UNCLASSIFIED

## AD NUMBER

ADC021924

## CLASSIFICATION CHANGES

TO: unclassified

FROM: confidential

## LIMITATION CHANGES

TO:

Approved for public release, distribution unlimited

FROM:

## AUTHORITY

DSWA ltr., 13 Apr 1998; Same

THIS PAGE IS UNCLASSIFIED

AD-E300832

**CONFIDENTIAL**

DNA 5056F

AD C021924

# MAGNETICALLY DRIVEN FLYER PLATE SIMULATION OF A RADIATION ENVIRONMENT ON A COMPOSITE MATERIAL (U)

Kaman Sciences Corporation
P.O. Box 7463
Colorado Springs, Colorado 80933

② LEVEL II

31 October 1979

"NATIONAL SECURITY INFORMATION"
"Unauthorized Disclosure Subject to Criminal Sanctions"

Final Report for Period 15 January 1979—31 October 1979

CONTRACT No. DNA 001-77-C-0106

THIS WORK SPONSORED BY THE DEFENSE NUCLEAR AGENCY UNDER RDT&E RMSS CODE B342077464 N99QAXAC31220 H2590D.

DTIC
S ELECTE D
JUL 8 1980
B

Prepared for
Director
DEFENSE NUCLEAR AGENCY
Washington, D. C. 20305

CLASSIFIED BY DDST/DNA.
REVIEW ON 6 September 1985.

DDC FILE COPY

**CONFIDENTIAL**

80 6 2 503

# CONFIDENTIAL

(This page is unclassified)

UNCLASSIFIED

SECURITY CLASSIFICATION OF THIS PAGE (When Data Entered)

## REPORT DOCUMENTATION PAGE

READ INSTRUCTIONS BEFORE COMPLETING FORM

| | | |
|---|---|---|
| 1. REPORT NUMBER<br>DNA 5056F | 2. GOVT ACCESSION NO.<br>AD-C021 | 3. RECIPIENT'S CATALOG NUMBER<br>934 |
| 4. TITLE (and Subtitle)<br>(6) MAGNETICALLY DRIVEN FLYER PLATE SIMULATION OF A RADIATION ENVIRONMENT ON A COMPOSITE MATERIAL (U) | | 5. TYPE OF REPORT & PERIOD COVERED<br>Final Report for Period<br>15 Jan 79—31 Oct 79 |
| (8) | | 6. PERFORMING ORG. REPORT NUMBER<br>K-79-307(R) |
| 7. AUTHOR(s)<br>(10) William S. Doane<br>David H. Seitz | | 8. CONTRACT OR GRANT NUMBER(s)<br>(15) DNA 001-77-C-0106 new |
| 9. PERFORMING ORGANIZATION NAME AND ADDRESS<br>Kaman Sciences Corporation<br>P.O. Box 7463<br>Colorado Springs, Colorado 80933 | | 10. PROGRAM ELEMENT, PROJECT, TASK AREA & WORK UNIT NUMBERS<br>(16) ~~Subtask~~ N99QAXAC312-20 |
| 11. CONTROLLING OFFICE NAME AND ADDRESS<br>Director<br>Defense Nuclear Agency<br>Washington, D.C. 20305<br>(17) C312 | | 12. REPORT DATE<br>31 October 1979 |
| | | 13. NUMBER OF PAGES<br>146 |
| 14. MONITORING AGENCY NAME & ADDRESS (if different from Controlling Office)<br>(14) K-79-307(R) | | 15. SECURITY CLASS (of this report)<br>CONFIDENTIAL |
| | | 15a. DECLASSIFICATION/DOWNGRADING SCHEDULE<br>Review on 6 Sep 85 |

16. DISTRIBUTION STATEMENT (of this Report)

(9) Final rept. 15 Jan-31 Oct 79,

17. DISTRIBUTION STATEMENT (of the abstract entered in Block 20, if different from Report)

(18) DNA, SBIE (19) 5056F, AD-E300 832,

18. SUPPLEMENTARY NOTES

This work sponsored by the Defense Nuclear Agency under RDT&E RMSS Code B342077464 N99QAXAC31220 H2590D. (12) 140

19. KEY WORDS (Continue on reverse side if necessary and identify by block number)

Facility Correlation Study
Impulsive Loading
UGT Simulation Study
Magnetically Driven Flyer Plates
Pressure-Time Pulse Shaping Using Advanced Capacitor Bank Techniques

20. ABSTRACT (Continue on reverse side if necessary and identify by block number)

The goals of the program were to: (1) Correlate the KSC magnetically driven flyer plate facility test techniques with those of another facility; (2) define AGT test techniques which successfully duplicate UGT test results; (3) expand the 3DQP material data base; and (4) establish 3D quality control procedures (3DQC) through analytics, NDM, NDT, resonance test techniques, and flyer plate loading procedures. KSC participation in the program touched on all four program goals. KSC impulsive load testing was most heavily concentrated in goals

DD FORM 1 JAN 73 1473 EDITION OF 1 NOV 65 IS OBSOLETE

UNCLASSIFIED

SECURITY CLASSIFICATION OF THIS PAGE (When Data Entered)

# CONFIDENTIAL

(This page is unclassified)

389119 slt

20. ABSTRACT (Continued)

1) and 2) under the facility Correlation Study and the UGT Simulation Study. KSC analytical capability was concentrated in areas 3) and 4), expanding the 3DQP data base and establishing 3DQC procedures.

This program consists of two phases:

1) To develop, demonstrate and assess the ability of magnetically driven flyer plates to duplicate the combined shock and structural response caused by a selected underground test (UGT) environment on 3DQP; and,
2) To correlate the magnetically driven flyer plate facilities of KSC with those of the Atomic Weapons Research Establishment (AWRE) in the United Kingdom.

The simulation development has been tailored to match the pressure vs. time and total impulse measurements obtained on UGT events. This matching of experimental data required considerable development of capacitor bank technology to develop the proper magnetic pressure vs. time profile. Sensitivity studies conducted during the course of this program vividly demontrated that two different waveforms with the same prompt and total impulse values could produce radically different response modes and failure levels. The proper simulation environment is realized by the proper control of the post-impact magnetic pressure amplitude and decay time. This significant achievement represents the first known time that these parameters have been utilized to control damage mode and level.

Evaluations of the degree of simulation have been made by detailed examinations of the damage modes and level in addition to correlation of mag flyer induced data with UGT data of pressure vs. time, total momentum and strain signatures on ring specimens. These mag flyer experiments were conducted on 11 arc specimens and 2 rings or 19.6-cm diameter C cycle 3DQP. (The UGT material was the same size and pedigree.)

Included in the damage mode assessment were measurements of the apparent degradation of the dynamic modulus as determined by Electromagnetic Excitation (EME) testing at KSC of both UGT and aboveground (AGT) rings. KSC then utilized this dynamic data to correlate measured strain vs. time signatures from firing specimens. The modeling for the ring analyses included variable thickness and degraded modulus as a function of angle. Incremental machining and resonant testing experiments yielded preliminary data through the thickness degradation of modulus for both AGT and UGT rings. KSC also conducted ultrasonic, radiographic, and shock tube NDT inspections of 3DQP samples. The overall agreement between the response of the UGT and final optimized AGT simulation is very good and is explained in detail herein.

Damage experiments continued to suggest a 10%-15% difference in the quoted impulse values necessary to produce equivalent damage in 3DQP samples by the AWRE and KSC facilities. Detailed discussions on diagnostics, flyer edge curl, backstrap deformation and other criteria have been conducted. KSC feels that the absolute value of current and impulse to be somewhere between those presently quoted by each facility.

*While individual paragraphs, sections, tables, graphs, etc. of the report are unclassified, the report is overall classified CONFIDENTIAL because the aggregate of information reveals new U.S. magnetic flyer technology development.*

# PREFACE

This report describes both the experimental and analytical efforts conducted by KSC for the UGT Simulation Program. The work was conducted as part of DNA's 3DQC Program and was authorized by DNA Contract 001-77-C-0106. This program was conducted under the direction of Mr. Donald Kohler, DNA.

Particular thanks go to Mr. Rex Bealing from AWRE, who spent several days at KSC, providing great insight into capacitor bank operation and the 3DQC Program. Again, special thanks to Mr. Angus MacAulay AWRE, who provided many years of assistance concerning test techniques and program guidance. KSC gratefully acknowledges the cooperation and contributions from the "3DQC Committee":

| | |
|---|---|
| Southern Research Institute (SoRI)<br>C. Pears and G. Fornaro | Material Properties and damage data, timeliness of action. |
| Science, Systems, & Software ($S^3$)<br>T. McKinley and G. Gurtman | Presentation of KSC data at AWRE, interpretations and program guidance, and both structural and material response calculations. |
| Air Force Weapons Laboratory (AFWL)<br>D. Newlander | Shockwave calculations and pulse shaping. |

Conversion factors for U.S. customary to metric (SI) units of measurement

(This Table Is Unclassified)

| To Convert From | To | Multiply By |
|---|---|---|
| angstrom | meters (m) | 1.000 000 X E -10 |
| atmosphere (normal) | kilo pascal (kPa) | 1.013 25 X E +2 |
| bar | kilo pascal (kPa) | 1.000 000 X E +2 |
| barn | meter$^2$ (m$^2$) | 1.000 000 X E -28 |
| British thermal unit (thermochemical) | joule (J) | 1.054 350 X E +3 |
| calorie (thermochemical) | joule (J) | 4.184 000 |
| cal (thermochemical)/cm$^2$ | mega joule/m$^2$ (MJ/m$^2$) | 4.184 000 X E -2 |
| curie | giga becquerel (GBq)* | 3.700 000 X E +1 |
| degree (angle) | radian (rad) | 1.745 329 X E -2 |
| degree Fahrenheit | degree kelvin (K) | $t_K = (t° f + 459.67)/1.8$ |
| electron volt | joule (J) | 1.602 19 X E -19 |
| erg | joule (J) | 1.000 000 X E -7 |
| erg/second | watt (W) | 1.000 000 X E -7 |
| foot | meter (m) | 3.048 000 X E -1 |
| foot-pound-force | joule (J) | 1.355 818 |
| gallon (U.S. liquid) | meter$^3$ (m$^3$) | 3.785 412 X E -3 |
| inch | meter (m) | 2.540 000 X E -2 |
| jerk | joule (J) | 1.000 000 X E +9 |
| joule/kilogram (J/kg) (radiation dose absorbed) | Gray (Gy)** | 1.000 000 |
| kilotons | terajoules | 4.183 |
| kip (1000 lbf) | newton (N) | 4.448 222 X E +3 |
| kip/inch$^2$ (ksi) | kilo pascal (kPa) | 6.894 757 X E +3 |
| ktap | newton-second/m$^2$ (N-s/m$^2$) | 1.000 000 X E +2 |
| micron | meter (m) | 1.000 000 X E -6 |
| mil | meter (m) | 2.540 000 X E -5 |
| mile (international) | meter (m) | 1.609 344 X E +3 |
| ounce | kilogram (kg) | 2.834 952 X E -2 |
| pound-force (lbf avoirdupois) | newton (N) | 4.448 222 |
| pound-force inch | newton-meter (N·m) | 1.129 848 X E -1 |
| pound-force/inch | newton/meter (N/m) | 1.751 268 X E +2 |
| pound-force/foot$^2$ | kilo pascal (kPa) | 4.788 026 X E -2 |
| pound-force/inch$^2$ (psi) | kilo pascal (kPa) | 6.894 757 |
| pound-mass (lbm avoirdupois) | kilogram (kg) | 4.535 924 X E -1 |
| pound-mass-foot$^2$ (moment of inertia) | kilogram-meter$^2$ (kg·m$^2$) | 4.214 011 X E -2 |
| pound-mass/foot$^3$ | kilogram/meter$^3$ (kg/m$^3$) | 1.601 846 X E +1 |
| rad (radiation dose absorbed) | Gray (Gy)** | 1.000 000 X E -2 |
| roentgen | coulomb/kilogram (C/kg) | 2.579 760 X E -4 |
| shake | second (s) | 1.000 000 X E -8 |
| slug | kilogram (kg) | 1.459 390 X E +1 |
| torr (mm Hg, 0° C) | kilo pascal (kPa) | 1.333 22 X E -1 |

*The becquerel (Bq) is the SI unit of radioactivity; 1 Bq = 1 event/s.
**The Gray (Gy) is the SI unit of absorbed radiation.

UNCLASSIFIED

## TABLE OF CONTENTS

## TABLE OF CONTENTS

## LIST OF ILLUSTRATIONS

## LIST OF ILLUSTRATIONS

## LIST OF ILLUSTRATIONS

## LIST OF ILLUSTRATIONS

## LIST OF ILLUSTRATIONS

## LIST OF ILLUSTRATIONS

## LIST OF TABLES

## 1.0 INTRODUCTION

This report describes work performed by KSC in support of the DNA 3DQC Program. The objectives of this program are as follows:

1. Correlate results from KSC and AWRE flyer plate facilities

2. Define an above ground test which duplicates underground test damage

3. Expand the 3DQP data base
   - higher impulse level data
   - porosity effects
   - combined response (shock and structural) effects

4. Establish 3D Quality Control (3DQC) procedures for
   - analytics
   - Non-destructive measurement (NDM) and non-destructive test (NDT) techniques
   - flyer plate loading which produces damage correctly

Tailored loading techniques[1] developed jointly by the AWRE and KSC flyer facilities demonstrated nearly ideal above ground test (AGT) simulation of the UGT effects experienced by Ring Z. Ring Z is a 3DQP ring, 19.56 cm O.D. x 0.14 cm thick, fielded in Husky Pup and is officially designated as M381-1. This simulation was based on duplication of four material property or material response parameters:

- transmitted P-t
- material damage mode/level
- 180° early time structural response
- material degradation gradients

Extensive use was made of the TINC hydrocode to produce P-t wave shapes as a basis for magnetic flyer pulse shaping.[6] Only the inability to produce a strong mid-plane delamination in a ring geometry kept the magnetic flyer AGT simulation from being totally complete.

To overcome this deficiency, further testing on 11 arcs and 3 rings was conducted in search of the proper tailored loading waveform which would produce the desired damage, along with the other stated response parameters. The demonstration of a complete damage mode along with material degradation, proper structural response, and transmitted pressure-time by AGT methods was the prime experimental objective of this contract.

KSC developed several new analytical codes and incorporated new methodology to strengthen existing codes in order to more accurately treat both the resonant testing/incremental machining experiments and the strain-time structural response measurements. The analytical methodology necessary to support the resonant testing was developed under IR&D funding, and was applied to the resonant testing/incremental machining data. These data and analysis were combined to obtain both the dynamic transverse shear and Young's moduli degradation gradients of several AGT and UGT damaged rings. These moduli values were then used as input to the recently developed RNGSHR Code to predict strain-time structural response modes of both AGT and UGT rings. These experimental/theoretical correlations are presented. As an

aid to the evaluation of the quality of these correlations, a correlation coefficient code was developed and correlation coefficients for AGT and UGT data are reported. To facilitate the handling of these experimental/theoretical arrays of data, a Plot Group of Records (PGR) code was developed to overlay the experimental data with the analytical predictions.

Analytical studies were also conducted to judge the sensitivity of both the virgin and degraded shear and Young's modulus to the frequency data recorded during resonant testing.

A shock tube capability was developed in order to conduct an NDT test which would establish the A or C process origins of 3DQP material. IR&D funds for the shock tube and instrumentation development were utilized through tests on flat and circular aluminum samples. DNA funds were used to test the 3DQP samples.

The experiments reported here are part of a comprehensive program by DNA to expand above ground test techniques in order to requalify a hardened heatshield material (3DQP) without the use of underground tests. Extensive analytic and laboratory test technique improvements were accomplished by Systems, Science and Software, the Air Force Weapons Laboratory, and Southern Research Institute which are reported in other DNA reports related to this 3DQC program. An integrative report of the efforts of this program is being prepared by $S^3$. A chronological viewpoint of the experiment is taken in this report in order to indicate the factors which influenced the methodology development by the "3DQC Committee."

## 2.0 IMPULSIVE LOAD TEST TECHNIQUES

### 2.1 Capacitor Bank Description

The samples were tested in the Kaman 220-kJ magnetic flyer plate facility. This capcitor bank consists of 36 capacitors storing 220 kJ of energy at 45 kV. The output parameters of the bank are several megamperes at a ringing frequency of 120 kHz. The electrical circuit consists of 36 capacitors, a Blumlein-triggered solid dielectric switch, and a flyer plate assembly. The discharge of the stored energy is initiated by a high voltage pulse induced into the solid dielectric switch to produce multiple current carrying channels. The discharging current produces a magnetic field which then produces an accelerating force on the flyer plate, itself a current carrying part of the circuit. The flyer plate is thus accelerated to a predetermined velocity, at which point it then strikes the target. The flyer plate velocity and, thus, the impulse is controlled by varying the width of the flyer plate, the flyer plate free run, and the stored energy in the capacitor bank. The posttest impact magnetic push is controlled both by the free run distance and by capacitor bank crowbar techniques.

### 2.2 Foil Chop Techniques

The KSC capacitor bank was altered to produce a tailored loading waveform for the damage shots conducted in the UGT Simulation Program. The tailored loading waveform was produced on the KSC capacitor bank by the addition of a ballast inductor and a foil chop crowbar technique. The KSC

capacitor bank and inductance schemes used early in the program have been reported.[1] However, as the program progressed to the shots being described in this report, the ballast inductor was discovered in a badly eroded condition due to high current densities. An improved inductor was inserted into the discharge circuit after performing 12 (arc and ring) damage shots. Ring 7.1.4#4 was the last sample impacted with the old inductor, while arc A73 and all remaining samples were impacted with the new discharge circuit parameters. Five calibration shots were conducted to insure repeatable discharge waveforms and compliance with previous data prior to impacting the samples with the new discharge circuit.

## 2.3 Flyer Plate Description

One of the most important items in obtaining good magnetic flyer experimental data is the quality control of the flyer plate assembly. Due to the criticality of the flyer assembly, Kaman has expended considerable effort to insure repeatibility in each of the assembly steps. Flyer plate shape is established by a template which is designed and fabricated for each new test assembly. Each flyer plate is individually fabricated by a special process which enables the flyer plate to conform to the precise dimensions of the template with edges which are smooth and free of burrs, machine marks, etc. The flyer plate/insulation/backstrap layout is then assembled in a controlled environment such that dust particles are virtually eliminated. The repeatability on the overall assembly thickness is normally less than 0.0127 mm.

In these experiments, flyer plates 7.62 cm wide were used to impact the arc and ring samples. All flyer plates were made from 0.64 mm thick aluminum and were sized in length to load 160° of arc.

Initially, the flyer/insulation/backstrap was fabricated flat and then curved to the proper radius before being placed in the massive aluminum backing block. The thicker 0.64 mm aluminum flyers did tend to lift, however, indicating that residual stresses had been built in during the assembly process. To overcome the flyer lift, the flyers were assembled over a curved mandrel, and then placed in the aluminum backing block. Fabrication by this technique allowed stress-free flyer assemblies, and the lift was eliminated.

KSC performed several shots with a different flyer plate to backstrap width ratio. These shots were conducted to eliminate flyer edge curl. This flyer/backstrap geometry was not used to perform damage shots, however. Details of this shot series are presented in Appendix A.

## 2.4 Momentum Calibration

Of prime importance to the understanding of any flyer plate experiment is the knowledge of the flyer plate behavior. To meet this requirement, Kaman has developed a flyer plate diagnostic scheme capable of determining the imparted magnetically derived momentum in a flyer plate experiment.

Kaman determines the flyer plate impulse versus capacitor bank voltage by means of a velocity measurement of a known mass density flyer plate. The basic measurement technique relies on a calibrated Rogowski coil to determine the "effective" current through the flyer plate. The time resolved "effective" current is then used to input the computer code Veldet such that the flyer plate performance (displacement, velocity, and momentum density) can be determined. The momentum density at impact and at the end of current ring-down are obtained by this method.

The "effective" current calibration is determined from time-of-arrival measurements and correlated by flyer plate velocity measurements as derived from offset pin switch closures. These data have been previously correlated to within ±5 percent for a 5.59 cm wide flyer as shown in Figure 1. Further diagnostic cross checks[1] including TOA pins, streak cameras, and quartz gage measurements show agreement to ±7.5 percent. The pin switches (either shorting or PZT pins) for these experiments are monitored on high-speed oscilloscopes. The standard data display for these recordings includes a timing wave on each channel and a fiducial mark which is common to the Rogowski coil measurement of the bank current (Figure 2) and all pin switch records (Figure 3). The timing marks are used to calibrate the sweep speed of the oscilloscope beams on each test and the fiducial mark is utilized to establish a positive reference time between all events including the start of current flow from the capacitor bank. These data are used as input to the Veldet computer code. The Veldet output includes printouts of the time varying items of interest (current, displacement, velocity, etc.).

The KSC and AWRE facilities continue to show 10-15 percent difference in the impulse value necessary to produce equivalent damage in 3DQP samples. KSC consistently quotes a lower impulse value than does AWRE. This difference was discussed in detail at the June 1978 visit by AWRE to KSC. Since both facilities use measured current waveforms to evaluate the flyer impulse, current measurement techniques, current distribution across the flyer width, flyer edge curl, and backstrap performance were discussed. However, the technical discussions did not conclude which facility is in error. KSC feels that the absolute values of current and impulse be somewhere between the quoted values of each facility.

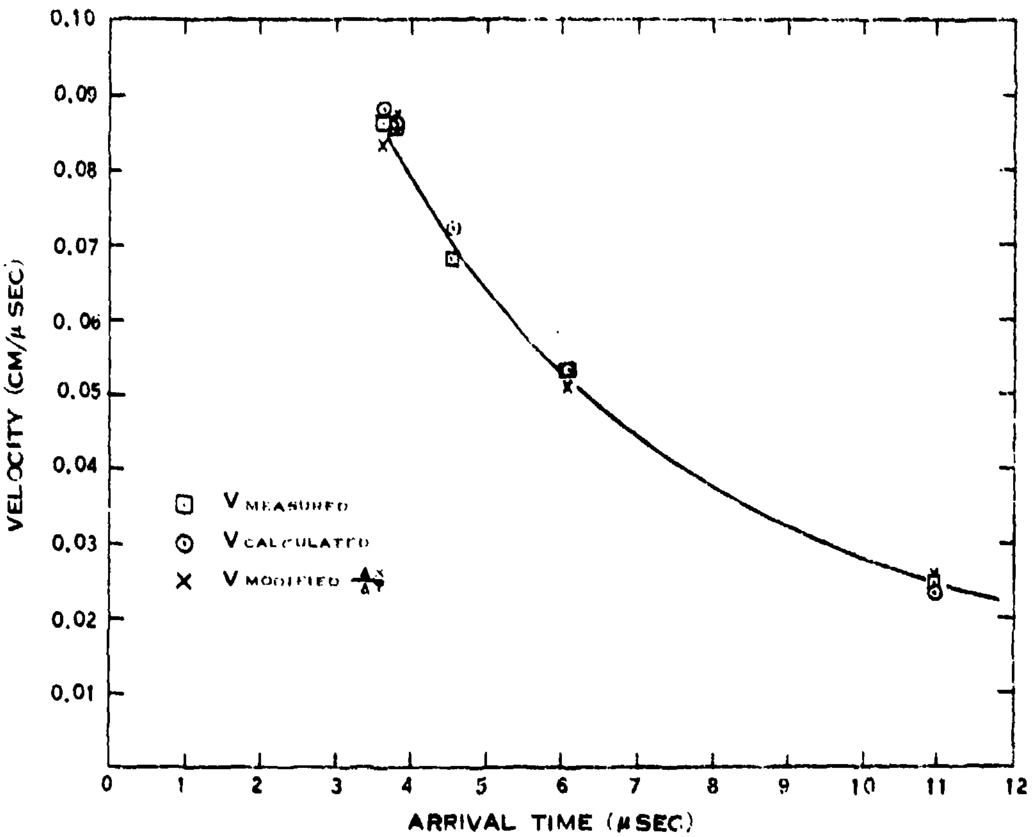

COSINE FLYER – 22.86 CM DIAMETER
2 MM FREE RUN
0.0305 CM THICK ALUMINUM FLYER
54 KILOJOULE BANK

FIGURE 1 0° FLYER VELOCITY VS. ARRIVAL TIME
(FLUSH AND OFFSET PIN SWITCH DATA)

FIGURE 2 CURRENT WAVEFORM RECORDING

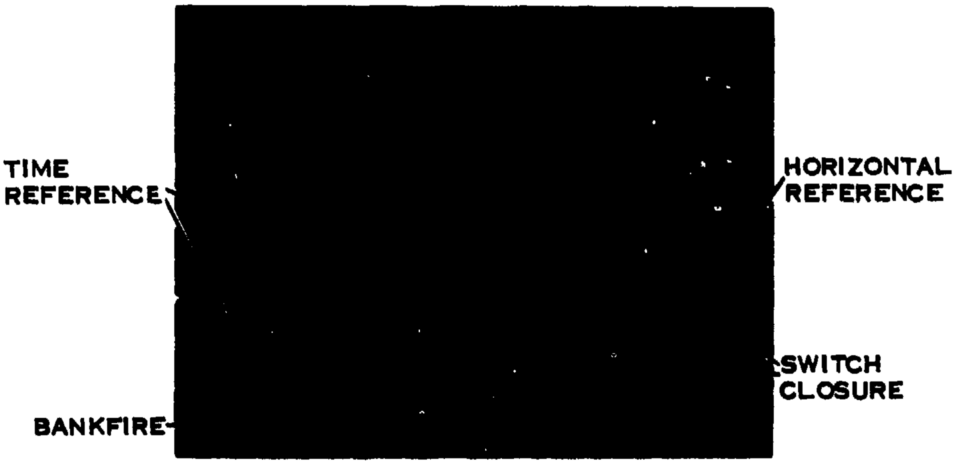

FIGURE 3 OFFSET PIN SWITCH RECORDING

## 2.5 Sample Support/Release Schemes and General Test Information

All arcs were impacted with the arc supported in an aperture plate. The arc sample, time-of-arrival pin and the adiprene shock blocks were placed in the aperture of this fixture. The sample was then attached to the aperture plate by gluing small, hollow glass rods across the top and bottom of the adiprene shock blocks and also gluing the rods to the fixture. The glass rods provide enough support to hold the sample in the target holder without any sag; however, the shock pulse impact shatters the glass and the arc sample is released after one shock wave transit time through the adiprene shock block thickness.

All shots documented in this report were conducted with a free-flying backstrap. Since all materials were fabricated as an arc or ring geometry, the same load coil, with a free-flying backstrap was used such that both sample geometries were tested under identical loading conditions.

The purpose of the free flight backstrap is to insure the free response of the rings tested in this program. As the impulsive load is applied, the ring surface begins to move radially inward and away from the flyer assembly at 0°. Shortly afterwards, the combined membrane and flexural response of the ring causes it to expand radially outward at ±90°. The ring expands such that it impacts the load coil before the rigid body displacement can remove the ring from the load coil extremeties. Structural response of the ring can be suppressed in addition to the point loading induced by the ring-coil impact.

Adiprene shock blocks 1.27 cm wide were placed around all samples in order to provide lateral constraints to effect a quasi-one-dimensional strain condition in the material during the initial shock wave transits. To the extent that the adiprene shock impedance matches that of the test sample, the effect of the adiprene shock blocks is to approximate a one-dimensional strain condition and suppress lateral release waves from traveling into the sample during the shock wave transits. The shock blocks also prevent undue side loads resulting from flyer plate edge curl. These shock blocks are also self releasing from the arc holder such that the sample is released immediately upon flyer impact. These criteria are thought to be extremely important for prompt shock damage evaluation. The adiprene shock blocks were, therefore, used on both the arc and ring samples. The shock blocks used on the ring samples were of identical width as those used for the arcs. They extended around the ring such that 160° of arc was subtended, protecting the ring from flyer edge curl, and were also self releasing from the ring. Small amounts of vacuum grease were used to join the shock blocks to either the arc or ring to insure intimate fit on all contact surfaces.

The arc holding scheme is devised so that the flyer-target spacing can be set very precisely. With the target placed on the flyer plate, six micrometer heads are used to raise the sample and aperture plate until the appropriate free run is attained. The proper orientation between the target surface and flyer surface is maintained by noting that the readings on the micrometer heads are identical.

The ring holding scheme used many of the same principles developed for the arc holder. Glass rods are used to support the ring, and when these rods are impacted by the flyer, they

shatter and release the ring. The ring-flyer plate spacing and orientation is controlled by exactly the same techniques described for the arc holding scheme.

Initially, mylar was placed over the impact surface of all 3DQP samples (both arcs and rings) as a standard practice. However, concern over potential deleterious effects on damage mode caused termination of the practice as a precautionary measure. Since the 3DQP samples were nonconductive, high voltage protection wasn't a consideration; the TOA pin shielding was altered to prevent arcs from the flyer to the pin.

Arc samples K60, K62, K64, K66, K68, K70, A65, K72, A61, A69, and A71 were the arcs tested with full front surface mylar. Except for the mylar/no mylar study, all samples starting with arc A73 were tested with a bare front surface. All rings, without exception, were tested with a bare impact surface.

## 2.6 Instrumentation and Data Recording

Current waveforms, time-of-arrival, sample velocity, and ring sample strain-time histories were recorded on this program. These parameters were measured to provided data for momentum calculations and for ring structural response calculations.

The Dynafax framing camera was used to record the displacement-time histories of the arc or ring samples after impact with the flyer plate. The lighting technique was a

backlight scheme in which a floodlamp, through a Fresnel lens, shines directly into the objective lens of the camera. The arc interrupts the light as it flies across the field of view of the camera and the image is exposed on the film. Knowing the distance the sample travels during each frame, and knowing the time interval between frames allows calculation of the late-time sample velocity. From the sample velocity the late-time impulse of the sample can be obtained.

An electronically integrated Rogowski coil is used to record the current waveform while time-of-arrival is measured with PZT pins.

All electronic instrumentation were recorded in an electrically isolated screen room. The isolation was obtained by lifting the double-walled screen room six inches off the floor onto insulating pads and powering the recording instrumentation with a motor generator which is also electrically floating. The purpose of this elaborate isolation is to insure that the instrumentation sees a minimum of electromagnetic interference.

The current waveforms from the Rogowski coils were recorded on fast oscilloscopes, hand digitized using a traveling microscope, then submitted to Veldet computer codes. These codes apply amplitude and time base calibrations to the current traces and then print the plot and plot the data.

Table 1 presents a summary of the instrumentation and data recording techniques used on this program.

Table 1. Instrumentation and Data Recording Techniques

| EVENT TO BE RECORDED | SENSOR | RECORDING INSTRUMENTATION | DATA REDUCTION PERFORMED |
|---|---|---|---|
| TOA | PZT Pins | | Hand digitize with traveling microscope, submit data to VELDET code to obtain TOA |
| Current Waveform | Rogowski Coil | Oscilloscopes | Hand digitize with traveling microscope; submit data to VELDET or Mandat computer code to obtain calibrated current or pressure waveforms |
| Strain Waveform | Strain Gages | 40 kHz bandwidth FM tape recorder | Analog-digital conversion at 2 μsec intervals |
| Free Flight Velocity | Dynafax Camera | Dynafax Camera | Read negative on film reader, submit data to code |

## 3.0 MATERIAL DESCRIPTIONS CUTTING DIAGRAMS, AND TEST MATRIX

### 3.1 Material Descriptions

All materials tested and reported here were nominal C process 3DQP material. All material used for impulsive loading tests was supplied by AWRE in ring geometry, 19.56 cm diameter 1.40 cm wall thickness, and 3.81 wall height. Materials reported for this contract were supplied from five rings, 7.1.4#9, 7.1.4#15, 7.1.4#16, 7.1.3#1, and 4.1.3#1. Ring 7.1.3#1 was cut into 13 arcs, 2 arcs for SoRI and 11 for KSC. The arcs were machined from rings to sample length and width of 3.81 cm and thickness of 1.40 cm. All samples were fabricated with a radial side cut.

Material properties from these rings vary due to inconsistencies of the fabrication process. As documented by SoRI[2] and KSC, the range of virgin properties values are: density of 1.66 - 1.67 gm/cm$^3$, plies/inch from 90 to 105, open porosity of 2.5 to 3.9 percent, and $A_R/A_T$ ratio of 0.70. A more complete listing and values for individual rings are listed in Table 2.

Ring Z has been documented by AWRE to have been from Cylinder 4.1.5. As a result five rings from this cylinder were allocated for AWRE and KSC testing. These rings have been dubbed as the "golden material" and their virgin material properties are listed in Table 2. A cursory examination of the properties presented in Table 2 show large differences between Ring Z and 4.1.5 materials, clouding the assumption that Ring Z is indeed from Cylinder 4.1.5. However, this program has seemed to show that the differences in material properties have not had major effects on shock wave

Preceding Page Blank

propagation, material degradation, or damage mode. As a result, the differences between Ring Z and 4.1.5 material may not be serious, and the 4.1.5 material could damage exactly as Ring Z.

## 3.2 Test Matrix

Prior to June 1978, work at KSC and AWRE had demonstrated that AGT technology could duplicate UGT effects. Ring 7.1.4#4 and 7.1.4#6 had been impacted as demonstrations of this technology, both had failed to exhibit the clear mid-plane delaminations which appeared in Ring Z, though all other simulation parameters were successfully duplicated. The thrust of the new work, then, was to develop a loading waveform which would produce a clear mid-plane delamination as well as duplicating the correct pressure-time, 180° strain-time, and material degradation gradient in the samples to be tested.

The concensus opinion of the 3DQC Committee was to impact the one remaining arc with a magnetic pressure-time loading waveform whose peak would split the difference between the K70 and K66 waveforms. Since SoRI judged arc K66 to be about right in overall damage mode, and arc K70 too severe, it was believed that an intermediate loading waveform would be sufficient to produce damage in a ring. The following test matrix was employed:

- MATERIAL STATUS
  2 Rings at KSC
  R7.1.3#1
  R7.1.4#9
  1 arc at KSC
  A73
- TEST PLAN
  - Impact A73 Between K66 and K70
  - Compare Damage to Ring Z

| SUCCESSFUL COMPARISON | UNSUCCESSFUL COMPARISON |
|---|---|
| - Hit 2 Rings, Instrumented With 9 Strain Gages | - Cut R7.1.3#1 Into Arcs<br>- Obtain Proper damage on Arc Samples<br>- Hit R7.1.4#9 |

A73 was judged as an insufficeint simulation of Ring Z damage. Ring 7.1.3#1 was cut into arcs and a test matrix was devised. The arc and ring shot results are best described by grouping certain arcs by the shot series for which they were consumed. These shot series are identified by some informal phrases which gained common usage by the 3DQC committee.

| Shot Series | Arcs or Rings Consumed | Purpose, Comments |
|---|---|---|
| KSC Summer Series | K74, A75, K76<br>A77, K78, A79<br>K80, K84, A91<br>7.1.4#9<br>7.1.4#15 | ● Summer Series<br>- Mylar-No Mylar Study<br>- Dial-a-Crack Study<br>- A91 Golden Arc (From R4.1.5#3) |
| Search for K70 | 4 cal shots<br>A83<br>7.1.4#16 | ● Search For K70 Waveform<br>- Bank Rebuild, Ballast Inductor Adjustment, Anticipated High Voltage Made K70 Magnetic Waveform Difficult to Duplicate |

## 3.3 Cutting Diagrams

Arcs were cut from rings 7.1.4#1, 7.1.3#1, and 4.1.5#3. All machining on these rings was performed by KSC and the cutting diagrams are presented in Figure 4.

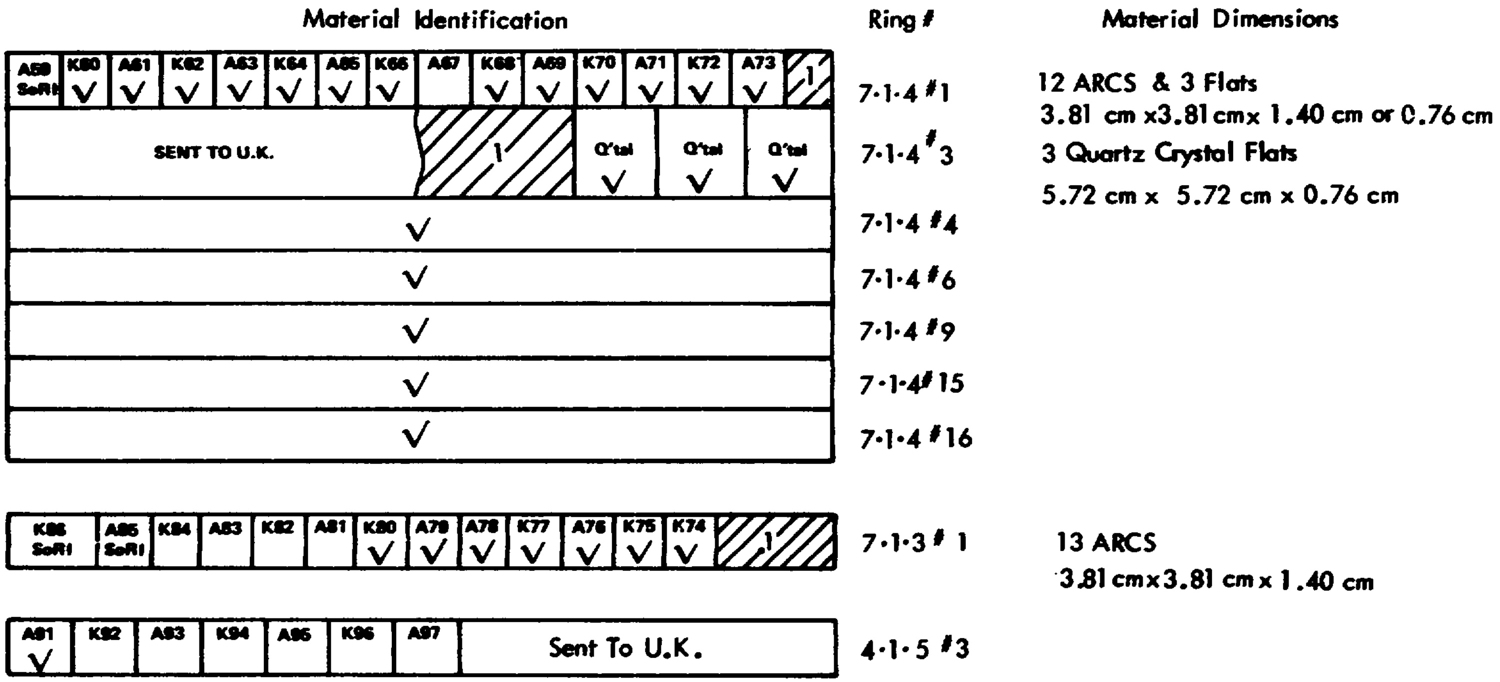

1 Material Lost In Machinging Process

√ Indicates Sample Has Been Shot

FIGURE 4 MATERIAL CUTTING DIAGRAMS

## 4.0 AGT RESULTS OF UGT SIMULATION TESTS

KSC tested 11 3DQP arc samples and three 3DQP rings in an attempt to exactly duplicate all UGT effects exhibited by Ring Z. The arc tests included the mylar, no mylar damage study, the Summer Series hunt for strong mid-plane damage (or so-called dial-a-crack shots), and a test on one golden arc, sample A91. Since material Z was in a ring geometry, the shots which were conducted as the final AGT simulation of UGT effects were performed on rings. Table 3 presents a complete summary for all shot parameters for all 3DQP samples tested to date. Figure 5 presents the pre and posttest radiographs of all samples tested for this contract. Damage descriptions are based on these radiographs and SoRI data.[2]

Twelve calibration shots were conducted throughout the arc and ring shots in order to calibrate for or verify the anticipated loading level. A detailed calibration was necessary because of the limited number of 3DQP samples available. The twelve calibration shots confirmed the relationship between the bank charging voltage, the flyer-to-target spacing, and the crowbar foil size in order to achieve the desired loading waveforms.

All damage and calibration shots were performed with 0.64 mm thick flyers. The flyer plate-to-target spacing was varied from 0.038 cm to 0.069 cm in order to achieve the desired loading waveforms.

As described in Section 3.3, Test Matrix, the 3DQC Committee believed that variations of the peak amplitude of the magnetic pressure-time loading waveform, in combination with the prompt impulse level and sample-flyer impact time, would duplicate Ring Z effects. As more tests were conducted, however, a strong bias developed between the arc and ring

results. This bias was observed both in damage mode as well as retained mechanical properties (such as strength and modulus; these data were measured and reported by SoRI[2]). Under the proper loading condition, the arcs developed strong mid-plane and rear surface cracks, nicely exhibiting the damage mode seen in Ring Z. However, when the rings were impacted under identical loading conditions, only the rear surface damage formed; the mid-plane delaminations so prevalent in the arc materials failed to develop in the ring geometry. SoRI presented mechanical property data which complemented this damage assessement in that the rings showed more retained strength and had higher retained modulus values than the arcs at similar impact levels. From these data, it was concluded that a bias existed between arc and ring test results (see reference 2, pages 27 and 28).

## 4.1 KSC Summer Series

Arc A73 was the first shot of the Summer series. This sample was pivotal in that it duplicated the Ring Z damage mode, then Rings 7.1.3#1 and 7.1.4#9 would be tested at A73 loading conditions. If the Ring Z damage mode did not appear in A73, then Ring 7.1.3#1 was to be cut into arcs. The desired loading condition was to achieve 6.0 prompt impulse, 13.0 Kilotaps total impulse, with a magnetic peak pressure of about 2.2 kilobars, splitting the difference between K70 and K66. The desired loading waveform was achieved. The sample, though correctly suffering mid-plane delamination, experienced too deep rear surface delamination, 9 to 12 plys deep (as compared to 4 plys deep in Ring Z). As a result of the lack of correlation between Ring Z and A73 rear surface damage Ring 7.1.3#1 was cut into 13 arcs. Eight arcs from this ring, A73 and A91 from the golden material comprised the arcs

| SoRI DATA | | | | | | | | | | | KSC DATA | |
|---|---|---|---|---|---|---|---|---|---|---|---|---|
| Virgin Material Properties | | | | | | Hoop Coupon Compression SCCC | | Ring Flexure RF2 | | ESE Vibrational Modulus | | |
| Ring # | Density$^7$ (gm/cc) | Attenuation (db$^1$) | Radial Velocity in/µsec | O.P. (%) | plies/in. | $E_\theta$ (in $10^6$ psi) | $\sigma_u$ (psi) | $E_H^2$ | $E_V^1$ | E (in $10^6$ psi | Shock$^2$ Speed (mm/ sec) | Modulus$^3$ GPa |
| 7.1.4/1 | 1.679 | 7 | 0.192 | 2.9 | 100 | 3.79 | 50,500$^6$ | - | - | - | | |
| 7.1.4/3 | 1.675 | 8 | 0.194 | - | 100 | - | - | 3.98 | 3.73 | - | | |
| 7.1.4/4 | 1.675 | 8 | 0.194 | - | 100 | belly<br>3.94 | belly<br>55,000 | 3.89 | 3.12 | - | | 26.1 |
| 7.1.4/5 | 1.674 | 8 | 0.194 | - | 100 | - | - | 3.89 | 3.12 | - | | |
| 7.1.4/6 | 1.675 | 6 | 0.194 | - | 100 | belly<br>3.74 | belly<br>57,000 | 3.84 | 3.21 | - | | 26.2 |
| 7.1.4/7 | 1.673 | 5 | 0.193 | - | 100 | - | - | 3.61 | 3.24 | - | | |
| 7.1.4/9 | -$^5$ | -$^5$ | -$^5$ | -$^5$ | -$^5$ | 3.58$^4$ | 75,500$^4$ | -$^5$ | -$^5$ | -$^5$ | | |
| 7.1.4/15 | 1.665 | 6 | - | 2.7 | 100 | 3.40$^4$ | 71.300$^4$ | 3.61 | 3.16 | 3.63 | 0°2.75 | 26.3 |
| 7.1.4/16 | 1.665 | 7 | - | 2.6 | 100 | $^4$ | $^4$ | 3.80 | 3.23 | 3.67 | 0°2.75 | 26.2 |
| 7.1.3/1 | 1.671 | 14 | | 3.9 | 105 | 3.72$^4$ | 63,000$^6$ | - | - | - | 225°2.50 | |
| Golden Rings: | | | | | | | | | | | | |
| 4.1.5/1 | 1.686 | 10 | 0.184 | 2.26 | 89 | - | - | 3.27 | 3.02 | 3.51 | | |
| 4.1.5/2 | 1.695 | 10 | 0.186 | 2.27 | 90 | - | - | 3.27 | 3.11 | 3.50 | | |
| 4.1.5/3 | 1.688 | 10 | 0.183 | 2.56 | 90 | - | - | - | - | - | 2.50 | 24.1(3.[illegible] |
| 4.1.5/4 | 1.685 | 9 | 0.184 | 2.35 | 90 | - | - | 3.35 | 3.21 | 3.48 | | |
| 4.1.5/5 | 1.687 | 8 | 0.185 | 2.06 | 90 | - | - | 3.35 | 3.29 | 3.54 | | |

1. These data published by SoRI in Reference 2
2. These Shock Speed data obtained by KSC Shock Tube Techniques
3. The data obtained by resonant testing techniques

Table 2 Virgin Material Property Data of AGT Rings

TABLE 3 OVERVIEW OF CAPACITOR BANK PARAMETERS
19.56 CM DIA. SAMPLE GEOMETRY

| SAMPLE # | SHOT # | VOLTAGE (kv) | CURRENT (MA) | FREE RUN (CM) | IMPULSE (KT) | | TOA (µsec) | | PEAK MAG PRESSURE (kb) | BANK INDUCTANCE (nH) | FOIL AREA ($CM^2$) |
|---|---|---|---|---|---|---|---|---|---|---|---|
| | | | | | $M_p$ | $M_t$ | VELDET | PIN | | | |
| K-60 | 2-338 | 24.1 | 1.50 | .114 | 8.3 | 14.5 | 5.9 | 5.7 | 2.20 | | 0.041 |
| K-62 | 2-342 | 35.1 | 2.00 | .051 | 7.9 | 14.4 | 3.5 | 4.3 | 3.80 | 100 | 0.165 |
| K-64 | 2-349 | 33.1 | 1.10 | .051 | 5.0 | 9.9 | 6.3 | 6.2 | 1.60 | 100 | 0.114 |
| K-66 | 2-350 | 35.0 | 1.20 | .064 | 6.2 | 11.3 | 6.6 | 6.5 | 2.00 | 100 | 0.114 |
| K-68 | 2-351 | 39.0 | 0.70 | .041 | 2.6 | 4.5 | 6.3 | 7.9 | 0.70 | 100 | 0.145 |
| | 2 | | | Crowbar Mylar Breakdown | | | | | | | |
| K-70 | 2-352 | 39.0 | 1.40 | .041 | 5.1 | 15.2 | 4.8 | 5.5 | 2.60 | 100 | 0.145 |
| A-65 | 2-356 | 35.1 | 1.20 | .053 | 5.7 | 12.8 | 5.3 | 5.9 | 2.20 | 100 | 0.124 |
| K-72 | 2-364 | 38.3 | 1.20 | .142 | 6.3 | 11.5 | 5.8 | 5.8 | 2.00 | 100 | 0.118 |
| A-61 | 2-365 | 20.1 | 1.10 | .051 | 5.3 | 13.5 | 5.1 | 5.6 | 1.70 | 35 | 0.036 |
| 7.1.4#6 | 2-366 | 35.0 | 1.20 | .064 | 6.0 | 10.9 | 6.2 | 1 | 1.90 | 100 | 0.114 |
| A-69 | 2-367 | 33.7 | 1.20 | .061 | 5.9 | 12.6 | 5.9 | 6.3 | 2.00 | 100 | 1.290 |
| 7.1.4#4 | 2-372 | 39.1 | 1.40 | .053 | 6.3 | 15.3 | 5.3 | 1 | 2.60 | 100 | 0.134 |
| 7.1.4.3. 1.F | 2-373 | 39.0 | 1.30 | .053 | 6.0 | 17.5 | 5.3 | 6.9 | 2.50 | 100 | 0.134 |
| A-73 | 2-445 | 32.8 | 1.30 | .058 | 6.1 | 12.9 | 5.6 | 6.4 | 2.20 | 100 | 0.114 |
| K-74 | 2-453 | 32.8 | 1.30 | .058 | 6.0 | 13.6 | 5.7 | 6.1 | 2.20 | 100 | 0.114 |
| A-79 | 2-469 | 32.9 | 1.30 | .058 | 6.2 | 16.7 | 5.6 | 7.0 | 2.30 | 100 | 0.114 |
| K-78 | 2-470 | 32.7 | 1.30 | .058 | 6.2 | 13.9 | 5.7 | 6.5 | 2.30 | 100 | 0.114 |
| A-75 | 2-472 | 32.1 | 1.30 | .038 | 4.7 | 13.0 | 5.1 | 6.0 | 2.20 | 100 | 0.114 |
| K-76 | 2-473 | 32.1 | 1.30 | .069 | 6.7 | 13.0 | 6.2 | 6.9 | 2.10 | 100 | 0.114 |
| A-77 | 2-474 | 32.1 | 1.30 | .069 | 6.8 | 13.4 | 5.9 | 6.6 | 2.20 | 100 | 0.114 |
| K-80 | 2-475 | 32.1 | 1.30 | .064 | 6.3 | 13.6 | 5.8 | 7.0 | 2.20 | 100 | 0.114 |
| 7.1.4#9 | 2-476 | Prefire 30 kv | 1.10 | .069 | 6.1 | 11.2 | 6.8 | 1 | 1.80 | 100 | 0.114 |
| K-84 | 2-487 | 31.0 | 1.20 | .069 | 6.4 | 12.9 | 6.1 | 7.1 | 2.00 | 100 | 0.114 |
| A-91 | 2-488 | 32.1 | 1.30 | .069 | 6.7 | 13.3 | 6.3 | 6.9 | 2.10 | 100 | 0.114 |
| 7.1.4#15 | 2-489 | 32.3 | 1.30 | .069 | 6.9 | 13.6 | 6.1 | 1 | 2.30 | 100 | 0.114 |
| A-83 | 2-505 | 34.5 | 1.40 | .041 | 5.2 | 15.03 | 5.0 | 5.93 | 2.60 | 90 | 0.124 |
| 7.1.4#16 | 2-506 | 34.5 | 1.40 | .041 | 5.3 | 16.4 | 4.9 | 1 | 2.80 | 90 | 0.124 |

1 Pin not run on experiment

| SAMPLE | RADIOGRAPHS | | DAMAGE* ASSESSMENT | | | | | |
|---|---|---|---|---|---|---|---|---|
| | PRETEST | POSTTEST | RRR | RL | RD | RND | MD | MND |
| A73 |  |  | 100% | 7/9 | 9/12 | 11/15 | 30/36 | -- |
| K74 |  |  | 100% | 2/5 | 2/7 | 7/9 | -- | 20/22 |
| A79 |  |  | 100% | 2 | 4 | 4 | 0 | 0 |
| K78 |  |  | 100% | 1/3 | 4/5 | 6/10 | 30/35 | 22/31 |
| A75 |  |  | 100% | 1/3 | 3/4 | 8/9 | 0 | 33/36 |
| K76 |  |  | 100% | 3/4 | 4/6 | 8 | 27/35 | 21/24 |
| A77 |  |  | 100% | 2/3 | 3/5 | 5/8 | 34/43 | 32/43 |

* Damage Assessments Obtained From Reference 2

FIGURE 5 KSC PRE AND POSTTEST RADIOGRAPHS AND SoRI DAMAGE ASSESSMENTS OF 3 DQP SAMPLES

| SAMPLE | RADIOGRAPHS | | DAMAGE * ASSESSMENT | | | | | |
|---|---|---|---|---|---|---|---|---|
| | PRETEST | POSTTEST | RRR | RL | RD | RND | MD | MND |
| K80 |  |  | 100% | 1 | 2/4 | 3/8 | 31/39 | 27/28 |
| 7·1·4 #9 |  |  | 90%<br>+30°<br>−35 | 2 | 3 | 0 | 0 | 0 |
| K 84 |  |  | 100% | 2 | 2/4 | 3/5 | None | 25/35 |
| A91 |  |  | 100% | 2 | 5/10 | 11/16 | 23/26 | None |
| 7·1·4 #15 | 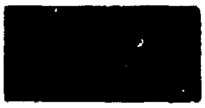 |  | 100% | 2/5 | 6/7 | 9/10 | 26/38<br>Bulk cracking extending 1—1 ½ cells<br>No connected MD | |
| A83 |  |  | 100% | 3 | 3/5 | 8 | 26/40 | See MD |
| 7·1·4 #16 | 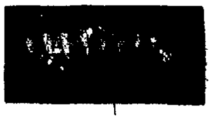 |  | 100% | 2/3 | 4/5 | 6 | 0 | 33/39 |

* Damage Assessments Obtained From Reference 2

FIGURE 5 (CON'T) KSC PRE AND POSTTEST RADIOGRAPHS AND SoRI DAMAGE ASSESSMENTS OF 3 DQP SAMPLES

tested in the KSC Summer Series. Data from these arc tests were used to complete the KSC Mylar-No Mylar study and the Dial-A-Crack Series.

The Mylar-No Mylar study was initiated to judge the effects of front surface mylar on the formation of mid-plane and rear surface damage. The premise was that the presence of mylar could alter the mid-plane and rear surface damage patterns as compared to samples impacted without mylar. The approach used to test this hypothesis was to place mylar on one half of the arc sample impact surface. So that the mylar would not protrude, a 0.0039 cm deep groove was cut into half the sample surface. In order to eliminate flyer bias, the location of the mylar was alternately placed on the left and right hand sides of the sample such that nonsymmetrical flyer performance, if present, could not affect the sample damage. The front surface mylar had been used as a standard procedure for years, originating as a technique to prevent arcing from the high voltage on the flyer plate to a conductive sample at ground potential. Previous use had not suggested an alteration of the front surface loading condition.

The results of Mylar-No Mylar Study showed the presence of the mylar made no deleterious effects on the arc damage modes. Samples A75, K76 (no mylar on the impact surface) and K78, K80, A77, and A79 (half mylar, half no mylar) were used in the study. Posttest damage was evaluated by sectioning the sample at the mylar/no mylar interface. SoRI then provided damage assessments based on all the exposed faces. SoRI also examined the impact surface to evaluate front face differences due to the mylar. Citing sample A77 as the foremost example, the four no mylar faces showed mid-plane damage at a depth of 34 to 43 plys, while the four mylar faces showed

mid-plane damage at a depth of 35 to 42 plys. Rear surface delaminations occurred to a depth of 3 to 4 plys on no mylar faces, and 4 to 5 plys on mylar faces. Therefore, both mid plane and rear surface damage seemed unperturbed by the presence of the mylar. Further, front radial recession was 90 percent complete on both mylar and no mylar impact surfaces, indicating inconsequential front surface effects due to the mylar. Radiographs and glossy photo's of A77 and K80 are presented in Figure 6 for visual confirmation.

The six arcs identified from the Mylar-No Mylar Study plus arc K74 comprised the Dial-A-Crack Study. All arc samples were cut from Ring 7.1.3#1. In KSC's opinion, this series seemed to indicate that increasing the prompt impulse measured the probability of mid-plane damage in the arc samples. Early shots in this study were at the following loading conditions: 6.2 ktap prompt impulse, 13.5 ktap total impulse, and 2.2 kbar peak magnetic pressure. This level split the loading conditions between K70 and K66 and was thought to be sufficient to cause mid-plane damage. K74, the first arc sample tested at this level, did not suffer mid-plane damage. Sample K78 did suffer mid-plane, but A79 did not. These shots indicated the load level was barely sufficient to cause damage, with two samples failing to show mid-plane damage and only on sample showing damage. Again it seemed that this loading waveform was not sufficient to produce this desired damage with consistency.

At this point, the 3DQC Committee decided to try a modified K70 loading condition. This loading condition would hold the total impulse at 13.5 ktap and the peak magnetic pressure at 2.2 kbar, but the impact time was to be before the magnetic peak, as in the waveform for K70.

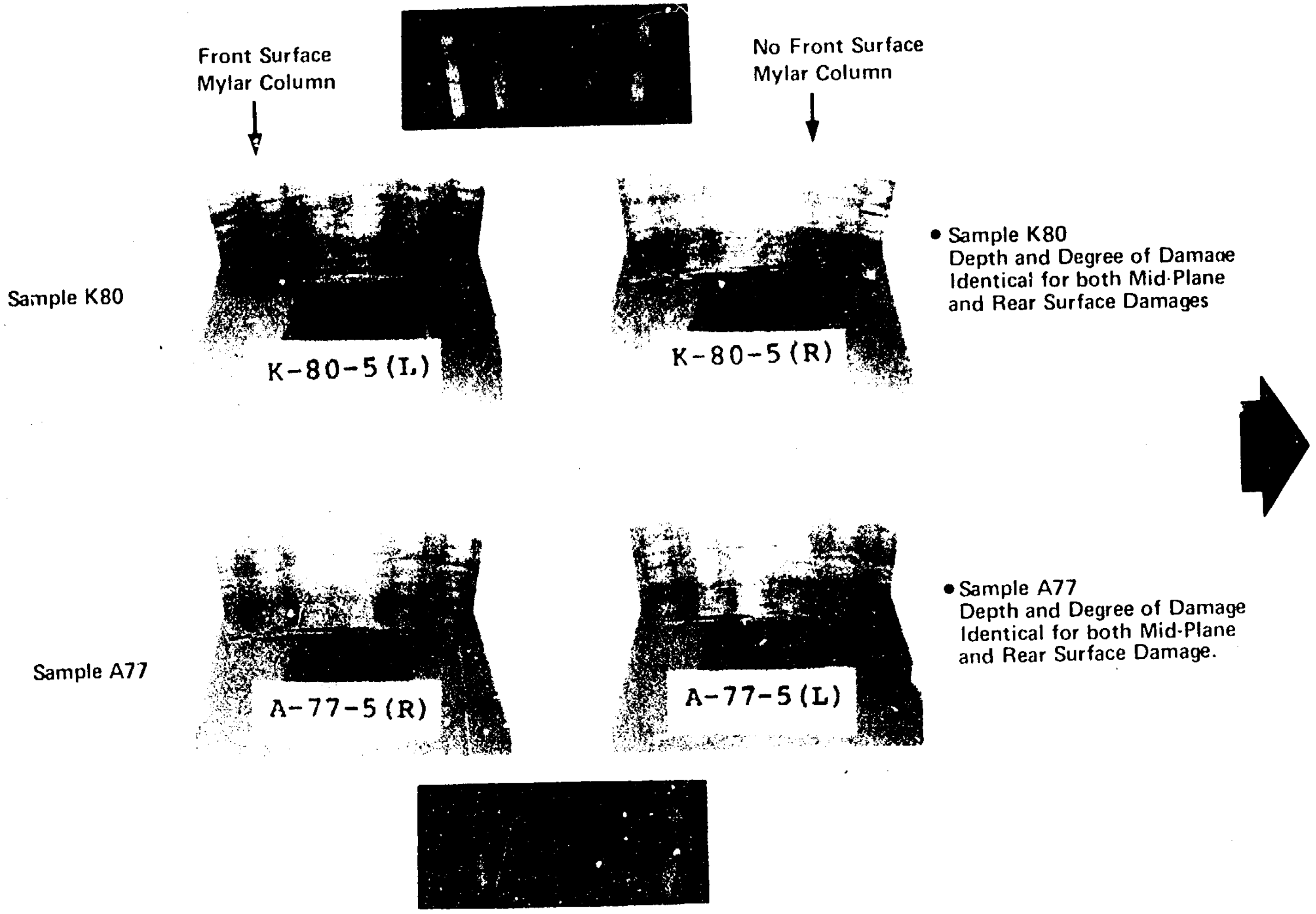

- Sample K80
  Depth and Degree of Damaoe
  Identical for both Mid-Plane
  and Rear Surface Damages

- Sample A77
  Depth and Degree of Damage
  Identical for both Mid-Plane
  and Rear Surface Damage.

- Conclusion
  Presence of
  Front Surface
  Mylar does
  not effect
  Damage Mode
  or Location.

FIGURE 6 EFFECTS OF FRONT SURFACE MYLAR ON 3DQP DAMAGE MODE

Sample A75 was thus impacted at 4.7 ktap prompt impulse, 13.0 ktap total, and 2.2 kbar peak pressure. Mid-plane damage was not observed as a result of this waveform.

The Dial-A-Crack Series then moved to a slightly higher prompt impulse, holding other loading parameters constant. The prompt impulse was increased to 6.7 ktap, while the 13.5 ktap total impulse and 2.2 kbar peak pressure were not altered. Samples K76 and A77 were tested at this level and both suffered mid-plane damage. Indeed, these samples suffered strong mid-plane damage described by SoRI as similar to K70. From these data, the supposition was proposed that strong mid-plane damage could be created routinely; hence, the phase Dial-A-Crack Study was formed.

To further test the Dial-A-Crack hypothesis sample K80 was impacted at a slightly reduced prompt impulse, hopefully, splitting the difference between the borderline K74, K78, A79 arcs (6.0 - 6.2 ktap prompt impulses) and the strong mid-plane damage K76, A77 arcs (6.7 - 6.8 ktap prompt impulse); K80 suffered strong mid plane damage at a loading level of 6.3/13.6/2.2. This loading level was close to that experienced by K74, K78, A79, and further indicates the borderline capability of that loading waveform to cause mid-plane damage.

Ring 7.1.4#9 was to be impacted at the K76, A77, load level. The bank prefired prior to reading full voltage and the resultant load parameters were woefully low, 6.1/11.2/1.8. The 1.8 kbar peak magnetic pressure was particularly inadequate; no previous data suggested this was a sufficient level to cause damage in arcs. Mid-plane damage was not observed in this ring as a result of the insufficient loading waveform. A posttest photograph of 7.1.4#9 is shown in Figure 7.

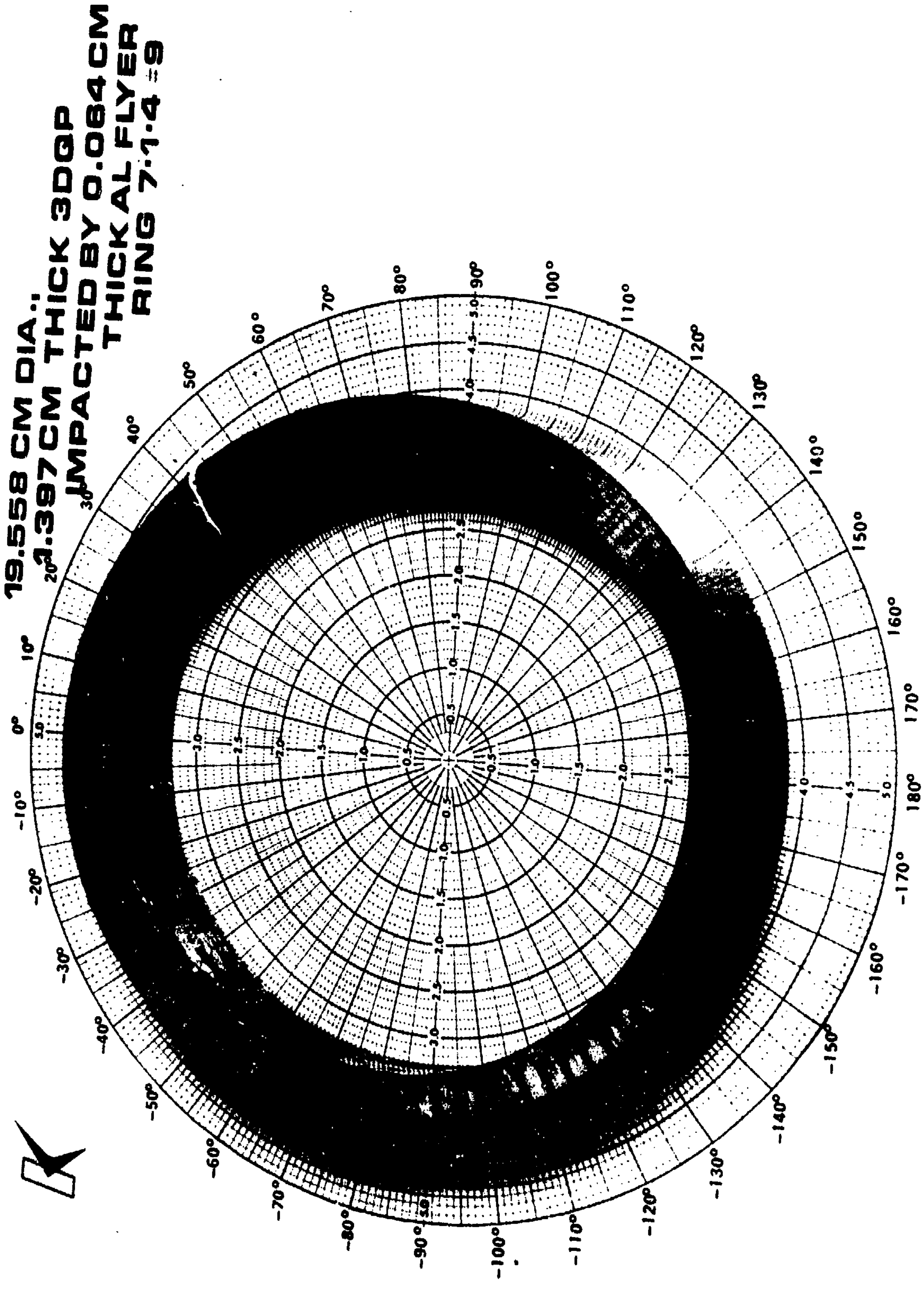

FIGURE 7 POSTTEST PHOTOGRAPH OF RING 7·1·4 #9

Reviewing all the arc data at a meeting held at DNA on 26 September 1978, the 3DQC Committee decided on the following test matrix:

- test arc K84 at 6.7/13.5/2.2
- if arc test is successful, hit Ring 7.1.4#15 at 6.7/13.5/2.2
- test golden arc A91 at 6.7/13.5/2.2

The loading conditions imposed on arc K84 provided a slight undertest due to an electrical arc between the flyer and return conductor plates. The values of the load were 6.4/12.9/2.0, and mid-plane damage was not observed. However, KSC felt strongly that the electrical arc had perturbed the loading conditions and decided to test Ring 7.1.4#15, confident that further calibration was not necessary in order tc obtain the desired loading waveform.

Ring 7.1.4#15 was tested at a loading condition of 6.9/13.6/2.3. This loading condition did not quite produce the desired damage, however. The rear surface damage was a slight overtest, producing rear delaminations to a depth 6/7 plys rather than the depth of 4 plys found on Ring Z. Perhaps more importantly, a clear mid-plane delamination did not form. The mid-plane damage described by SoRI was bulk cracking over one to two cell widths. These cracks did not coalesce to form connected cracks over a sufficient number of cell widths to be considered mid-plane damage. Near mid-plane delamination formed at a depth of 26 to 38 plys, encompassing the 25 to 30 ply depth of mid-plane damage experienced by Ring Z. In summary, the damage formed in 7.1.4#15 was a good, but not perfect duplication of the damage mode experienced by Ring Z. A posttest picture of 7.1.4#15 is shown in Figure 8.

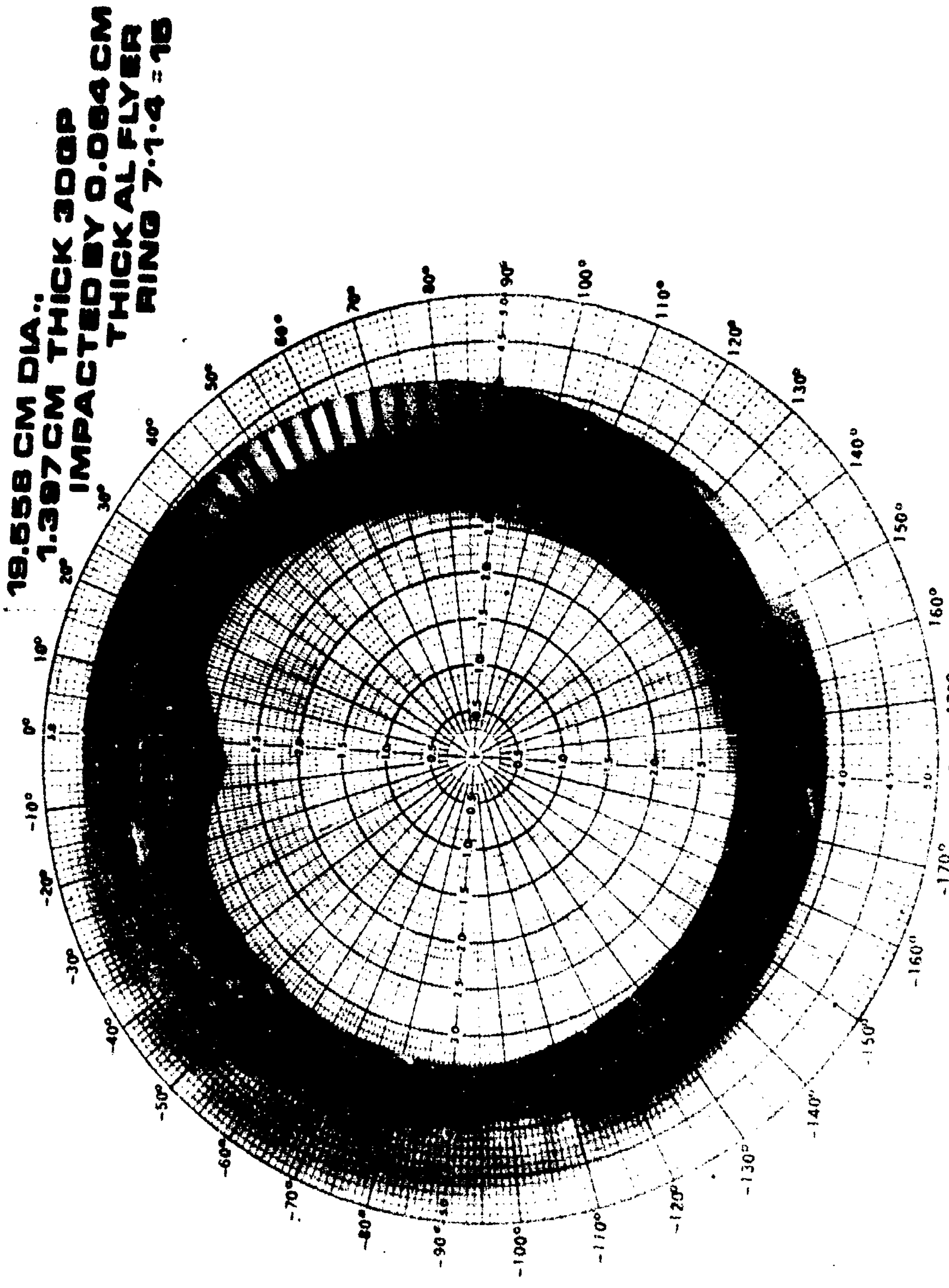

FIGURE 8 POSTTEST PHOTOGRAPH OF RING 7-1-4 #15

KSC EME and strain-time data suggested that the dynamic modulus degradation and the 180° strain-time comparisons are quite good between Ring 7.1.4#15 and Ring Z. The dynamic modulus degredation experienced by Ring 7.1.4#15 was 29 percent, while that of Ring Z was 28 percent. The correlation coefficients, comparing the strain time histories recorded by the inside and outside 180° strain gages of Ring 7.1.4#15 and Ring Z, were 0.97 and 0.887 (the modulus degradation and strain correlation is explained thoroughly in Section 7.0 UGT/AGT comparisons). Considering all available data, damage mode, modulus degradation, and strain-time correlations, KSC believes Ring 7.1.4#15 to be the best AGT simulation of Ring Z. The absence of a clear mid-plane delamination continued to be a dilemma. However, all other standards of comparison would suggest a high degree of success in the simulation of the UGT effects experienced by Ring Z.

Arc A91, obtained from the golden material Ring 4.1.5#3, was tested to establish its failure mode with respect to arc samples from 7.1.4 and 7.1.3 materials. Arc A91 was impacted at a 6.7/13.3/2.1 loading condition which was easily sufficient to cause mid-plane damage at a depth of 23 and 26 plys, comparable to the Ring Z mid-plane location of 25 to 30 plys; Arc A91 suffered rear surface delamination at a depth of 5 to 10 plys with near rear surface delaminations from 11 to 16 plys deep.

These shots comprised the KSC Summer Series. The range of magnetic pressure time waveforms for these 11 shots is shown in Figure 9.

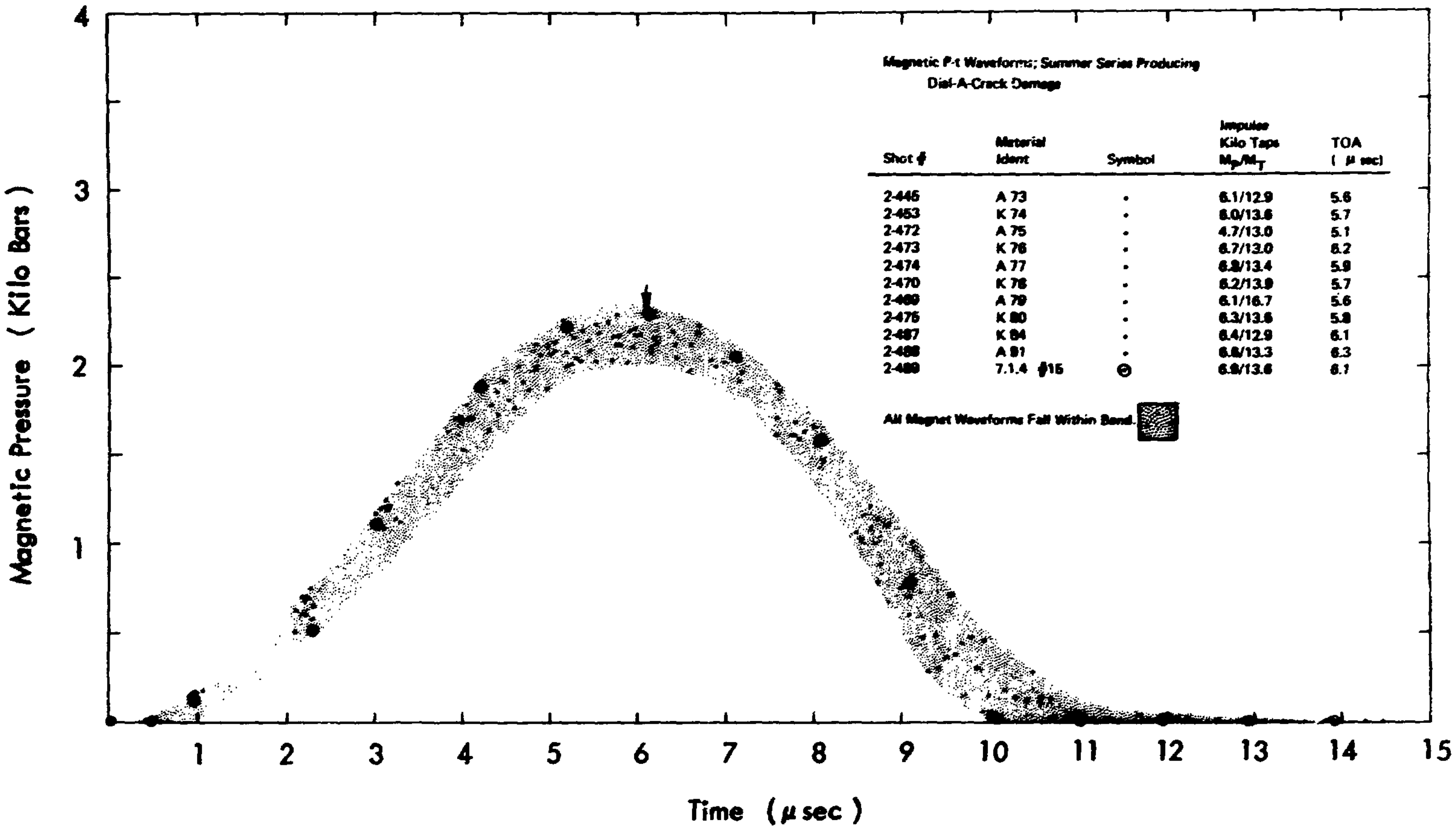

| Shot # | Material Ident | Symbol | Impulse Kilo Taps $M_p/M_T$ | TOA ( μ sec) |
|---|---|---|---|---|
| 2-445 | A 73 | • | 6.1/12.9 | 5.6 |
| 2-453 | K 74 | • | 6.0/13.6 | 5.7 |
| 2-472 | A 75 | • | 4.7/13.0 | 5.1 |
| 2-473 | K 76 | • | 6.7/13.0 | 6.2 |
| 2-474 | A 77 | • | 6.8/13.4 | 5.9 |
| 2-470 | K 78 | • | 6.2/13.9 | 5.7 |
| 2-469 | A 79 | • | 6.1/16.7 | 5.6 |
| 2-475 | K 80 | • | 6.3/13.6 | 5.8 |
| 2-487 | K 84 | • | 6.4/12.9 | 6.1 |
| 2-488 | A 81 | • | 6.6/13.3 | 6.3 |
| 2-489 | 7.1.4 #15 | ⊙ | 6.9/13.6 | 6.1 |

FIGURE 9 KSC SUMMER SERIES MAGNETIC PRESSURE WAVEFORMS

## 4.2 Search For K70 Series

The last series of shots was termed the Search For K70 Series. The purpose of this series was to duplicate the K70 loading conditions. Since Ring 7.1.4#15 did not show proper mode, the 3DQC Committee decided the best choice for developing a mid-plane delamination was the K70 waveform. Due to high voltage breakdowns and replacement of the original ballast inductor, KSC had to search for this loading condition developed over a year earlier. After four calibration shots, arc A83 was loaded at 5.2/15.0/2.6 with the rediscovered waveform. This sample showed strong mid-plane damage at a depth of 26 to 40 plys and rear surface damage to a depth of 3 to 5 plys. The rear surface damage nicely matched Ring Z, while the extent of the mid-plane damage bounded that found in Ring Z. As a result of these good matches of Ring Z damage mode, it was decided to load a ring with the new K70 waveform.

Ring 7.1.4#16 was successfully tested at a loading level of 5.3/16.4/2.7. This loading waveform produced a near mid-plane delamination at a depth of 33 to 39 plys. This delamination was connected at most, but not all, cell crossovers, and fell just short of being called a true mid-plane delamination. The rear surface damage was formed at a depth of 4 to 5 plys. In addition to these more typical damage modes, Ring 7.1.4#16 also suffered two hoop cracks due to the high total impulse exciting the structural response modes. One hoop crack developed to a depth of 5 plys on the outside diameter at 10°. The other hoop crack developed to a depth of 12 plys on the inside diameter at 0°. A posttest picture of 7.1.4#16 is shown in Figure 10.

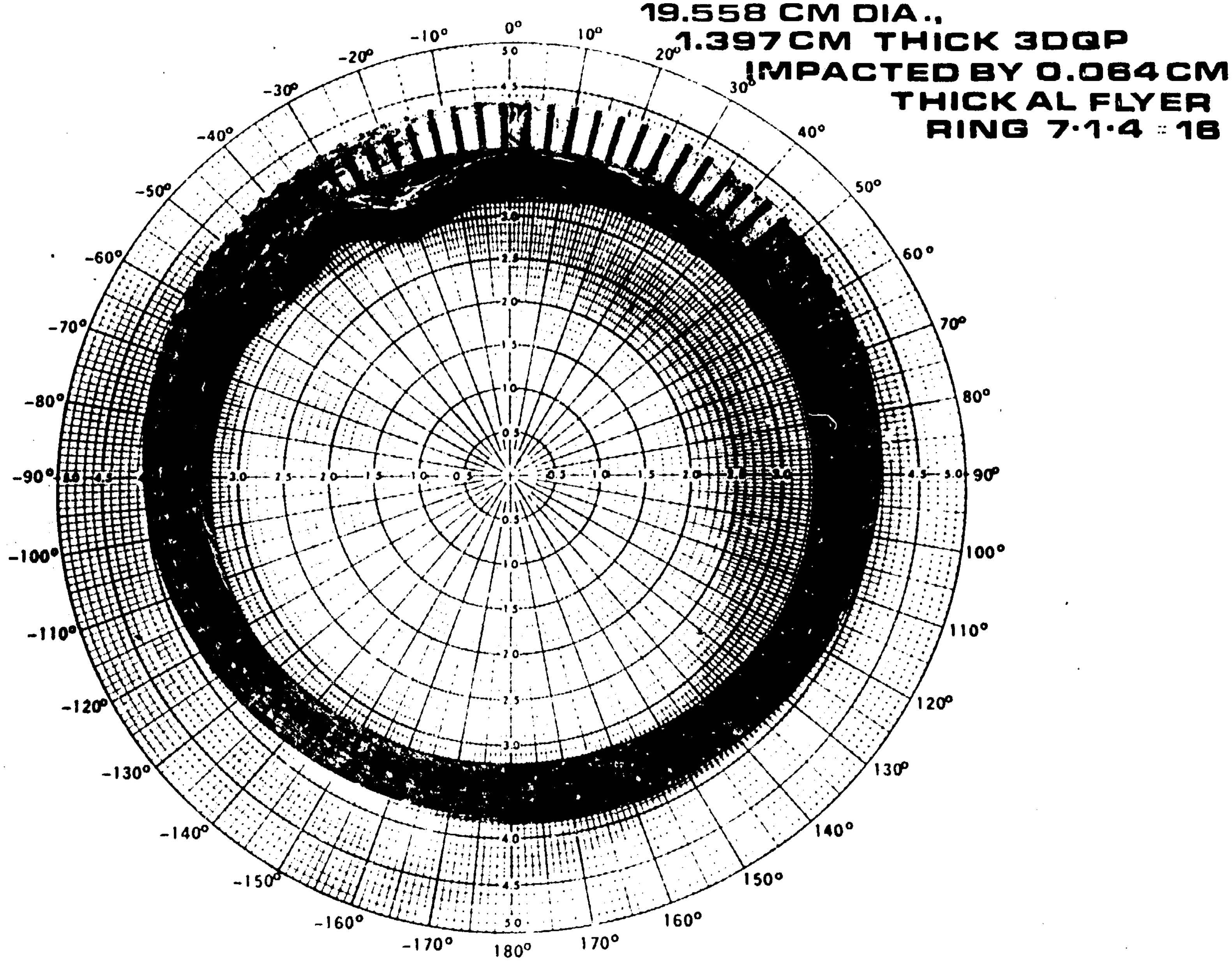

FIGURE 10 POSTTEST PHOTOGRAPH OF RING 7·1·4 #16

In addition to the development of two hoop cracks, the K70 loading condition also produced a degraded modulus and strain-time records which were too large in comparison to Ring Z data. These results were anticipated prior to the shot, but mechanical properties and strain time were de-emphasized in order to duplicate damage mode.

The modulus degradation experienced by 7.1.4#16 was 31 percent while that measured for Ring Z was 28 percent. The strain correlation coefficients comparing the 7.1.4#16 180° outer gage against the Ring Z 180° outer gage was 0.87. These data are presented in detail in Section 6.2, AGT Strain Correlation.

The magnetic pressure-time loading waveforms obtained from the Search For K70 Series are shown in Figure 11. This series concluded the damage shots conducted by KSC for the UGT Simulation Program.

### 4.3 Shock Tube Experiments

KSC loaded eight selected 3DQP samples by means of shock tube excitation. The shock tube produces a low amplitude air shock. A capacitance gage was used to detect the free surface motion of the sample rear surface. The output of the capacitance gage was differentiated and displayed on an oscilloscope so that the sample free surface velocity was recorded as a function of time. Experiments on aluminum samples to develop the shock tube capacitance gage and differentiation circuit were funded by KSC. Tests conducted on 3DQP samples were funded by DNA.

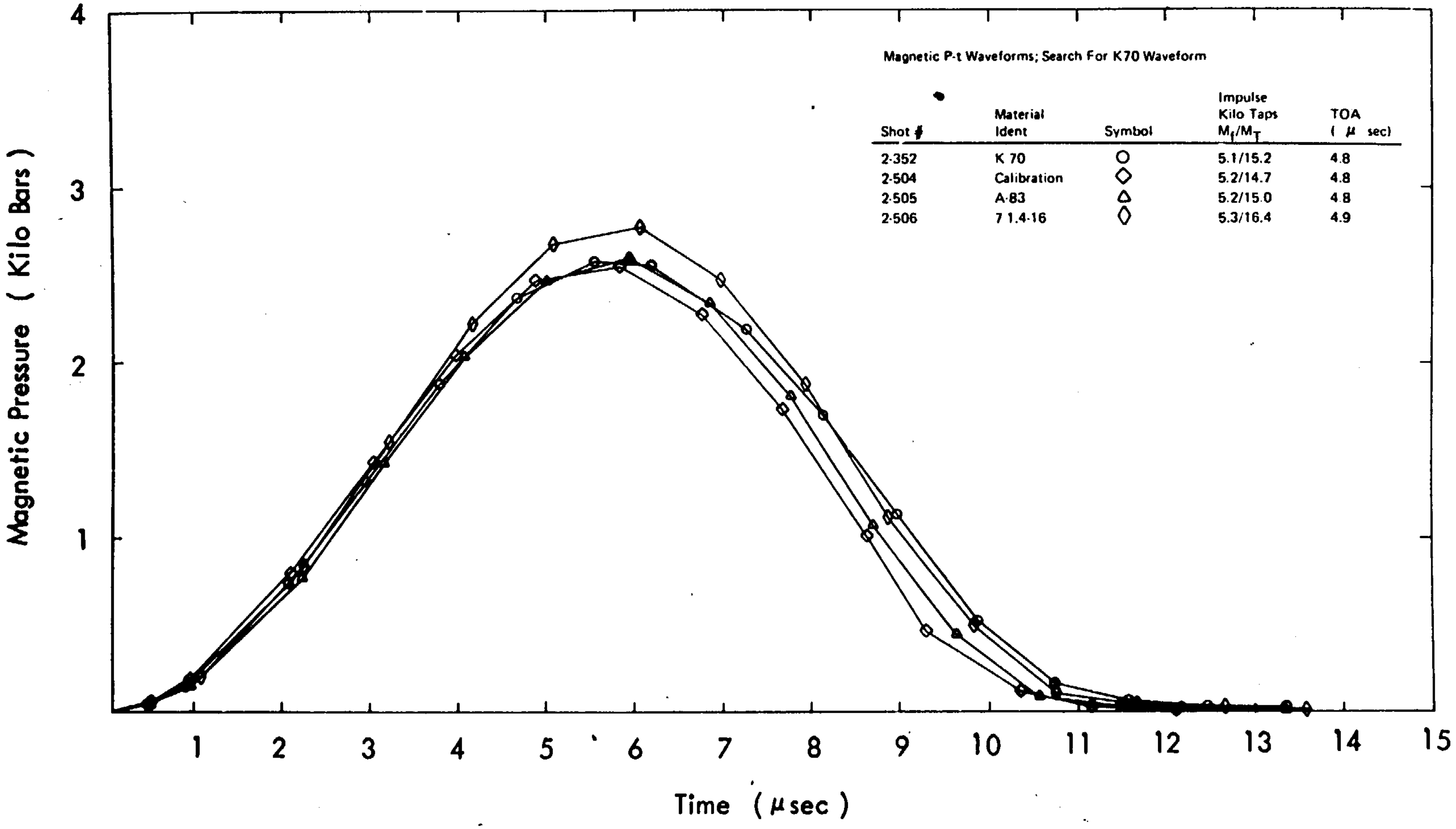

FIGURE 11 SEARCH FOR K70 MAGNETIC PRESSURE WAVEFORMS

Previous experimental[3] and analytical[4] work had suggested that the shock tube was capable of establishing the pedigree of 3DQP samples by non-destructive methods. It is also known that the pedigree (i.e., A or C) determines the dynamic failure mode of the 3DQP samples. Since the 3DQP samples being tested in this program possessed different virgin properties, the anticipated failure mode of the different batches of material was of concern. In particular, the 7.1.3, 7.1.4 and 4.1.5 (golden) materials showed slightly different virgin properties and apprehension grew that the tailored waveform, which produced the correct damage mode in 7.1.3 and 7.1.4 materials would not produce identical results in 4.1.5 material. For this reason, available materials were tested in the shock tube facility to determine their pedigree; and, thus, their failure mode.

Earlier experimenters[3] had shown that the risetime of the rear surface velocity waveform was the parameter capable of separating A and C process 3DQP. The trend established was that C process material had a shorter risetime than A process. Risetime data was measured at KSC on eight available 3DQP samples. A record typical of those measured is shown in Figure 12. This record details the region where the risetime measurement was made. Also shown in Figure 13 is the time increment which KSC assumes is a monitor of two transits of the thickness of the sample. From these time increments, a shock velocity was calculated.

The rear surface waveforms for the eight samples were normalized in both time and amplitude, and overplotted as shown in Figure 13. The risetimes were measured off of the normalized records. The risetime of the known A process

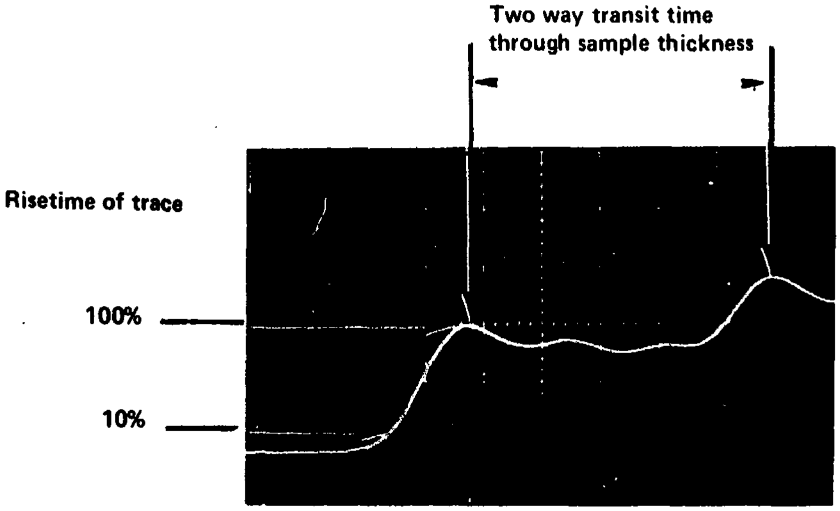

FIGURE 12 TYPICAL 3DQP REAR SURFACE PARTICLE VELOCITY OSCILLOGRAPH SHOWING LOCATIONS FOR OBTAINING RISETIME AND SHOCK VELOCITY DATA

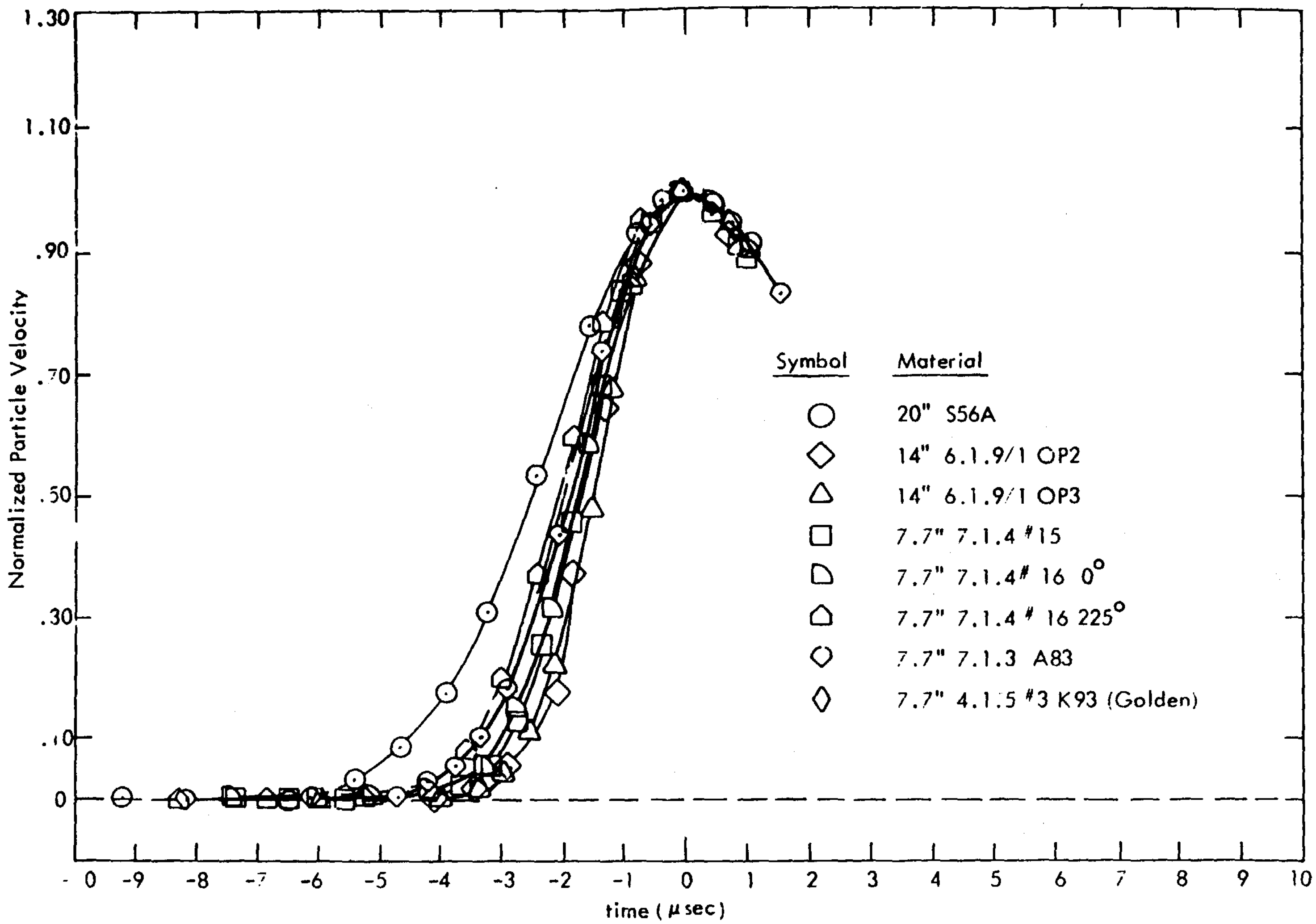

KSC SHOCK TUBE DATA

FIGURE 13 NORMALIZED RISETIME DATA FROM VARIOUS PEDIGREES OF 3DQP MATERIALS

TABLE 4 KSC SHOCK TUBE DATA

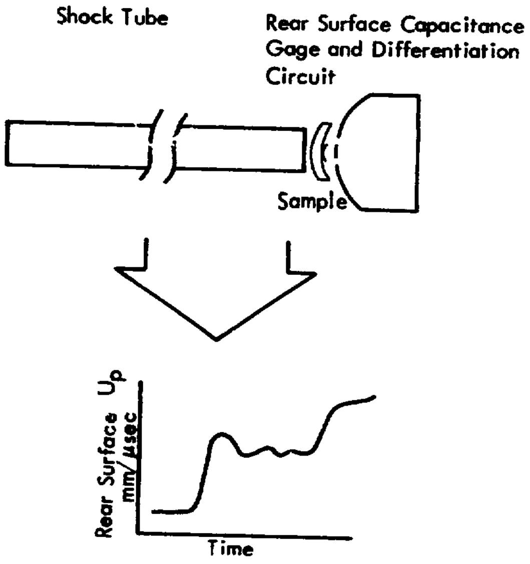

| MATERIAL IDENT. | MATERIAL PEDIGREE | RISETIME $t_{pk} - 0.10$ | VELOCITY mm/msec |
|---|---|---|---|
| 14" 6.1.9#1, OP3 | C | 2.6 | 2.80 |
| 14" 6.1.9#1, OP2 | C | 2.6 | 2.75 |
| 7.7" 7.1.4#15 | C | 2.9 | 2.75 |
| 7.7" 7.1.4#16, 0° | C | 3.0 | 2.75 |
| 7.7" 7.1.4#16, 225° | C | 3.5 | 2.50 |
| 7.7" 7.1.3, A83 | C | 3.3 | 2.33 |
| 7.7" 4.1.5#3, K93 | C | 3.4 | 2.50 |
| 20" S56A | A | 4.5 | 2.30 |

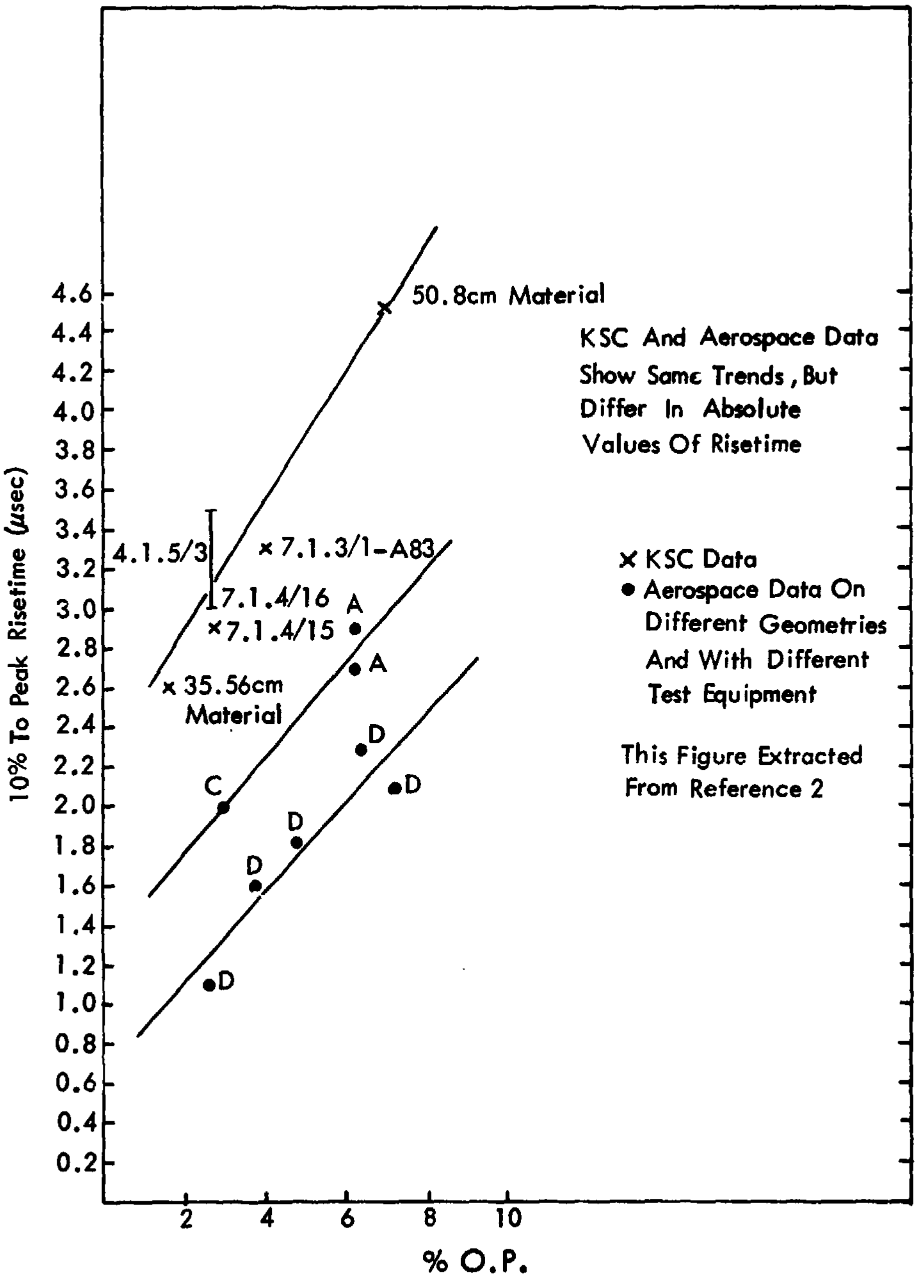

FIGURE 14 KSC AND AEROSPACE SHOCK TUBE RISETIME DATA VS SoRI OPEN POROSITY DATA

material, sample S56A from the 50.8 cm diameter 3DQP, was 4.5 μsec and, as shown in Figure 13, is by far the longest risetime recorded. Samples from 6.1.9 material, thought by SoRI to be the purest C process, had the shortest risetime. This is exactly as SoRI would have predicted from their virgin property data, that is, the 6.1.9 material had the shortest risetime while the 50.8 cm diameter material had the longest risetime.

The risetime and shock velocity data are presented in Table 4. Nominal C process material had risetimes which ranged from 2.6 - 3.5 μsec, while the A process sample had a risetime of 4.5 μsec. All risetimes disagree in absolute value with previously published data[3]; however, the trends established by past experimenters are duplicated by the KSC work. To give the reader an idea of the difference between the KSC and Aerospace work, data presented by SoRI[2] are shown in Figure 14 (the risetime data from both KSC and Aerospace is plotted against sample open porosity as measured by SoRI). These data suggest a risetime difference of 1.0 μsec for C process materials and a difference of 1.5 μsec for A process materials. Explanations for the different risetimes may be the difference in sample geometry (flats for the Aerospace work, arcs for the KSC work), different $A_R/A_T$ ratios, and different instrumentation circuits used by the two facilities.

## 5.0 ANALYTICAL TECHNIQUES FOR STRAIN CORRELATION

### 5.1 Ring Response Code Qualification

A sample ring configuration was subjected to dynamic response calculations under two magnitudes of half-cosine-distributed impulse in order to test the interchangeability of and expose any fundamental differences between U.S. ring response computer codes that were proposed for application to prediction and correlation work relative to the 3DQC effort. A parallel effort in the U.K. was undertaken in order to compare results of a U.K. code to those of the U.S. codes. KSC's work on this task is reported here.

The material of the subject ring was nominally aluminum. The dimensions, material properties, and impulse magnitudes are tabulated below.

| | |
|---|---|
| Diameter | 25.4 cm |
| Thickness | 0.51 cm |
| Impulses | 1.0 ktap, 5.0 ktap |
| Density | 2.70 $g/cm^3$ |
| Modulus | 72.4 GPa |
| Yield Stress | 275.8 MPa (perfectly plastic) |
| Damping | 0.05% (membrane) |

In the U.S. KSC ran these cases on its TWORNG code. Prototype Development Associates (PDA) used Lockheed's GIRLS I code. The TWORNG analyses were run for a period long enough to cover one complete flexural cycle of response. The GIRLS I results cover about one fourth of a flexural cycle.

Preceding Page Blank

KSC also ran the 5 ktap case without any damping to investigate the importance of the 0.05 percent membrane damping.

The strain plots of KSC's 9-millisecond runs are presented in Figures 15 to 20. Included are strains for 0, 90, and 180 degrees on both surfaces. Plots of the first 1.8 milliseconds of response are given here as Figures 21 to 26. PDA's GIRLS I results are overplotted thereon for comparison. Records are included for only the inner surface locations. The outer surface records are similar.

Comparison indicates that for the 1 ktap impulse, for which the response is completely elastic, the results are almost identical. The slight frequency shift is not real but due to parallax in a copying machine. For the 5 ktap case, which includes considerable plasticity, the agreement is fairly good for the first millisecond but degenerates thereafter. The general reason that the results are so close for the elastic case, but less so for the plastic case, is probably that the elastic analysis allows fewer theoretical options for the code writer, which lead to differences. There is apparently a difference between the plasticity models in these two codes which shows up even in this basic test case.

While it is definitely desirable to sort out and understand the differences between these codes and synthesize a code that best correlates data, it is probably of little importance to the 3DQC Program because 3DQP remains essentially elastic to failure.

The 0.05 percent damping has no noticeable effect on the results.

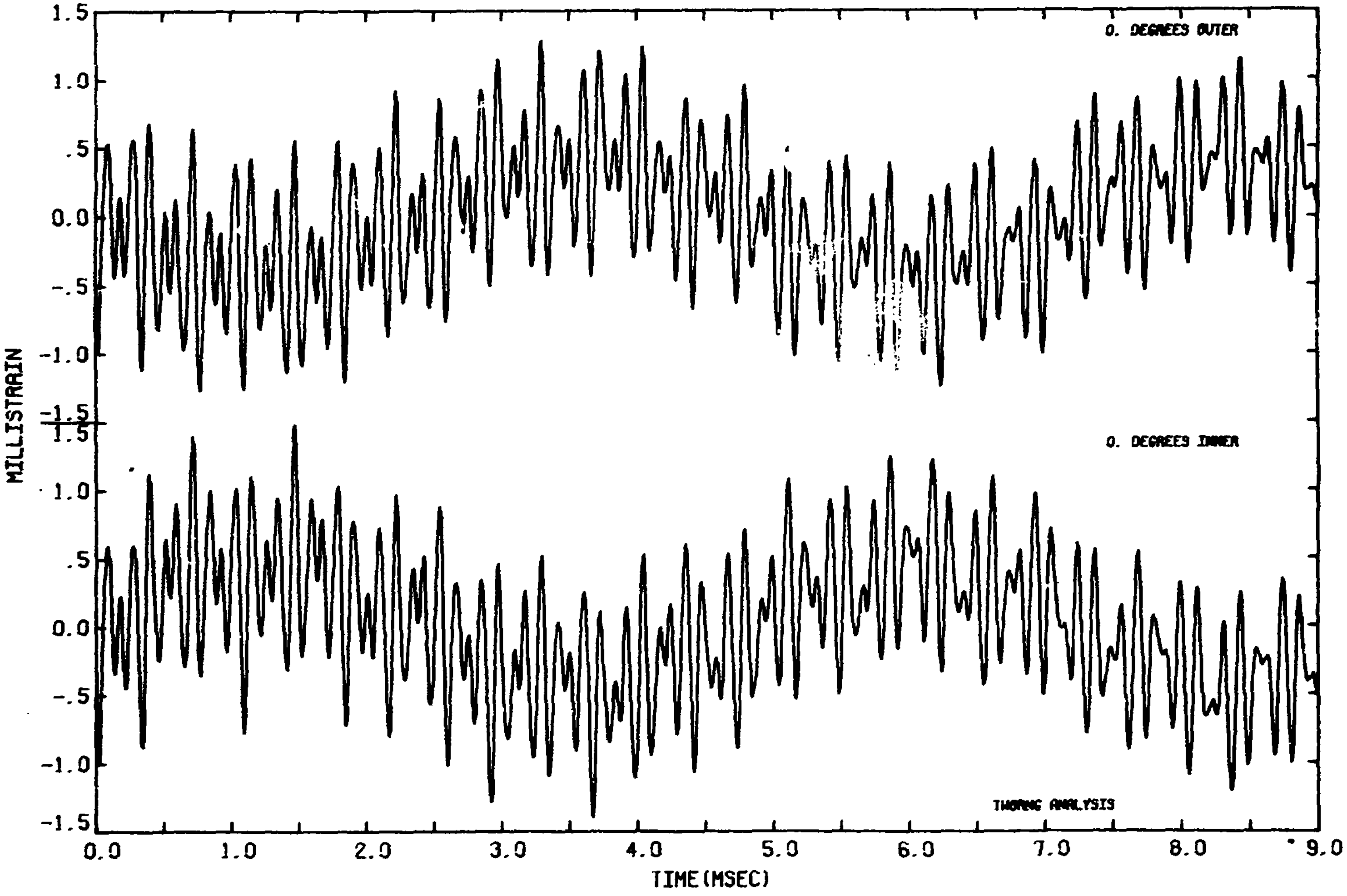

FIGURE 15

TWORNG ANALYSIS OF ALUMINUM RING - 1 KTAP.
O.D. 25.4 CM, THICKNESS 0.508 CM

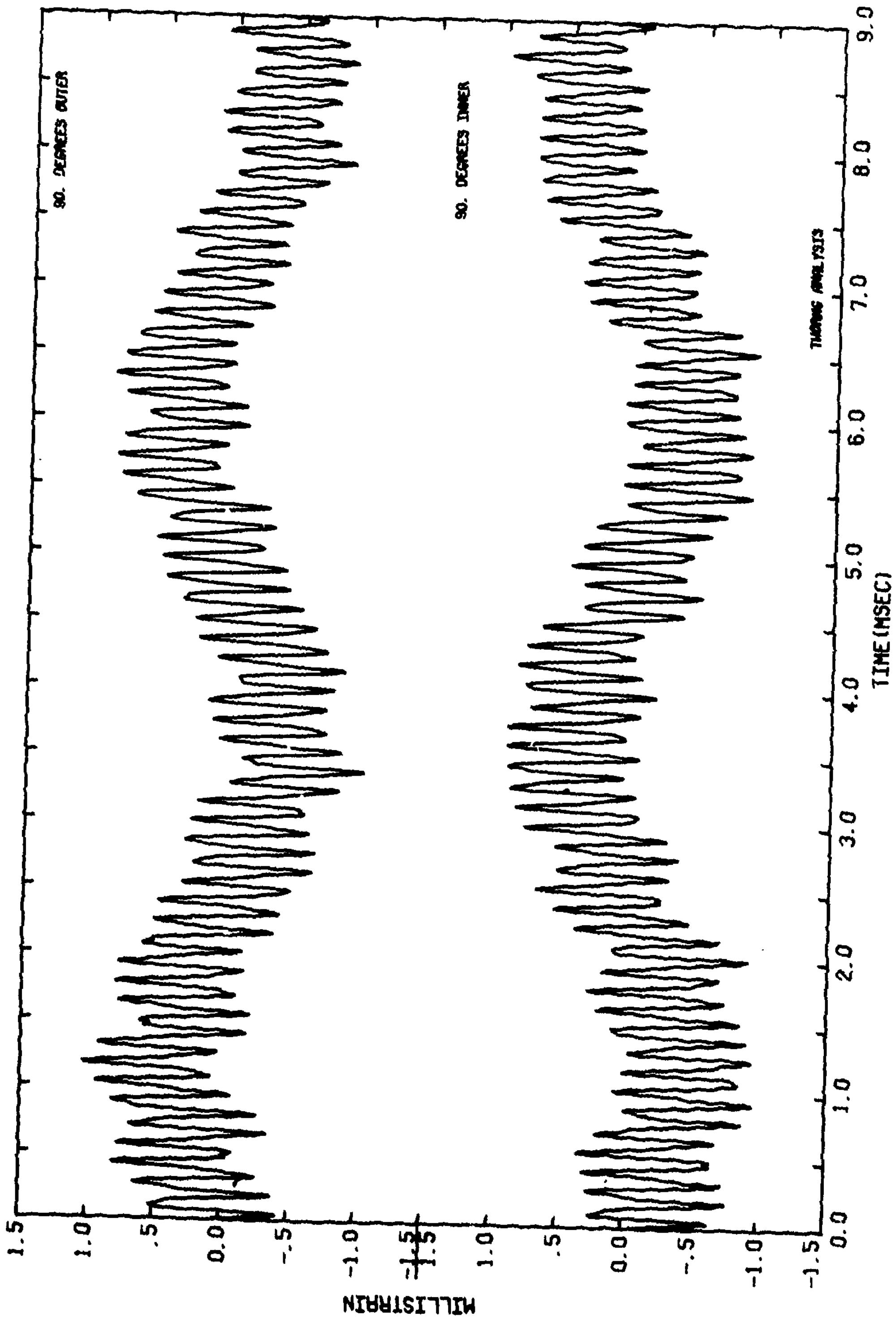

FIGURE 16

TWORNG ANALYSIS OF ALUMINUM RING - 1 KTAP.
O.D. 25.4 CM, THICKNESS 0.508 CM

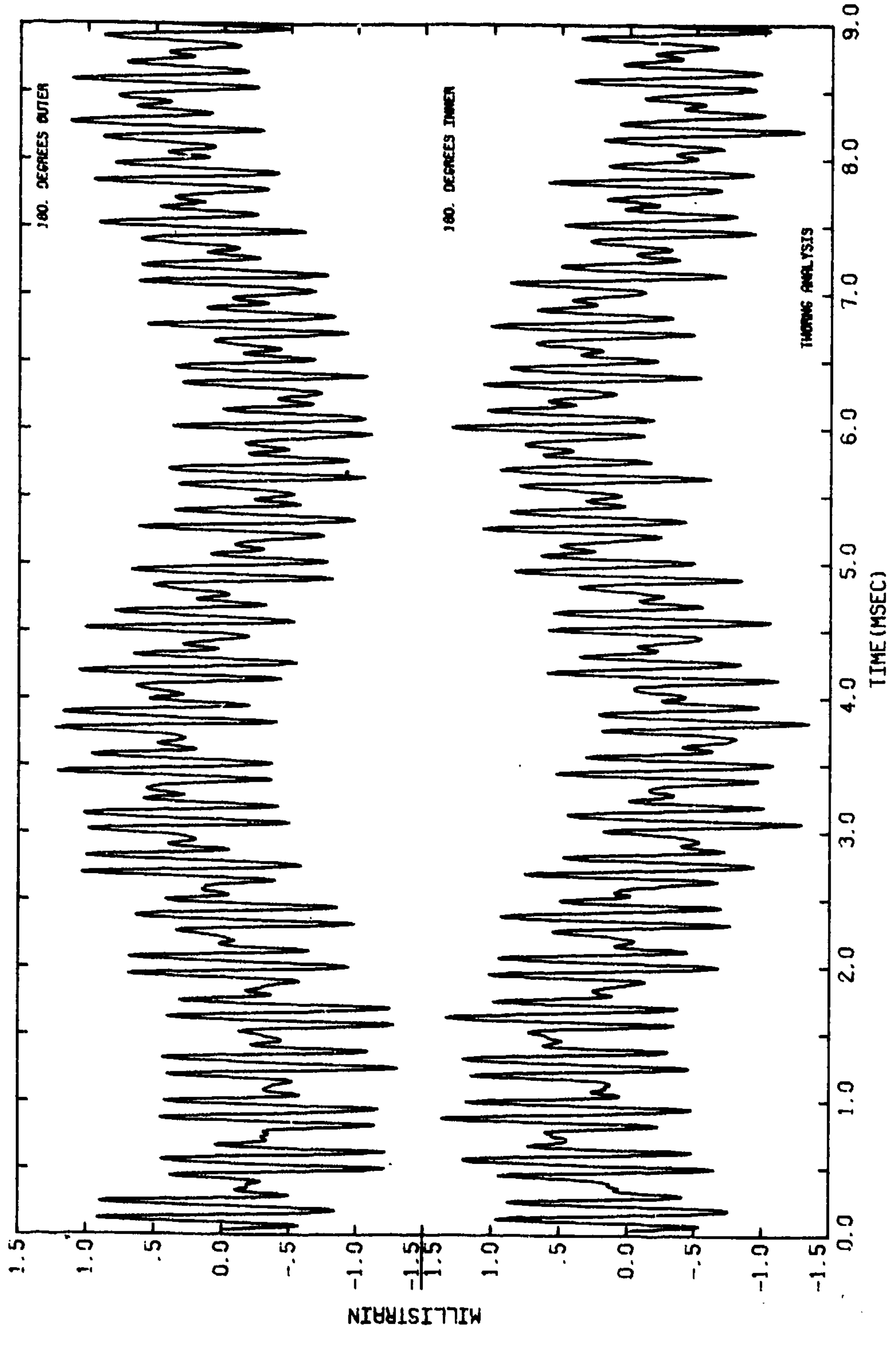

FIGURE 17

TWORNG ANALYSIS OF ALUMINUM RING - 1 KTAP.
O.D. 25.4 CM, THICKNESS 0.508 CM

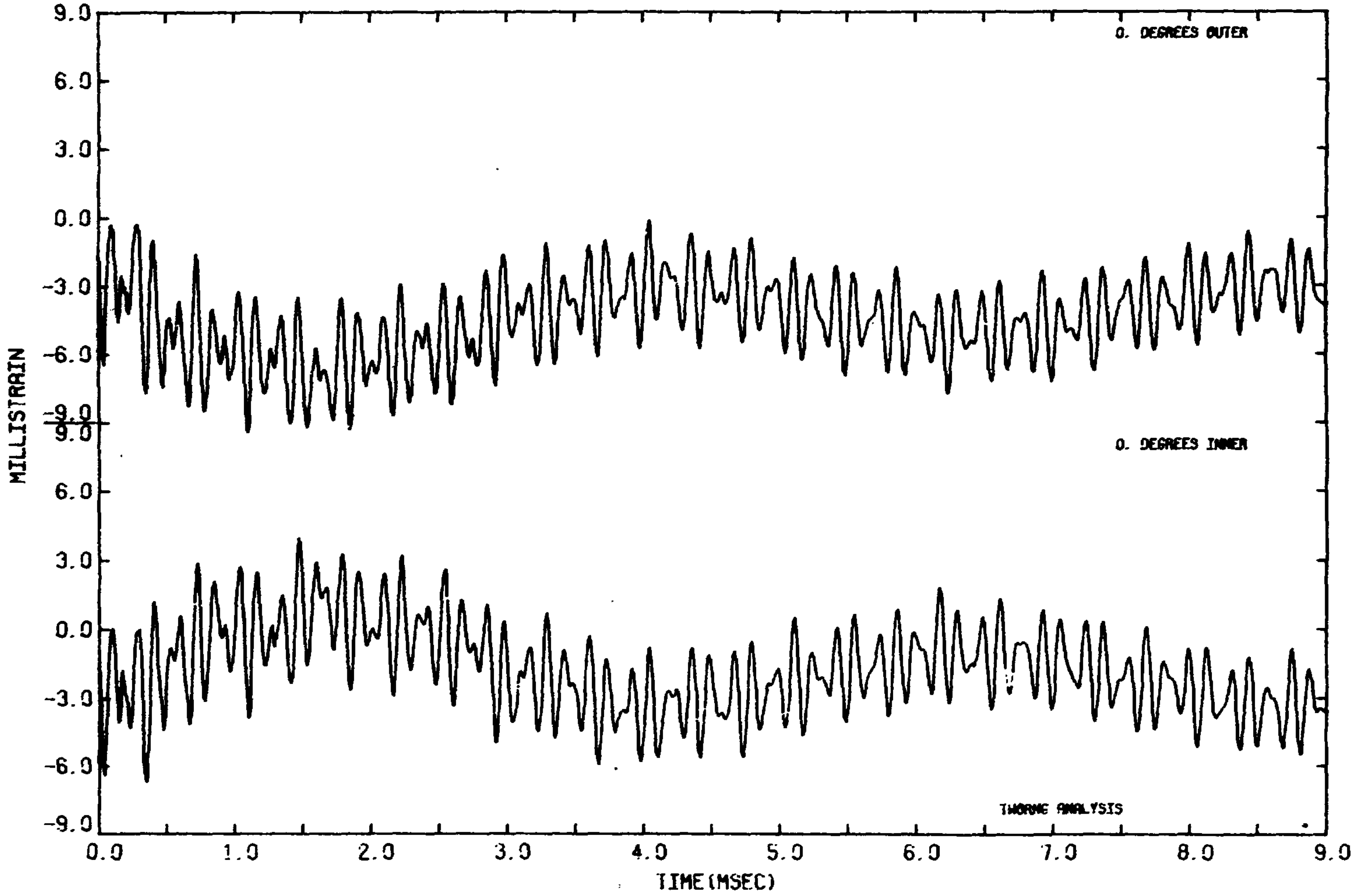

FIGURE 18

TWORNG ANALYSIS OF ALUMINUM RING - 5 KTAP.
O.D. 25.4 CM, THICKNESS 0.508 CM

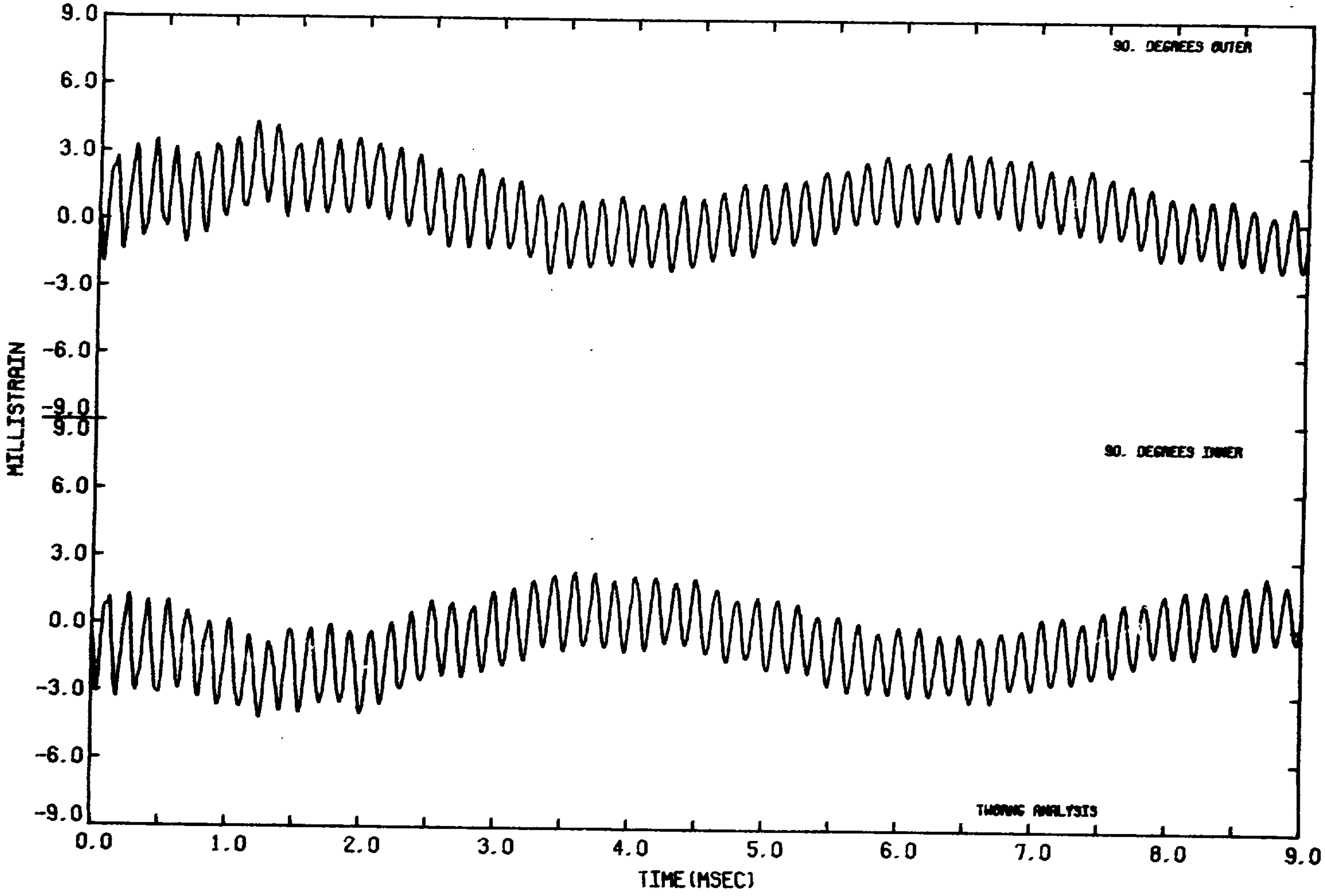

FIGURE 19

TWORNG ANALYSIS OF ALUMINUM RING – 5 KTAP.
O.D. 25.4 CM, THICKNESS 0.508 CM

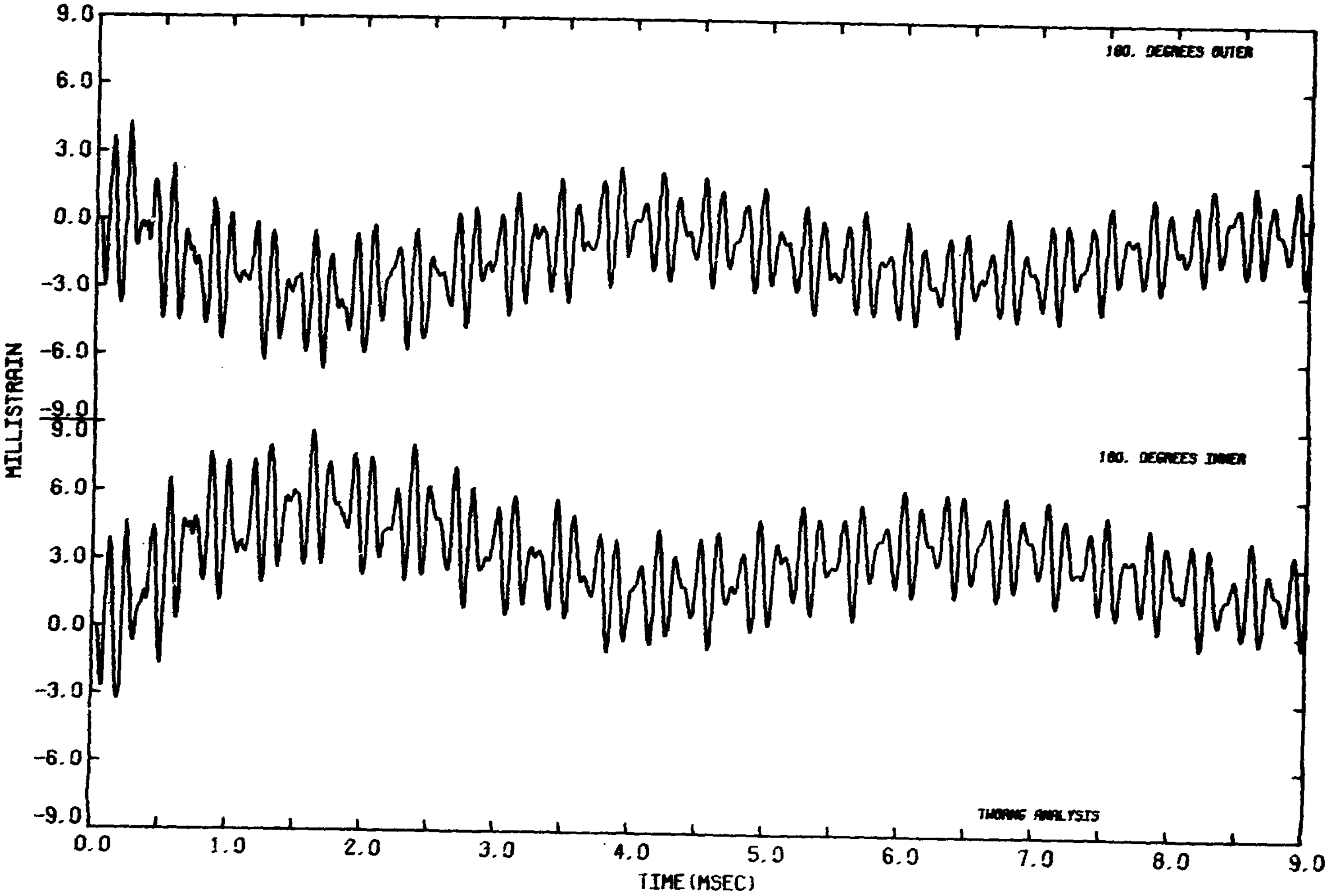

FIGURE 20

TWORNG ANALYSIS OF ALUMINUM RING - 5 KTAP.
O.D. 25.4 CM, THICKNESS 0.508 CM

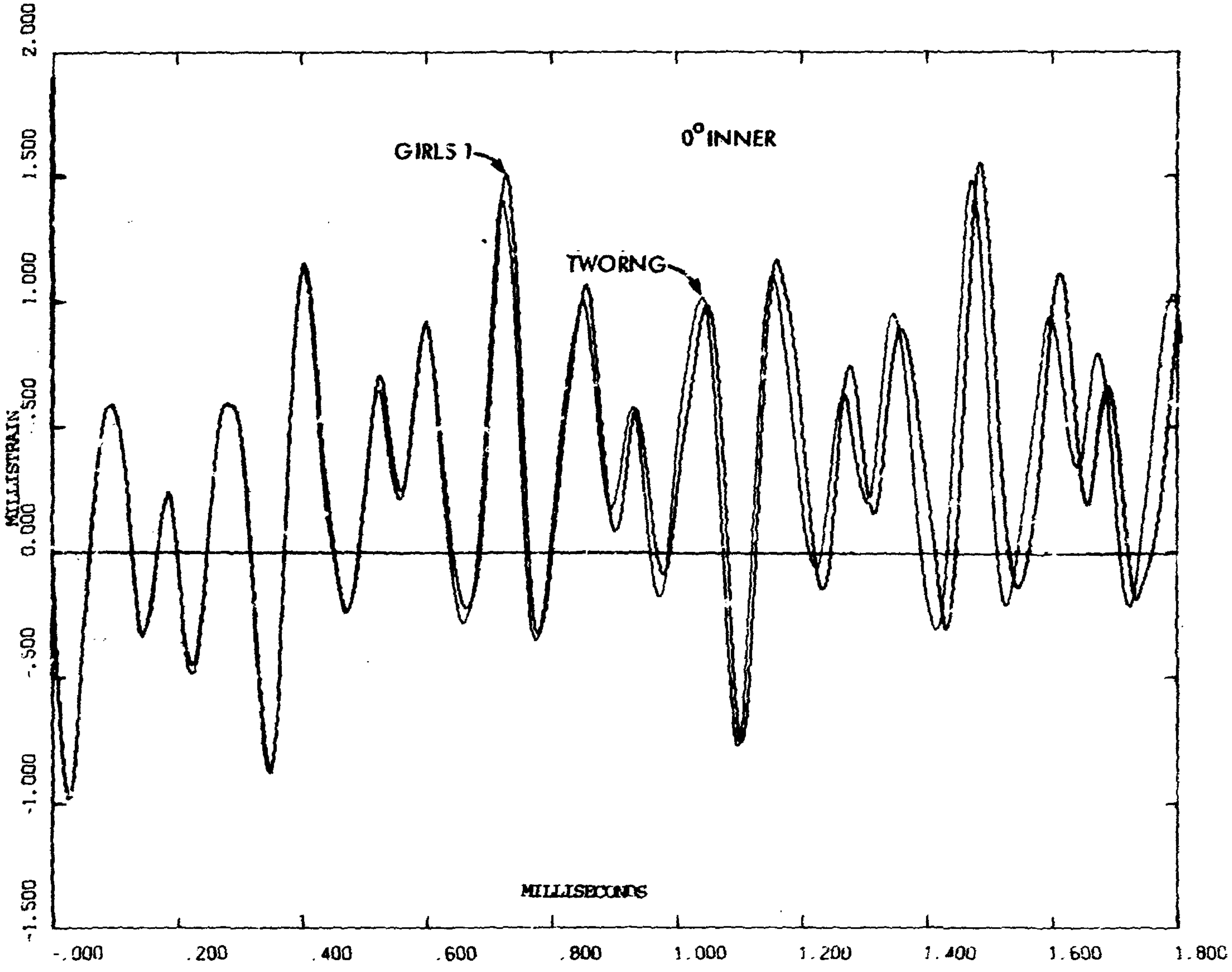

FIGURE 21

TWORNG AND GIRLS I ANALYSIS OF ALUMINUM RING - 1 KTAP.
O.D. 25.4 CM, THICKNESS 0.508 CM

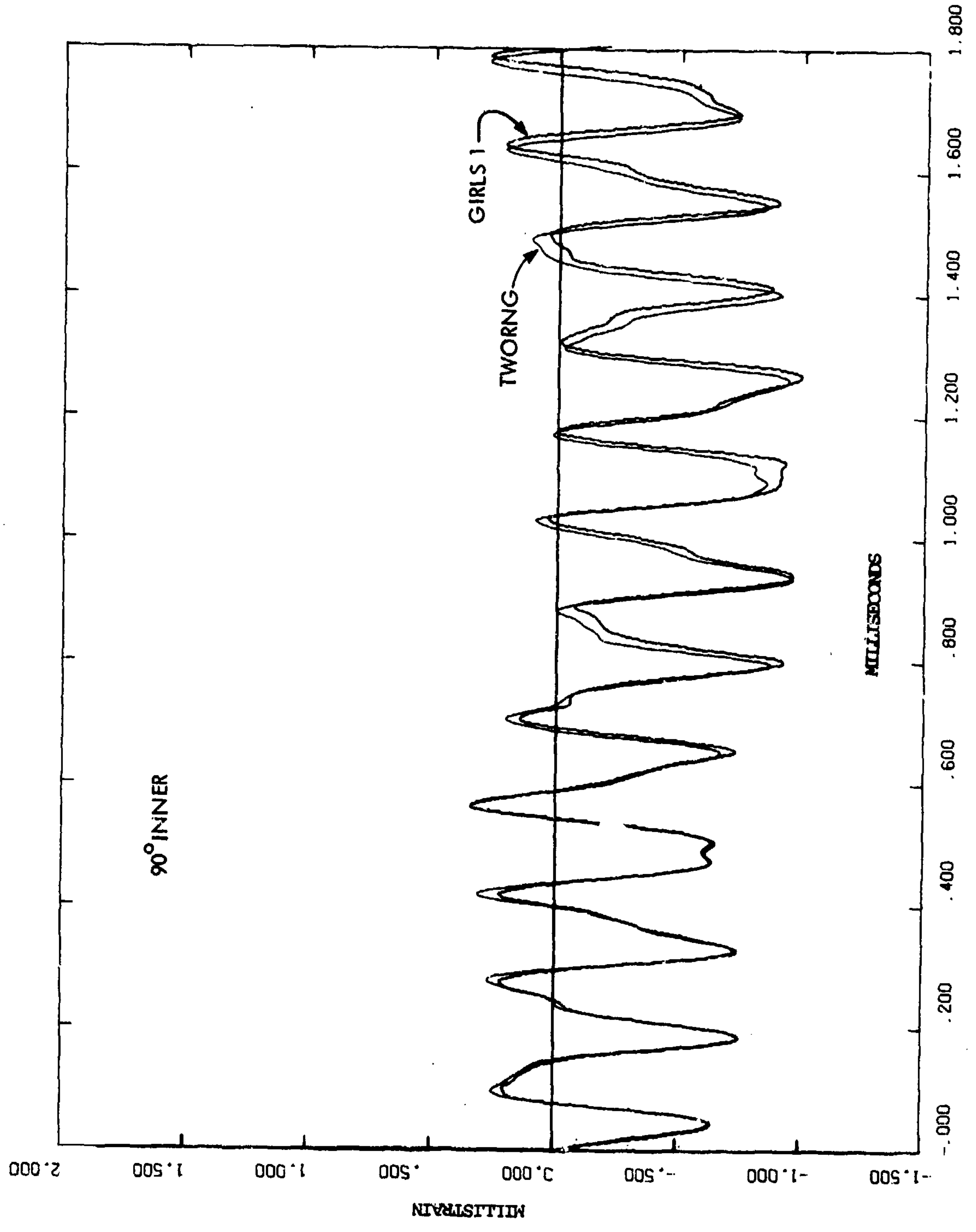

FIGURE 22

TWORNG AND GIRLS I ANALYSIS OF ALUMINUM RING – 1 KTAP.
O.D. 25.4 CM, THICKNESS 0.508 CM

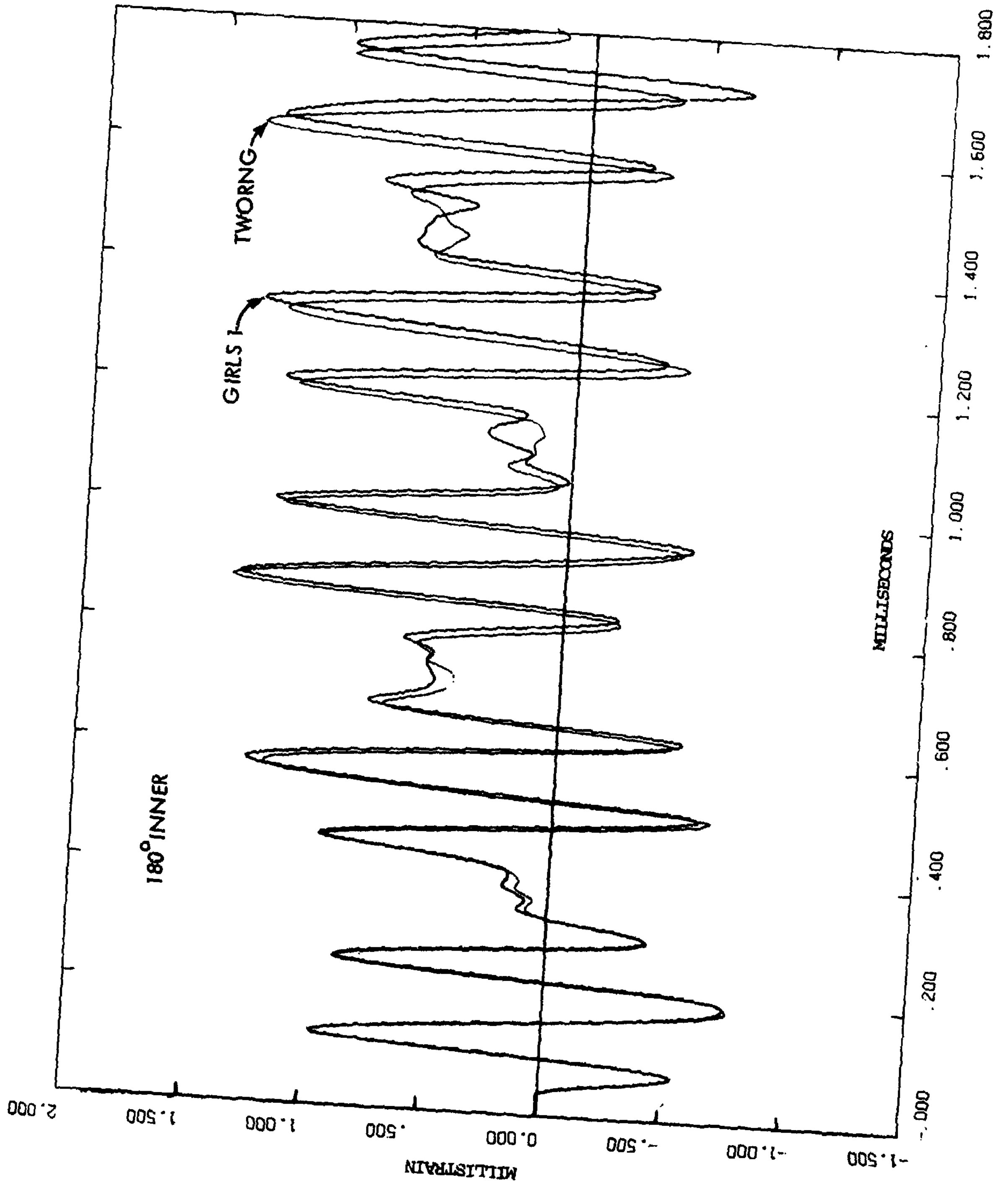

FIGURE 23

TWORNG AND GIRLS I ANALYSIS OF ALUMINUM RING - 1 KTAP.
O.D. 25.4 CM, THICKNESS 0.508 CM

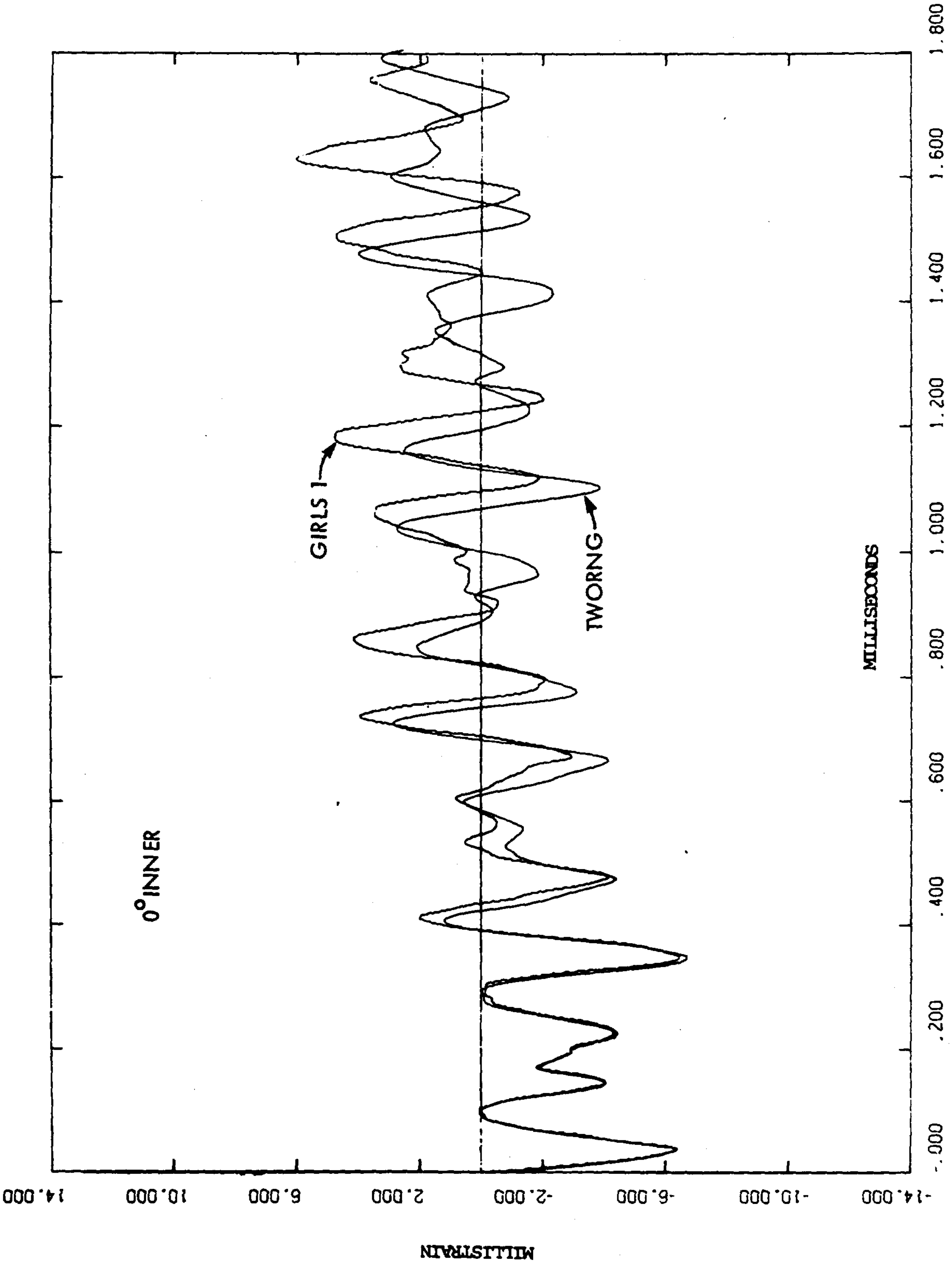

FIGURE 24
TWORNG AND GIRLS I ANALYSIS OF ALUMINUM RING – 5 KTAP.
O.D. 25.4 CM, THICKNESS 0.508 CM

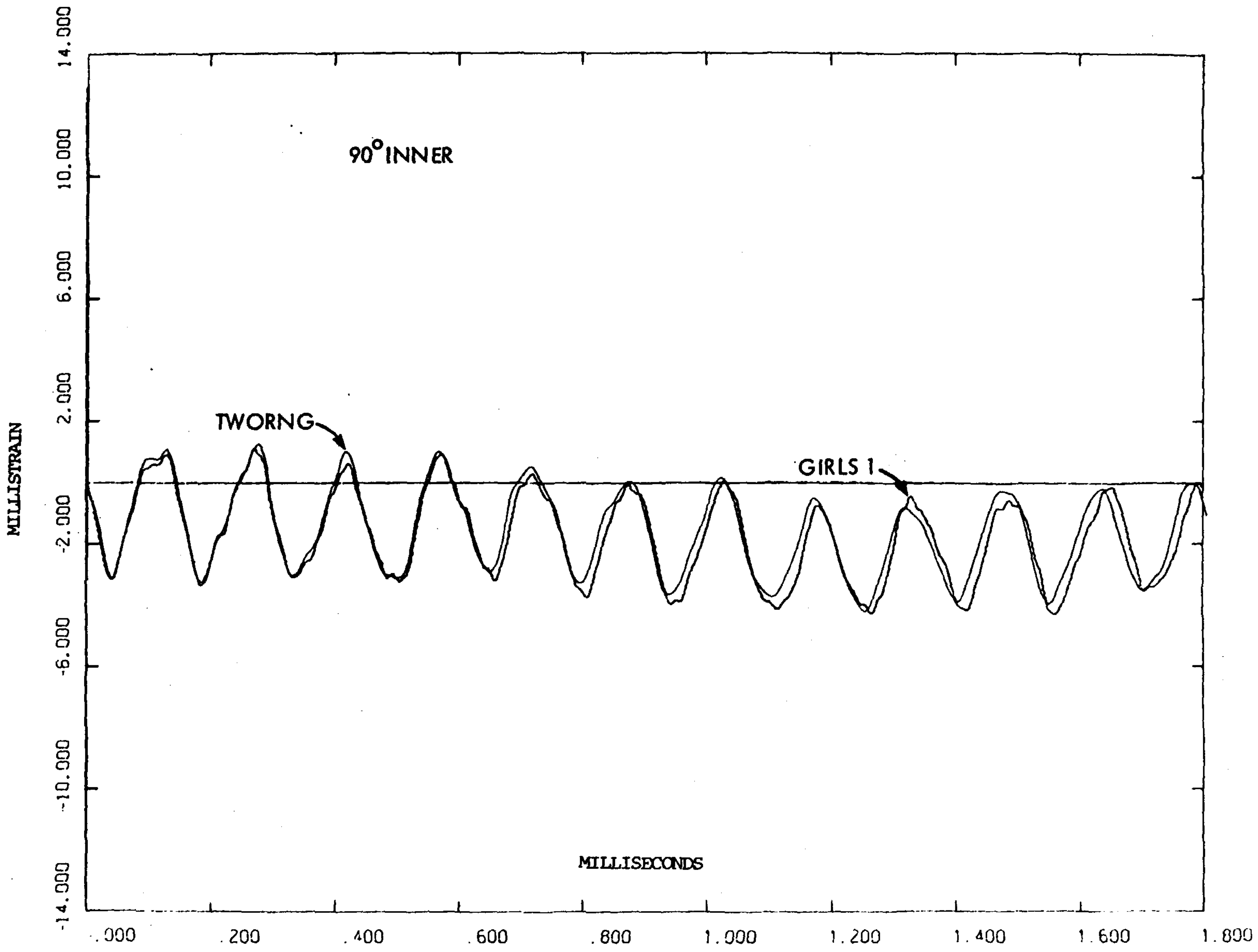

FIGURE 25

TWORNG AND GIRLS I ANALYSIS OF ALUMINUM RING - 5 KTAP.
O.D. 25.4 CM, THICKNESS 0.508 CM

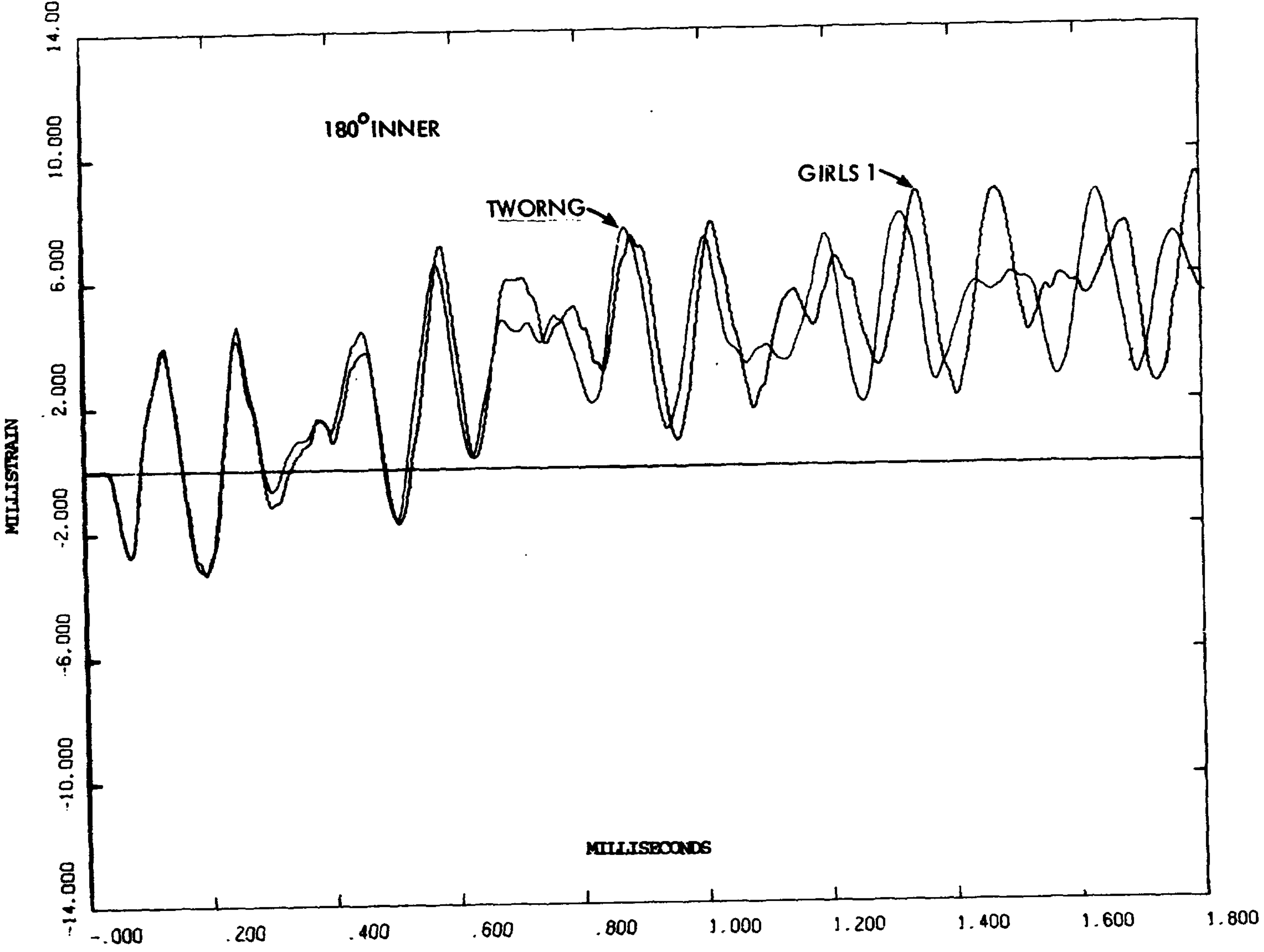

FIGURE 26

TWORNG AND GIRLS I ANALYSIS OF ALUMINUM RING - 5 KTAP.
O.D. 25.4 CM, THICKNESS 0.508 CM

## 5.2 Strain Correlation Methodology Developments

Strain calculations performed on this program and reported here incorporated three additions to the procedural technique, which are described as follows:

1. A fast and very economical printer plot generating computer code PGR was written to make initial comparisons of groups of strain records.

   The PGR code is used as a post-processor to strain computations. Economical printer overplots are made of the analytical and experimental results and the correlation is evaluated. Impulse, material parameters, and phase can be adjusted for subsequent analytical iterations. Only when the analyst is satisfied with the agreement of the records are the more costly graphic methods used for report-quality plots.

   The PGR code has also been used to make initial comparisons of UGT data with AGT data or of two AGT records.

2. An existing initial-value integration computer code was modified to do response of degraded rings to half-cosine-distributed impulse using linear elastic transverse shear theory. This theory includes a full treatment of rotary inertia and, therefore,

a sixth-order system of equations is integrated rather than the usual fourth-order system. The resulting code has been referred to as RNGSHR (Ring Shear). The primary reason for using transverse shear theory was to investigate the importance of the transverse shear modulus $G_{r\theta}$ relative to 3DQP ring response to half-cosine-distributed impulse.

Since the transverse shear modulus of 3DQP is a much smaller fraction of the circumferential modulus than it is in metals, one might expect significant differences in the theoretical results, if transverse shear flexibility is introduced. It has been found that resonant frequencies of 3DQP rings, for wave numbers greater than two, can be accurately calculated only if transverse shear flexibility is introduced in the theoretical formulation. This indicates that, for some loading conditions, transverse shear flexibility may be important.

By-products of the introduction of transverse shear flexibility are better formulations of rotary inertia and strain-rate damping. The optimum amount of strain-rate damping for correlation of strain in 3DQP appears to be about one percent of critical. The transverse shear theory and sixth-order system of equations handles that much damping without integration stability problems. A

disadvantage of the sixth-order theory is that a more precise integration technique than forward differencing and its enhancements is required because the frequency of the first shear mode is much higher than that of the first extensional mode.

A sample problem, representative of a 3DQP ring undergoing a 13.5 ktap half-cosine-distributed impulse, was run with and without transverse shear theory using TWORNG and RNGSHR. In order to make a separate analysis of the influence of shear flexibility and rotary inertia, negligible damping was prescribed. The parameters used in this exercise were the following:

| | |
|---|---|
| Diameter | 19.56 cm |
| Density | 1.67 g/cm$^3$ |
| Impulse | 13.5 KT |
| Damping | 0.0 |
| Circumferential Modulus | |
| $E_o$ | 25.9 GPa |
| $\Delta E/E_o$ | 0.28 |
| Degradation angle ±60° | |
| Shear Modulus | |
| $G_o$ | 2.59 GPa |
| $\Delta G/G_o$ | 0.28 |
| Degradation angle ±60° | |
| Thickness | |
| $h_o$ | 1.40 cm |
| $\Delta h/h_o$ | 0.065 |
| Degradation angle ±60° | |

The result plotted in Figures 27 and 28 indicates that the impact of the shear flexibility and rotary inertia on the half-cosine impulse response is small. The improved damping formulation does, however, improve correlations for late times (greater than one half millisecond).

3. A numerical temporal correlation function was defined for making direct quantitative comparisons of the similarity of two strain records. When combined with PGR, the result is a fast process for comparing the agreement of two records for various phase shifts.

The correlation coefficient used to quantitatively compare strain records is defined by the formula

$$cc = \frac{\displaystyle\int_{t_1}^{t_2} f\, g\, dt}{\left[\displaystyle\int_{t_1}^{t_2} f^2\, dt\right]^{1/2} \left[\displaystyle\int_{t_1}^{t_2} g^2\, dt\right]^{1/2}}$$

where f and g represent the two time functions being compared and $t_1$ and $t_2$ define the time interval of interest. It is observed that

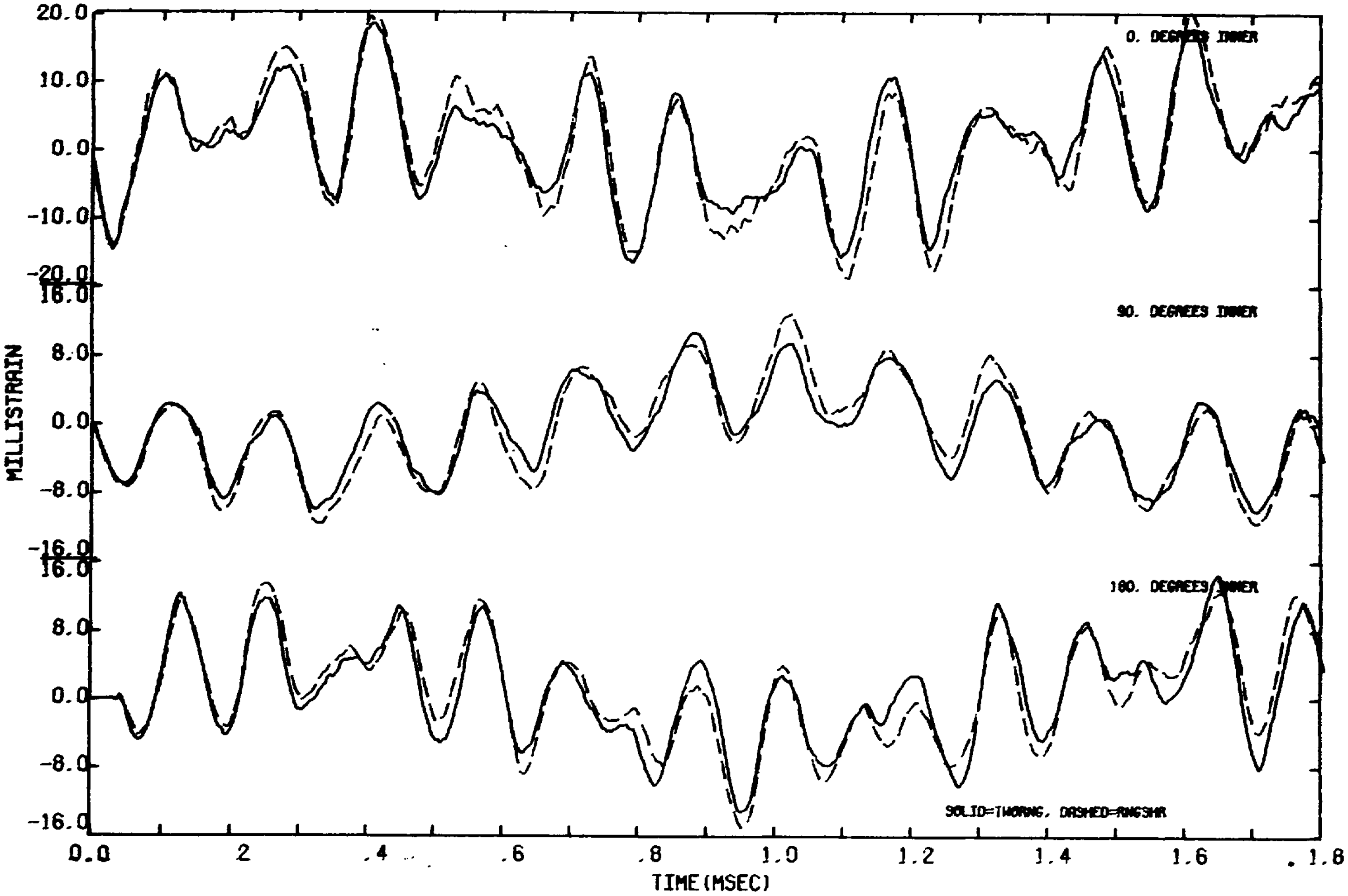

FIGURE 27

TWORNG - RNGSHR COMPARISON.
19.56 CM/1.40 CM DEGRADED 3 DQP RING, 13.5 KTAP

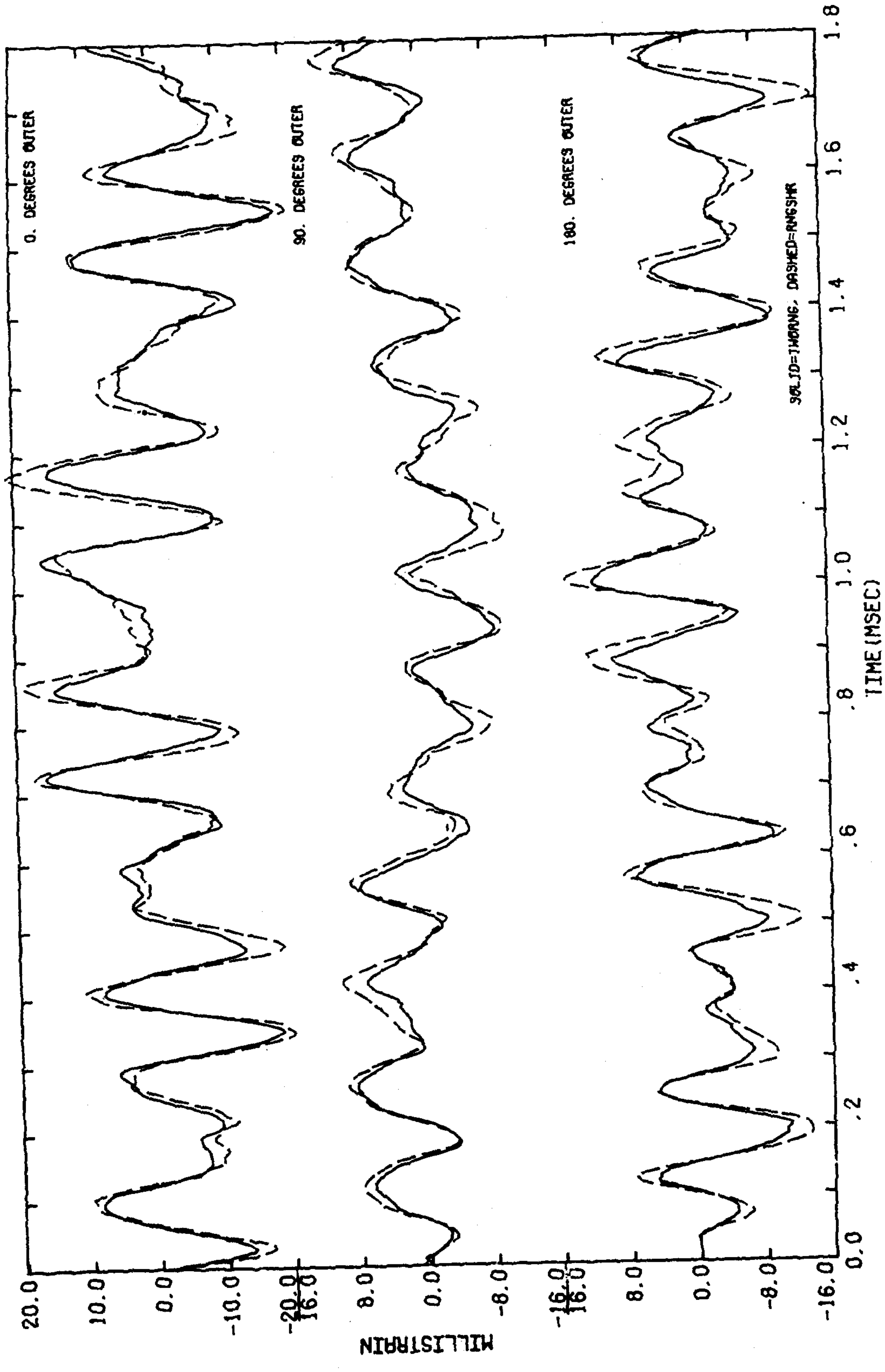

FIGURE 28

TWORNG - RNGSHR COMPARISON.
19.56 CM/1.40 CM DEGRADED 3 DQP RING, 13.5 KTAP

this function will approach plus one for closely correlated functions and minus one for functions which correlate closely except for sign. The result for uncorrelated functions will approach zero. This coefficient appears to satisfy the condition that, for functions for which the correlation is visibly good, it approaches plus one and, for functions visibly uncorrelated, it approaches zero.

## 6.0 STRAIN CORRELATIONS

### 6.1 UGT Strain Correlations

Analytical correlations were made for the strain measurements from three 3DQP rings from Husky Ace. The objective of this study relative to the 3DQC Program was to verify that the impulse experienced by the rings was understood as indicated by the agreement between calculated and measured strain. The assurance that these rings had a known history would qualify them for detailed damage assessment.

After studying the strain records from Husky Ace, three rings were selected for study. The selection was based on the following criteria:

1. Only bare 3DQP rings were considered.
2. The rings were to have been unsupported.
3. Only rings for which $A_r/A_t$ of the material was 0.65 were considered.
4. The rings were to have experienced impulse not greater than that imposed at Level 3 in the test.
5. The rings were to have experienced moderate damage but no gross cracking.

Those rings selected are listed below along with their dimensions and the impulse they experienced.

| RING | O.D. (cm) | THICKNESS (cm) | IMPULSE (ktap) |
|---|---|---|---|
| 277-1 | 19.56 | 1.40 | 10.0 |
| 380-1 | 35.56 | 1.40 | 13.5 |
| 381-1 | 19.56 | 1.40 | 13.5 |

The calculations were done using the transverse shear ring code RNGSHR. The strain measurements from ring 381-1 had previously been satisfactorily correlated using the TWORNG code.(1) The reasons for reanalyzing 381-1 were to see if the correlation would improve using shear theory and to obtain the data in a form accepted by the PGR code for calculation of the correlation coefficient.

The degradation model used in the computations included similar functional forms for circumferential modulus E, transverse shear modulus G, and thickness h. These degradation functions had the following mathematical forms:

$$E(\theta) = E_o - \Delta E \cos \frac{\pi\theta}{2\theta_E}; \qquad |\theta| < \theta_E$$

$$G(\theta) = G_o - \Delta G \cos \frac{\pi\theta}{2\theta_G}; \qquad |\theta| < \theta_G$$

$$h(\theta) = h_o - \Delta h \cos \frac{\pi\theta}{2\theta_h}; \qquad |\theta| < \theta_h$$

The value used for $E_o$ was taken from resonant frequency correlations on rings of similar material. $G_o$ was obtained from posttest resonance testing on 381-1. The ratios $\Delta E/E_o$ and $\Delta G/G_o$ were taken to be equal for a given ring. This ratio, for 381-1, was obtained from posttest resonance testing of that ring. The ratio for the other rings was obtained by scaling, using impulse/thickness as the scaling parameter.

The values of $\Delta h$ were obtained from posttest measurements made by the U.K.(5) $\theta_E$, $\theta_G$, and $\theta_h$ were based on observations made by Southern Research (SoRI).

The density assumed was 1.67 g/cm$^3$. One percent (1.0%) of critical damping was applied to both the extensional and shear strain rates. The properties used are summarized in Table 5.

Comparison plots of the analytical results and the experimental measurements are given in Figures 29, 30, and 31 for rings 277-1, 380-1, and 381-1, respectively. The quality of the correlation is apparently quite good. Correlation coefficients for selected time intervals are given in Table 6.

It is concluded from this effort that the history of the three subject rings is well enough understood to qualify them for more detailed study.

Table 5. Material Properties for UGT Strain Calculations

| RING | $E_o$ (GPa) | $\Delta E/E_o$ | $\theta_E$ | $G_o$ (GPa) | $\Delta G/G_o$ | $\theta_G$ | $h_o$ (cm) | $\Delta h/h_o$ | $\theta_h$ |
|---|---|---|---|---|---|---|---|---|---|
| 277-1 | 25.9 | 0.13 | 45° | 2.62 | 0.13 | 45° | 1.40 | 0.013 | 60° |
| 380-1 | 25.9 | 0.28 | 45° | 2.62 | 0.28 | 45° | 1.40 | 0.084 | 60° |
| 381-1 | 25.9 | 0.28 | 45° | 2.62 | 0.28 | 45° | 1.40 | 0.065 | 60° |

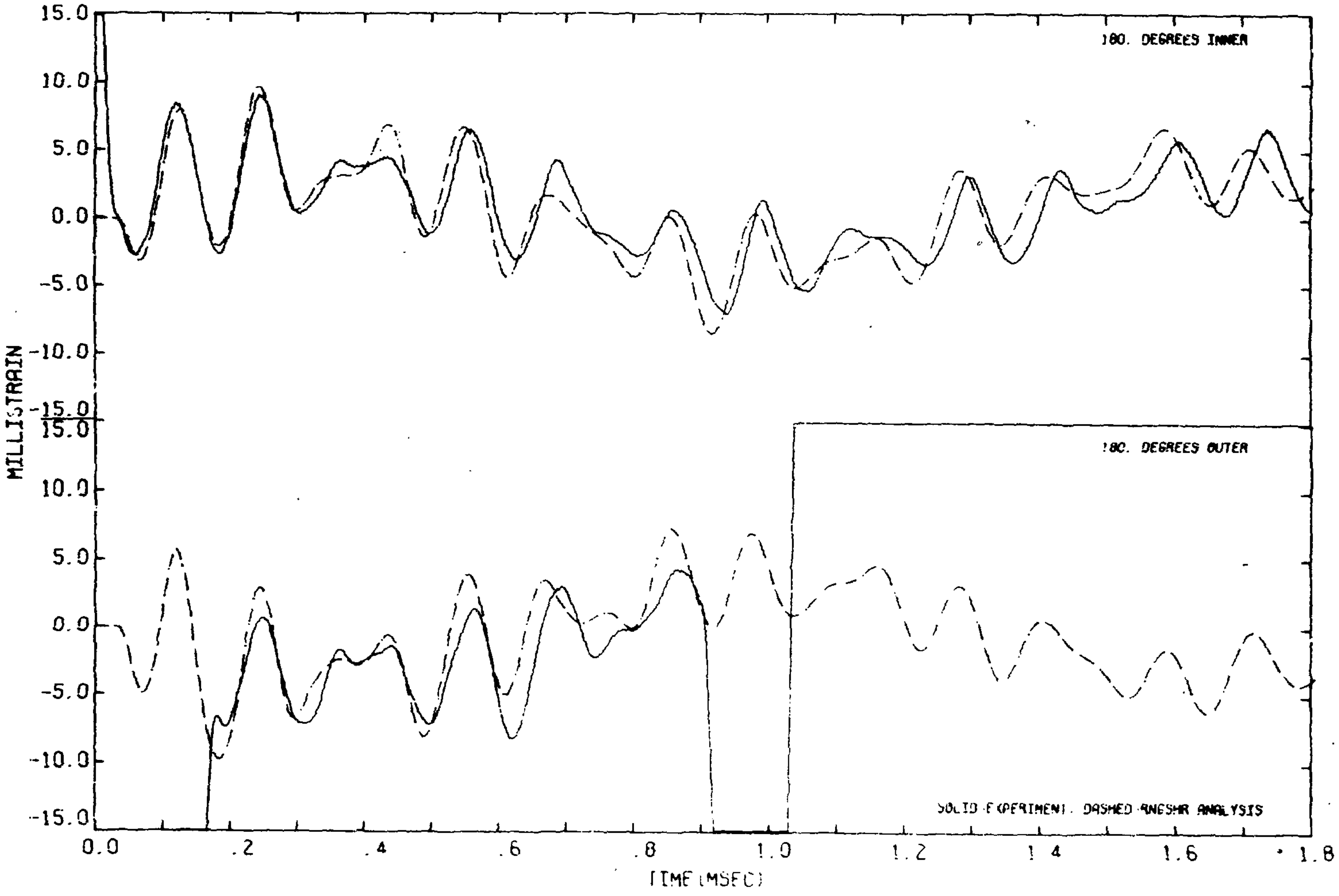

FIGURE 29

ANALYTICAL/EXPERIMENTAL STRAIN CORRELATION.
3DQP UGT RING M277-1

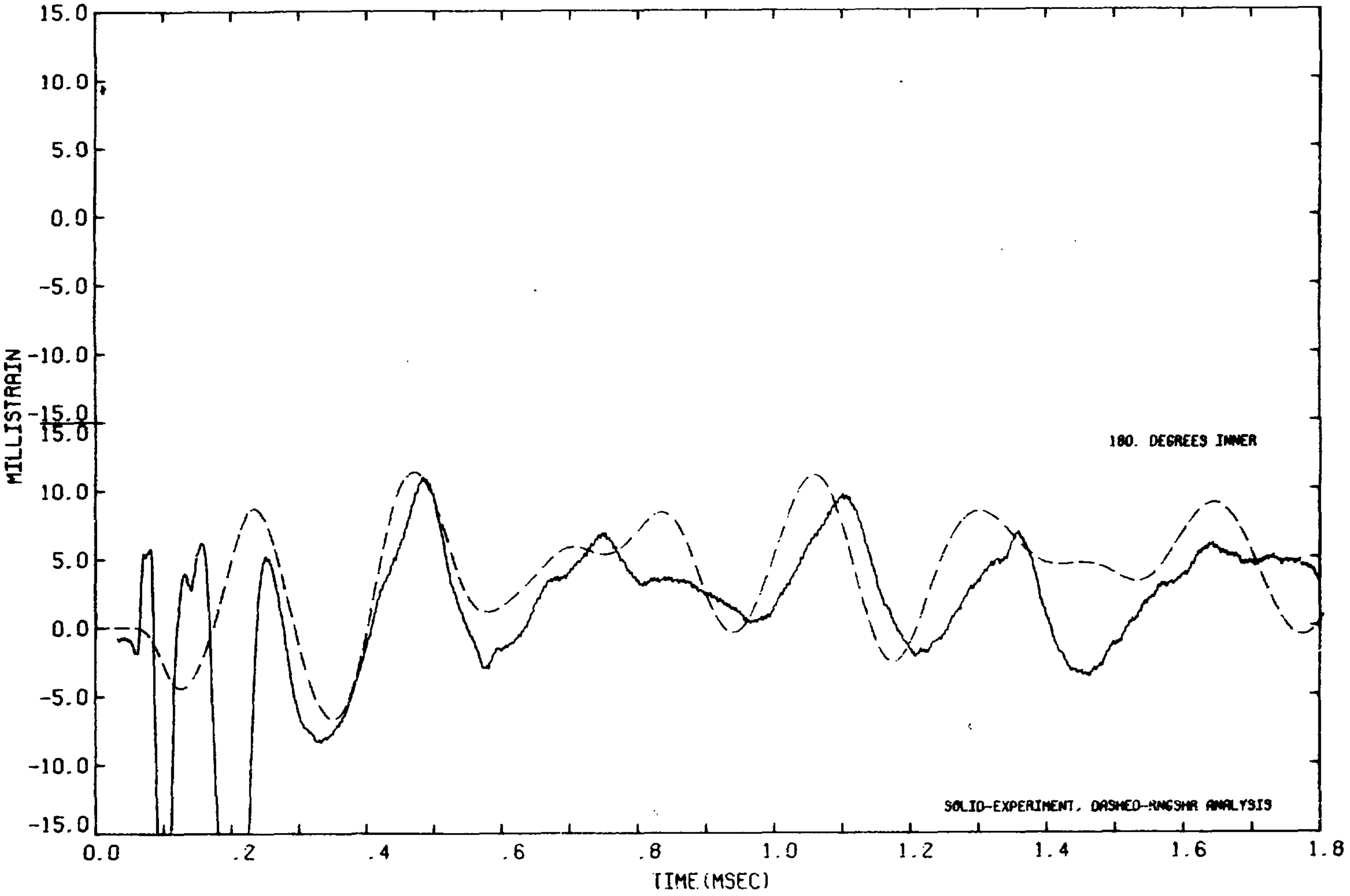

FIGURE 30

ANALYTICAL/EXPERIMENTAL STRAIN CORRELATION.
3DQP UGT RING M380-1

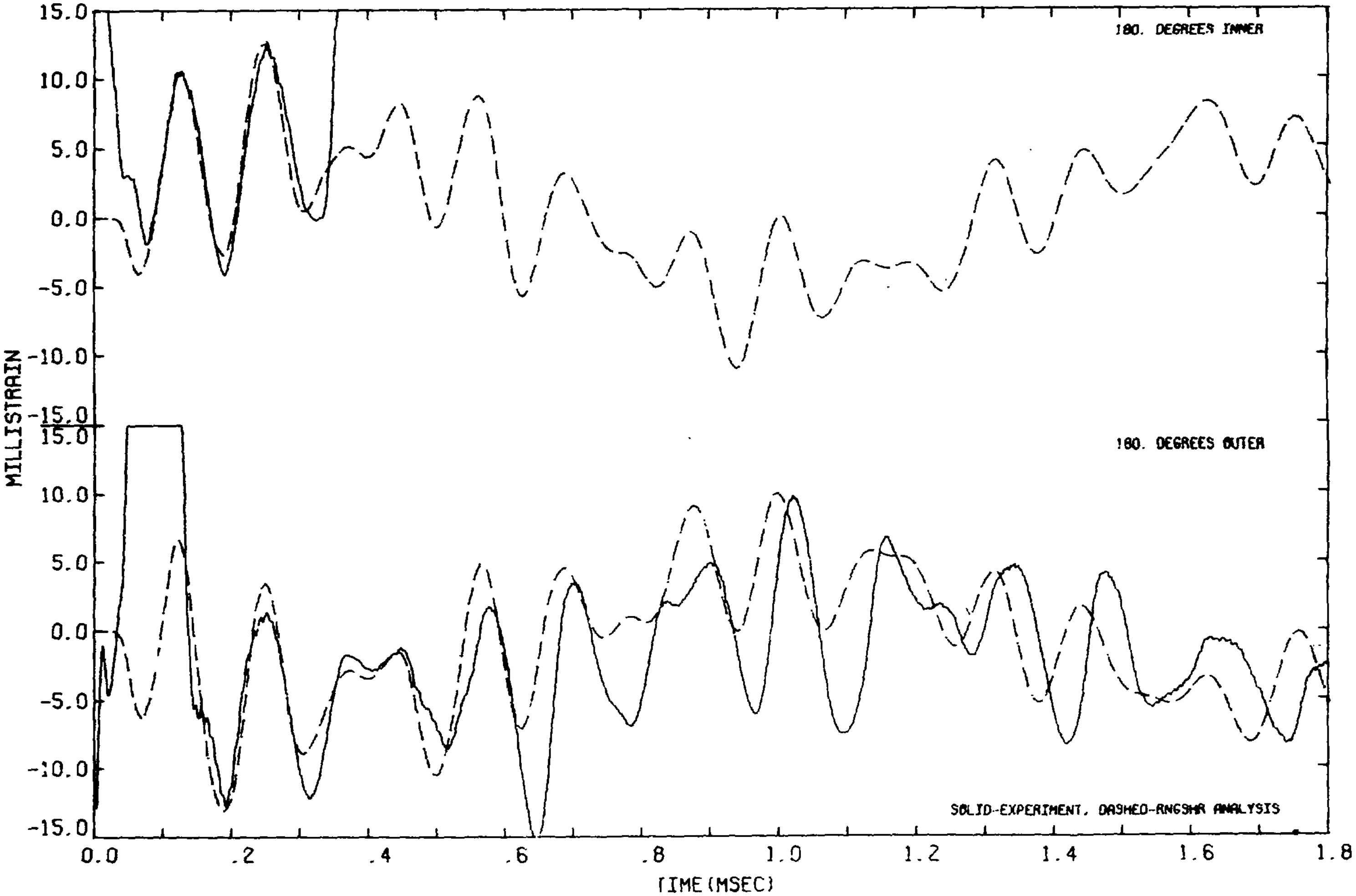

FIGURE 31

ANALYTICAL/EXPERIMENTAL STRAIN CORRELATION.
3DQP UGT RING M381-1

Table 6. UGT Strain Versus Calculated Strain

| Ring | Gage Location | Time Interval (ms) | Correlation Coefficient |
|---|---|---|---|
| 277-1 | 180° Inner | 0.05 to 0.3 | 0.987 |
| | | 0.05 to 2.00 | 0.899 |
| | 180° Outer | 0.18 to 0.90 | 0.859 |
| 380-1 | 180° Inner | 0.26 to 0.75 | 0.898 |
| | | 0.26 to 2.00 | 0.760 |
| 381-1 | 180° Inner | 0.08 to 0.33 | 0.980 |
| | 180° Outer | 0.14 to 0.60 | 0.926 |
| | | 0.14 to 1.95 | 0.626 |

## 6.2 AGT Strain Correlations

Preliminary strain calculations were made to correlate measured strains from the flyer plate experiments on 3DQP rings 7.1.4/15 and 7.1.4/16.

Since these rings were of basically the same material and configuration as ring 381-1, and since the impulse level was close to that experienced by ring 381-1, the same material properties and degradation model were employed in these calculations as were used for the correlation of the ring 381-1 strains. The impulse was adjusted for 7.1.4/16, but for 7.1.4/15 even the impulse was kept at the same level (13.5 ktap). The impulse on 7.1.4/16 that gave the best correlation was 14.2 ktap.

These correlations give one point of comparison between the results of flyer plate blowoff impulse simulation and actual UGT testing.

The results of the calculations are over-plotted with the measured strains for ring 7.1.4/15 in Figure 32 and for ring 7.1.4/16 in Figure 33. The measured strain at 180° on the outside of 7.1.4/15 experienced amplifier saturation at about 3.5 millistrain. This precludes an optimum correlation of that record. Ring 7.1.4/16 is thought to have experienced enough damage to distort its linear behavior. It may be adviseable to reanalyze 7.1.4/16 after the damage is more closely studied.

Overall, the preliminary correlations for these two AGT rings are fairly good. It is expected that these correlations would be improved if the assumed material properties are adjusted after close study of the damage and of the pretest resonance data.

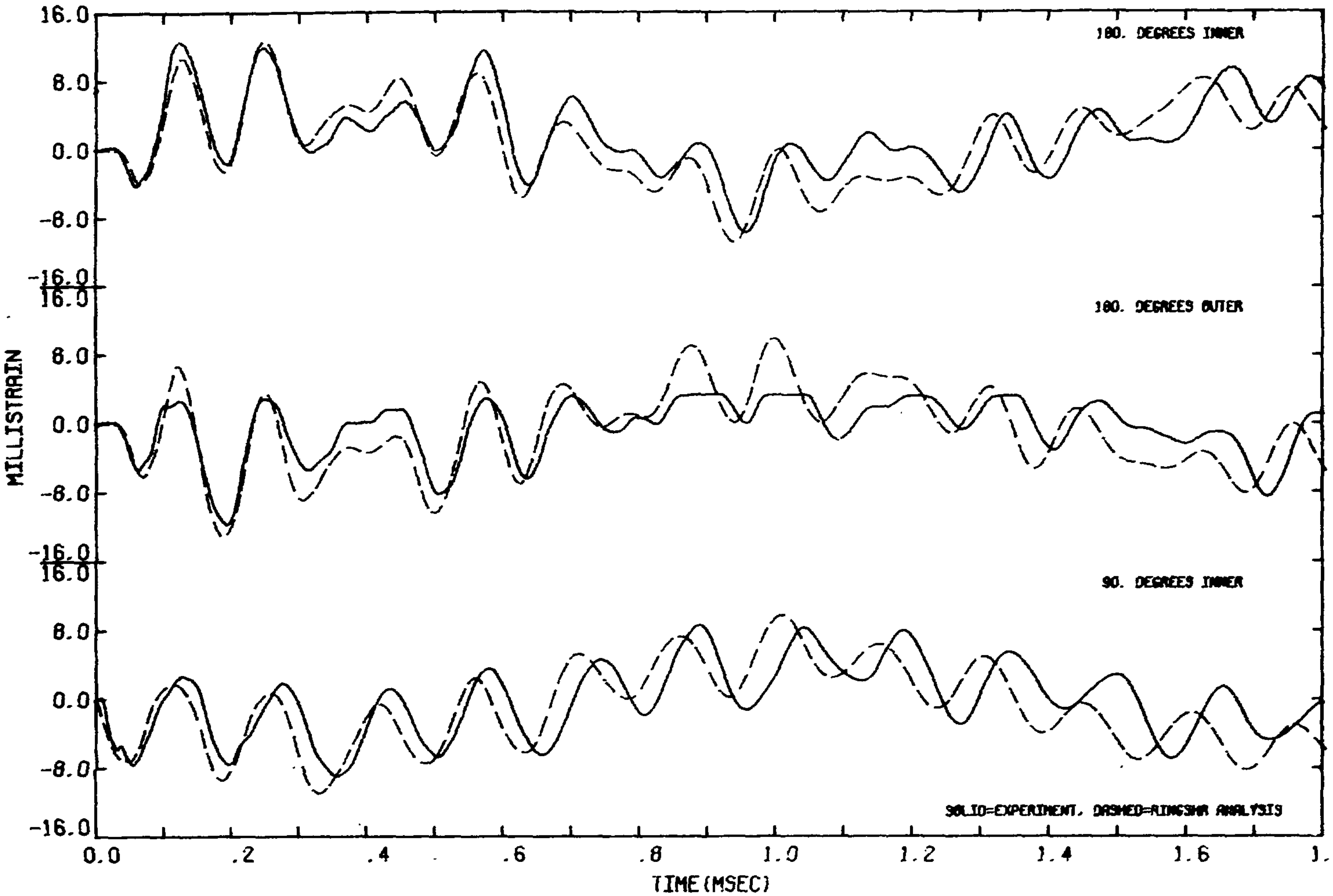

FIGURE 32

ANALYTICAL/EXPERIMENTAL STRAIN CORRELATION.
3DQP AGT RING 7.1.4/15

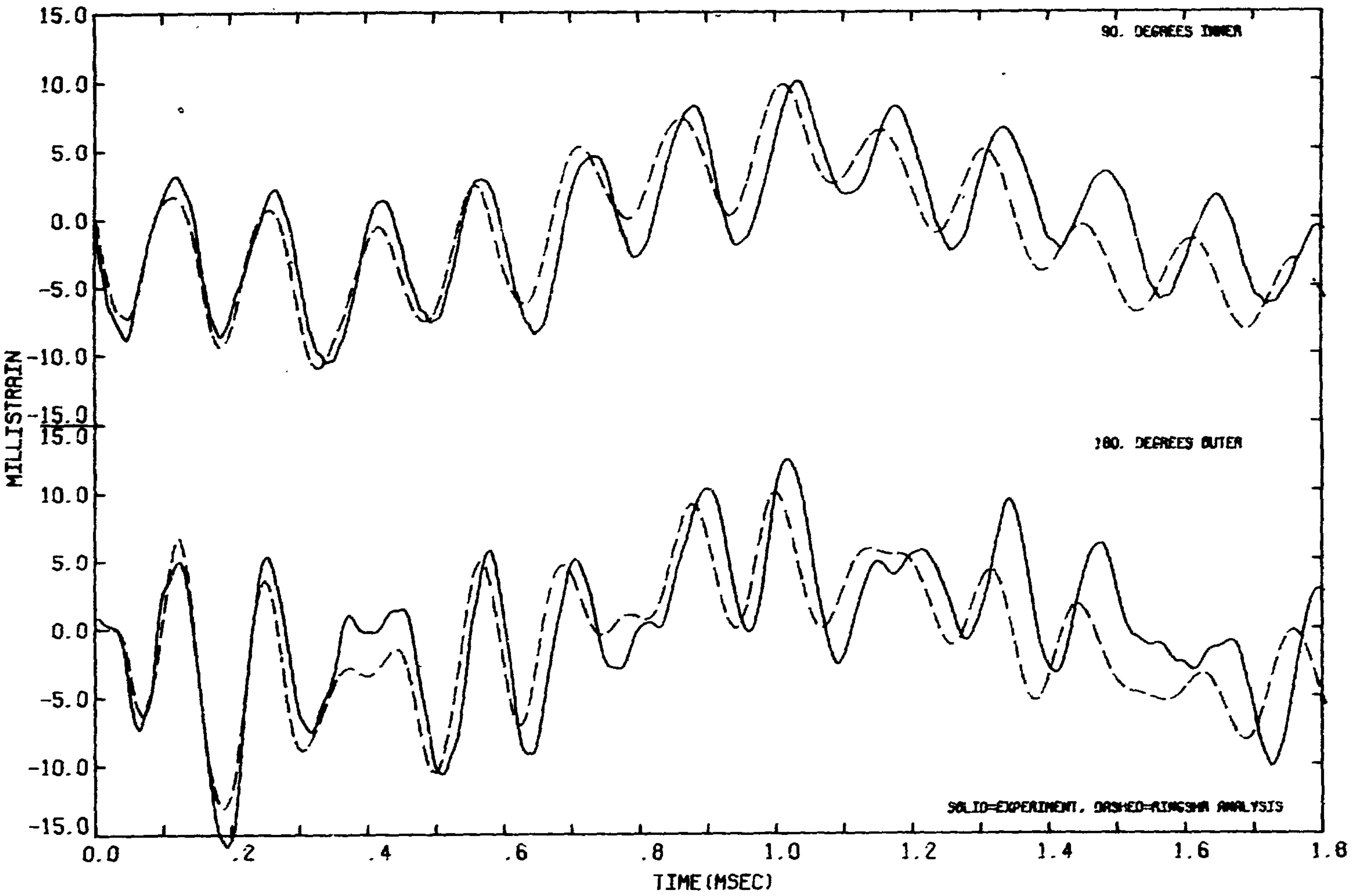

FIGURE 33

ANALYTICAL/EXPERIMENTAL STRAIN CORRELATION.
3DQP AGT RING 7.1.4/16

The correlation coefficients computed to compare the calculated and measured strains are listed in Table 7.

Table 7. AGT Measured Strain Versus Calculated Strain

| RING | GAGE LOCATION | TIME INTERVAL (ms) | CORRELATION COEFFICIENT |
|---|---|---|---|
| 7.1.4/15 | 180° Inner | 0-1.0 | 0.909 |
| | | 0-1.9 | 0.829 |
| | 180° Outer | 0-1.0 | 0.888 |
| | | 0-1.9 | 0.784 |
| | 90° Inner | 0-1.0 | 0.792 |
| | | 0-1.9 | 0.689 |
| 7.1.4/16 | 180° Outer | 0-1.0 | 0.872 |
| | | 0-1.9 | 0.746 |
| | 90° Inner | 0-1.0 | 0.908 |
| | | 0-1.9 | 0.816 |

## 6.3 Analysis of P-478-2

An analytical study was made of the response of a 3DQP ring to impulse and instantaneous heating. The attempt was made to represent analytically the conditions experienced by 3DQP rings in Ming Blade. The purpose of the study was to gain a better understanding of the results of the test relative to 3DQP. The condition analyzed was a half-cosine-distributed impulse of 13.5 ktaps delivered

to the ring. Energy deposition and temperature rise were computed by means of KSC's PUFF VI code. The calculated temperature rise distribution is shown in Figure 34 Dimensions of the ring and parameters used in the calculation are the following:

| | |
|---|---|
| O.D. | 19.56 cm |
| Thickness | 1.15 cm |
| $A_r/A_t$ | 0.65 |
| Density | 1.67 $g/cm^3$ |
| Reference Temperature | 20°C |
| Expansion Coefficient | 16.2 x $10^{-6}$/C° |
| Specific Heat | 0.250 cal/gC° |
| Circumferential Modulus: | |
| Bilinear variation | |
| 20°C | 24.45 GPa |
| 94°C | 23.51 GPa |
| 538°C | 0.70 GPa |

Initial thermally induced circumferential stress was imposed in accordance with the derived graph given as Figure 35.

KSC's TWORNG code was used for the response analysis. The following runs were made:

1. Thermal stress with thermally degraded modulus.
2. Impulse with undegraded modulus.

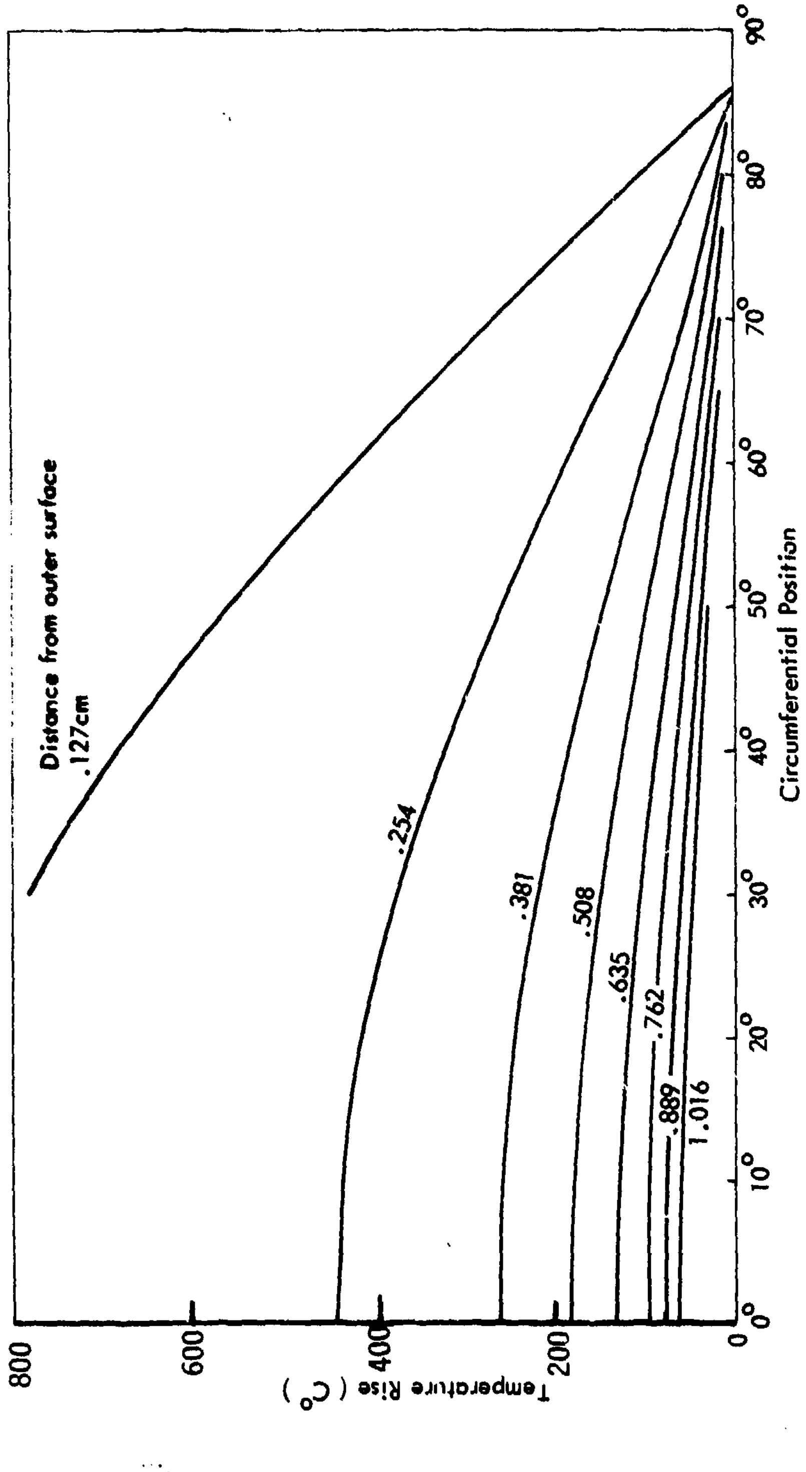

FIGURE 34

CALCULATED INSTANTANEOUS TEMPERATURE RISE.
MING BLADE RING P-478-2

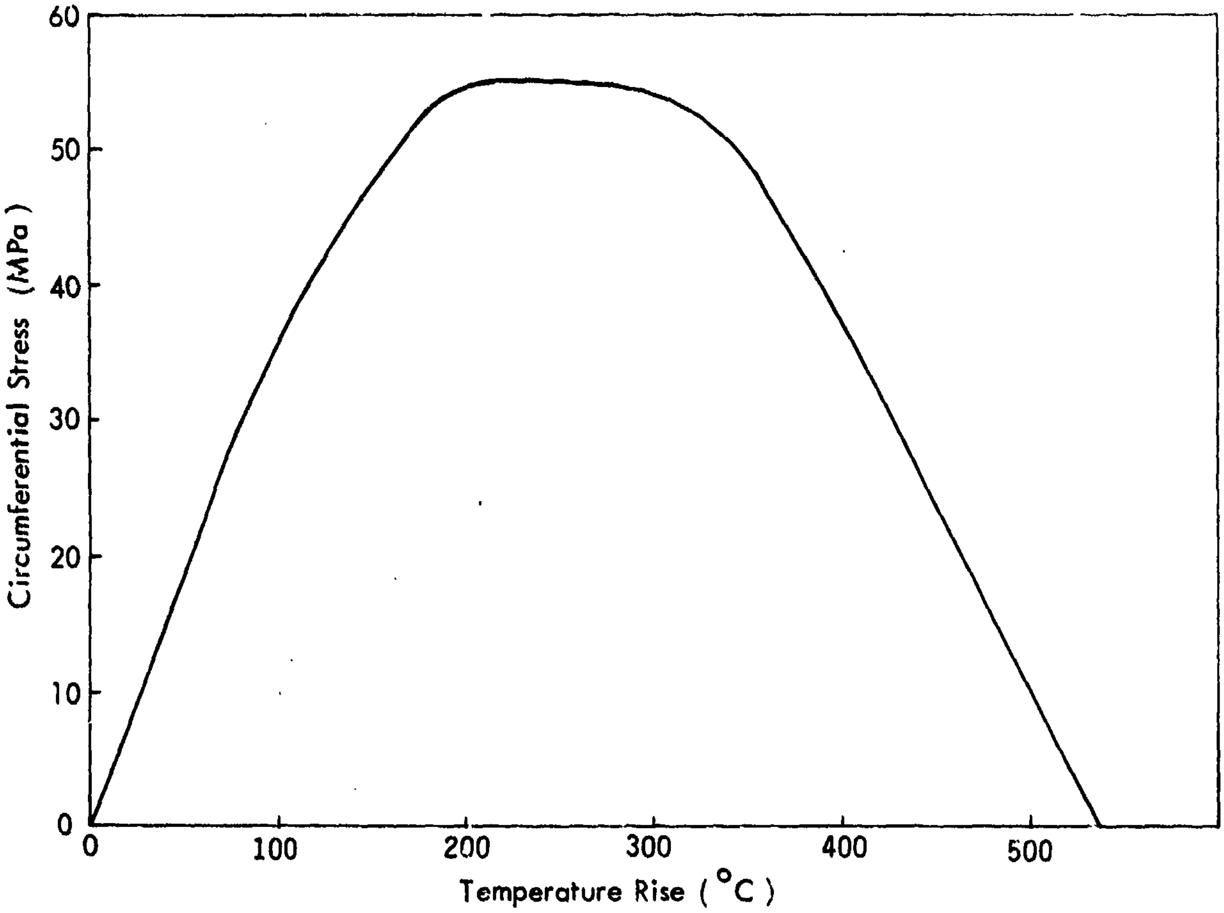

FIGURE 35

CALCULATED INITIAL CIRCUMFERENTIAL THERMAL STRESS VERSUS TEMPERATURE RISE, MING BLADE RING P-478-2

3. Impulse with thermal stress and thermally degraded modulus.

The results of run 1, thermal strain, are plotted in Figures 36 and 37. The results of runs 2 and 3 are overplotted for comparison in Figures 38, 39, and 40. Strain versus time graphs have been provided for 0°, 90°, and 180° on both the inside and outside surfaces.

From the graphs it is seen that the difference in strain magnitude between impulse with undegraded modulus and impulse plus thermal stress with degraded modulus is insignificant except near 0°, near the outer surface and this difference is primarily due to thermal degradation of modulus. The strain traces display a lower membrane frequency when part of the ring has degraded modulus. This result is as expected.

The difference between predicted strain at 0° outer, calculated for 13.5 ktap with and without thermally degraded modulus, is large enough that gross failure is predicted at 0° in the thermal case but not in the impulse only case.

Strain peaks at 0° outer without impulse (thermal strain with degraded modulus) are only about 9 percent of the strain peaks with impulse and degraded modulus. The strain records for thermal stress with degraded modulus (i.e. no impulse) have complicated waveforms, probably due to excitation of higher wave numbers of the response. Half-cosine-distributed impulse excites primarily n=0, 1, and 2 waves.

From this study it is concluded that

1. The thermal aspect of the problem is important in predicting failure.

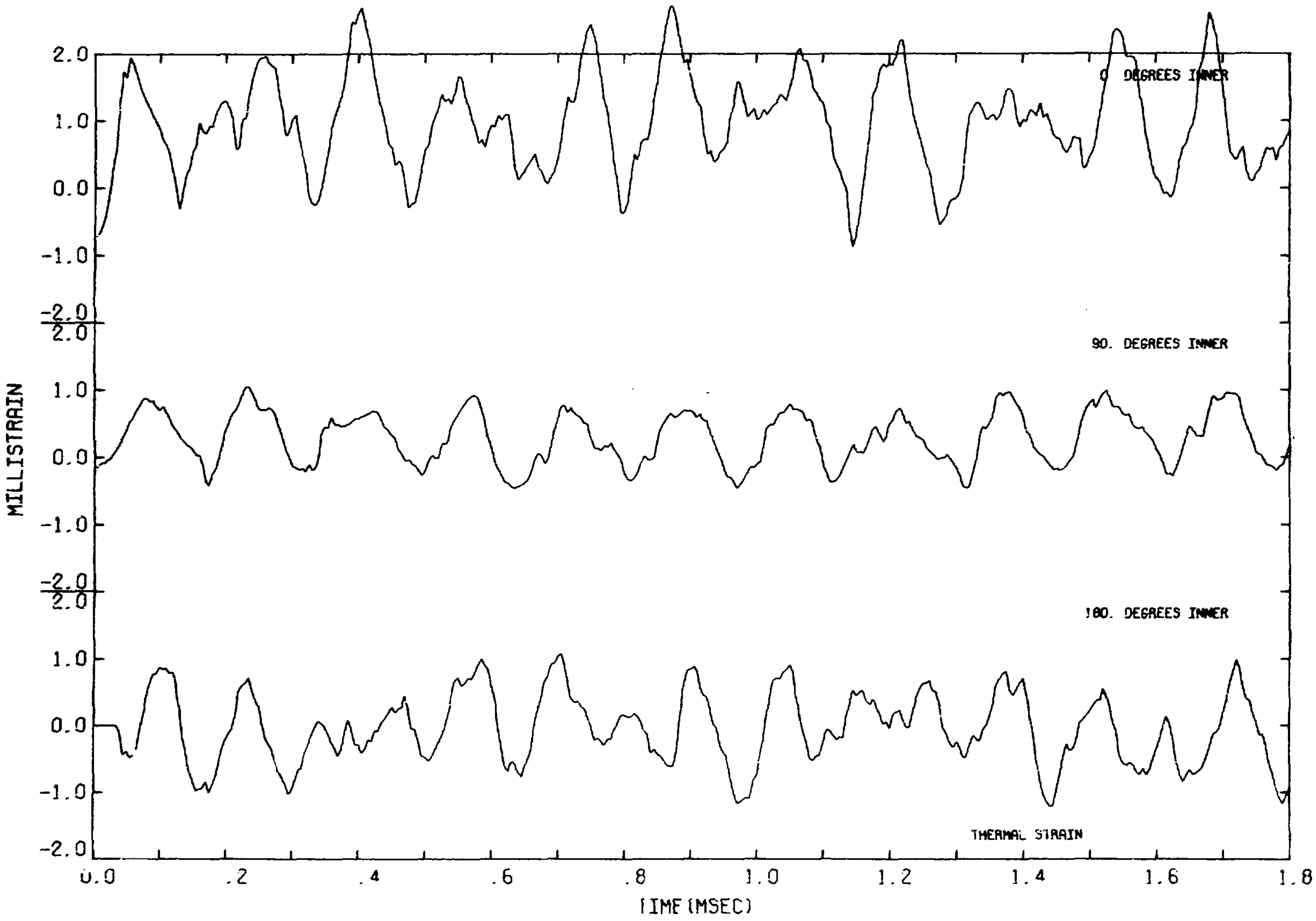

FIGURE 36

9/78

STRAIN CALCULATION, RING P-478-2
THERMAL STRAINS, NO IMPULSE, THERMALLY DEGRADED PROPERTIES

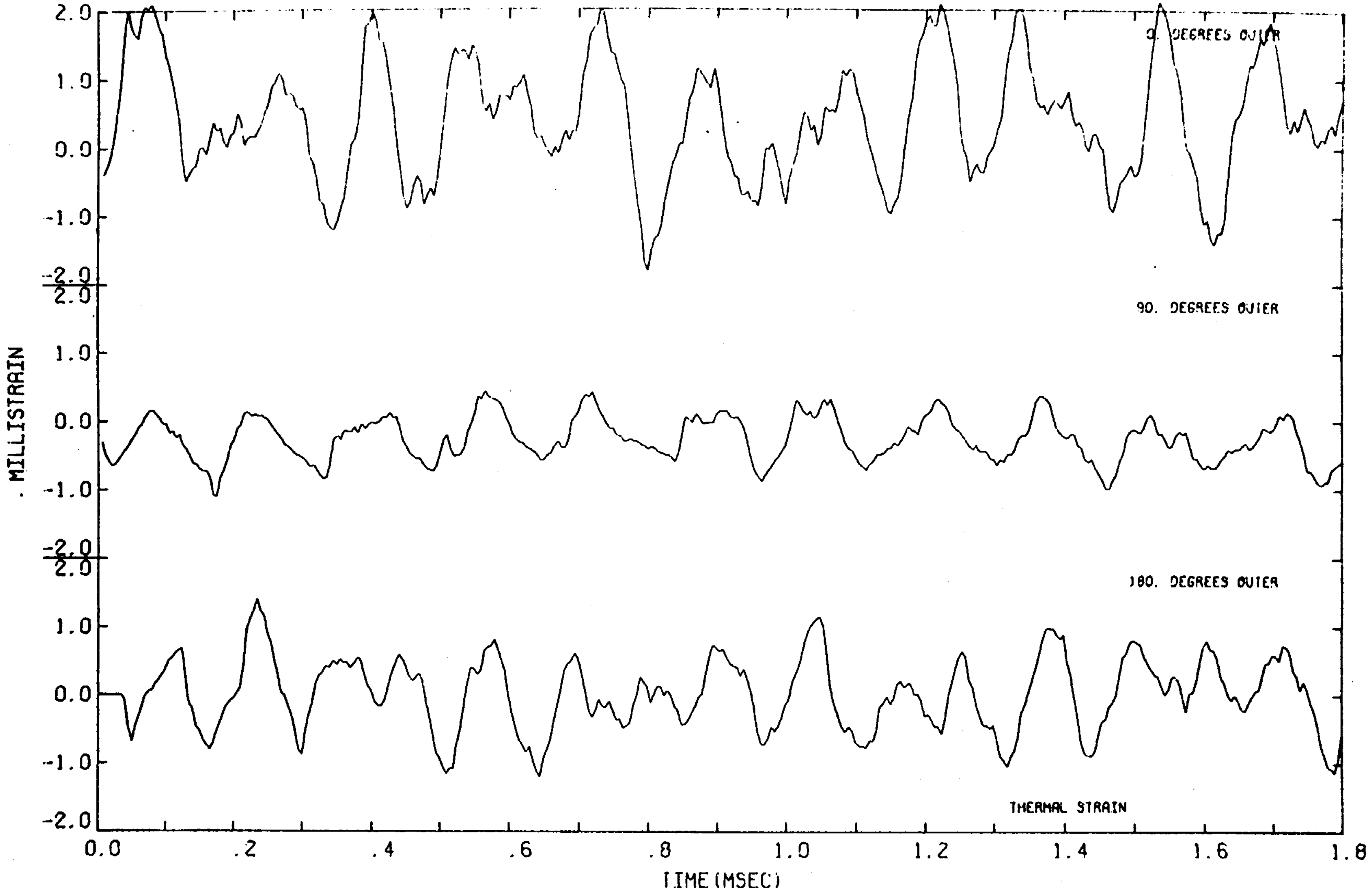

FIGURE 37

STRAIN CALCULATION, RING P-478-2
THERMAL STRAINS, NO IMPULSE, THERMALLY DEGRADED PROPERTIES

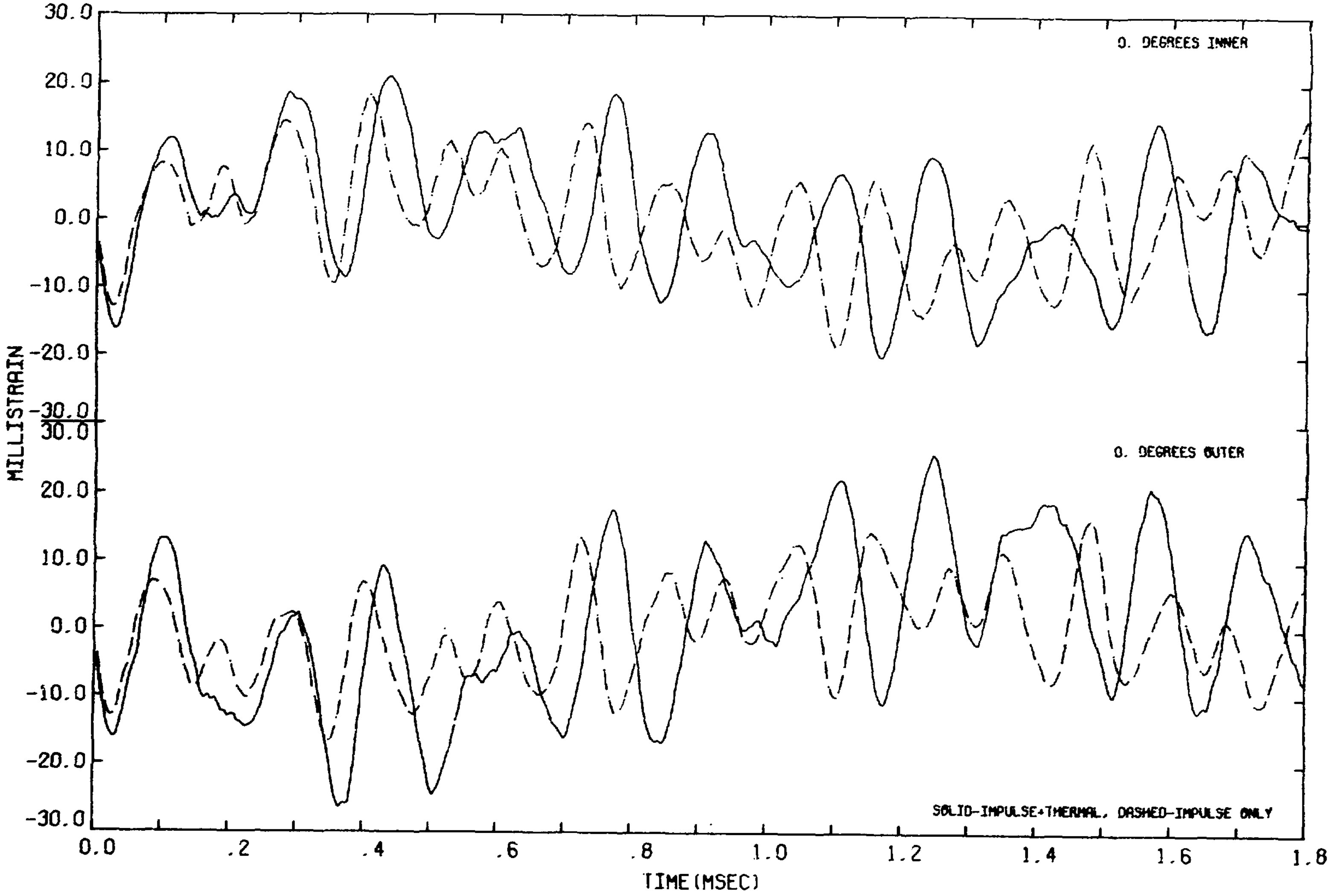

FIGURE 38

STRAIN CALCULATION, RING P-478-2
IMPULSE WITH AND WITHOUT THERMAL EFFECTS

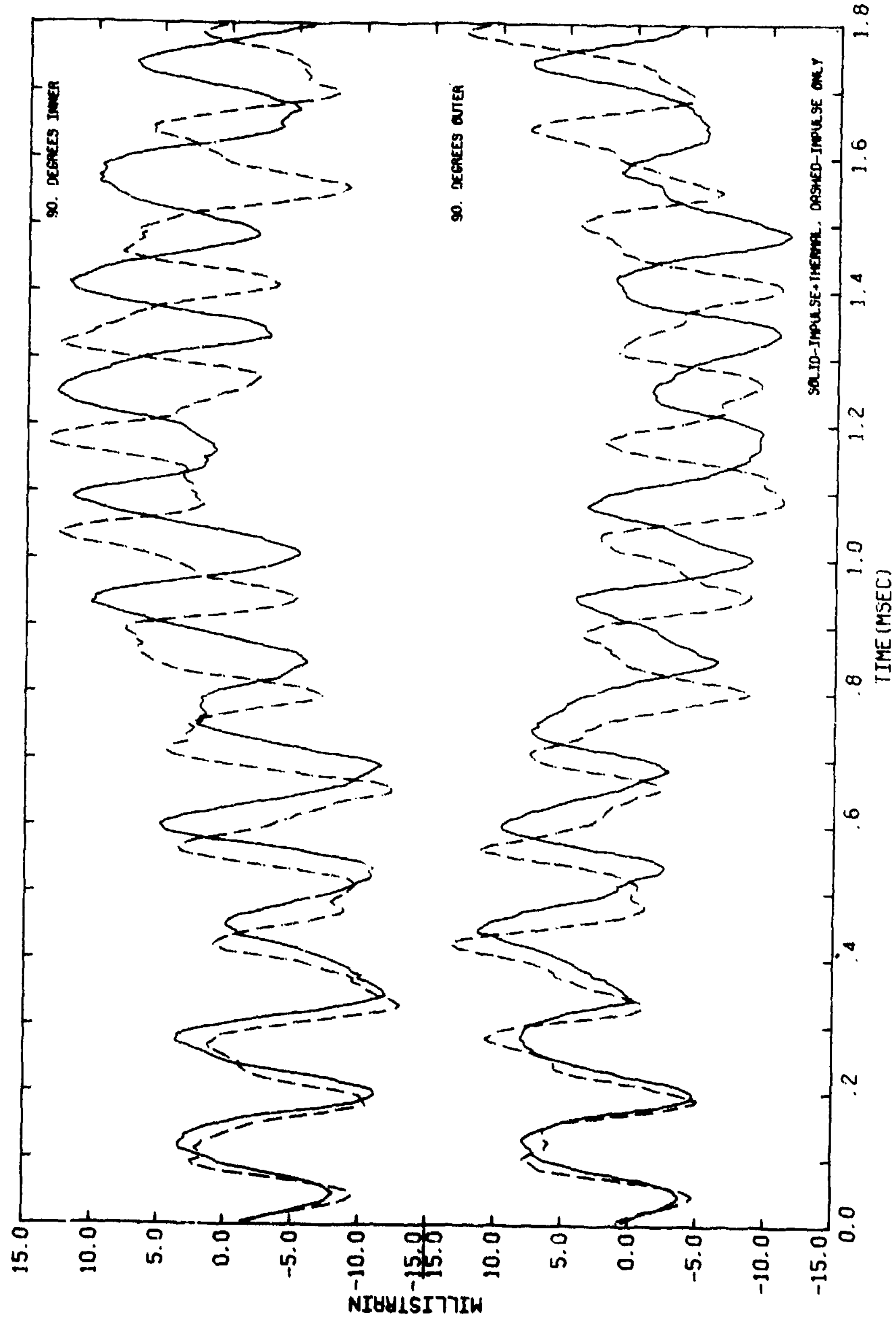

FIGURE 39

STRAIN CALCULATION, RING P-478-2
IMPULSE WITH AND WITHOUT THERMAL EFFECTS

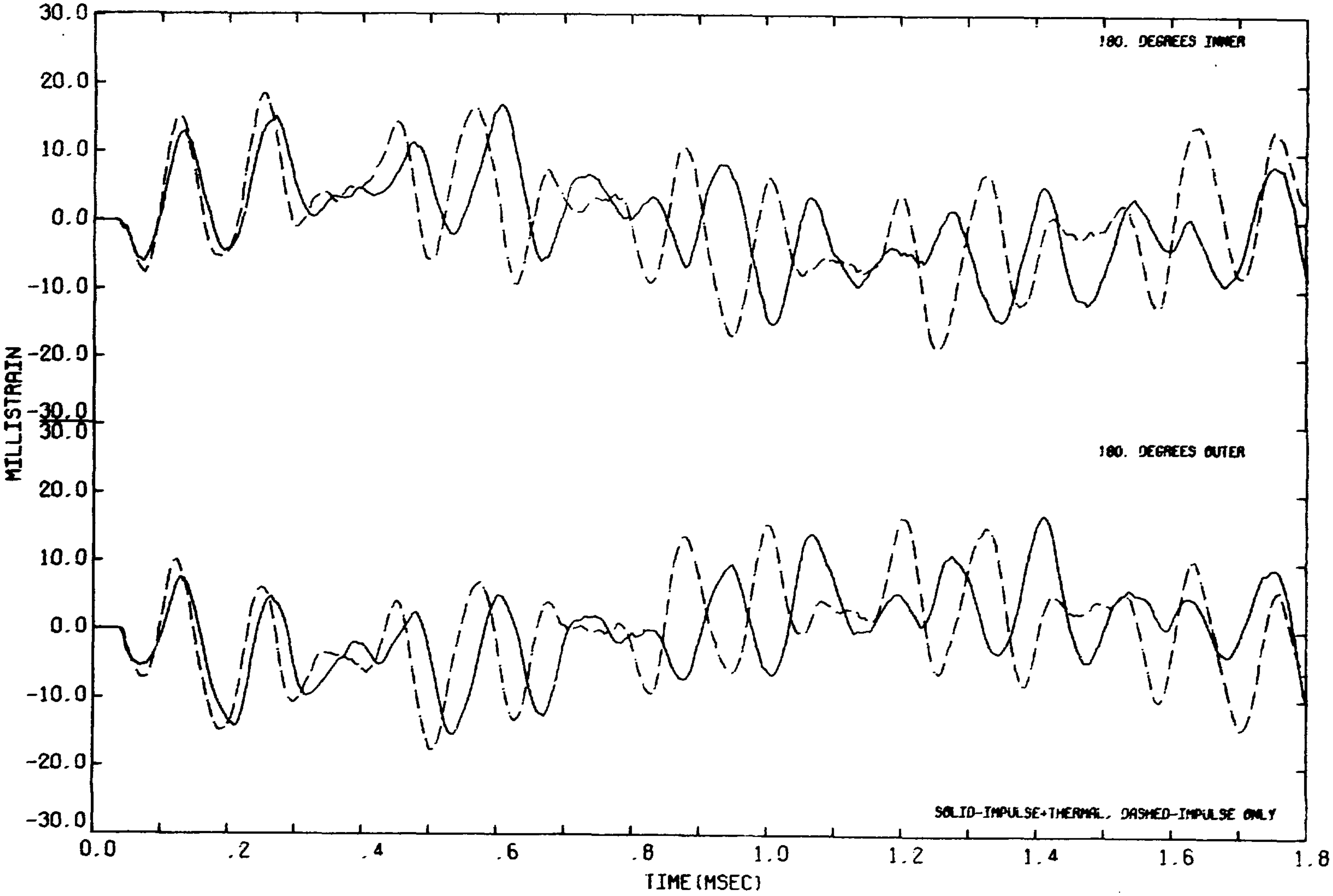

FIGURE 40

STRAIN CALCULATION, RING P-478-2
IMPULSE WITH AND WITHOUT THERMAL EFFECTS

2. The thermal strains are relatively small compared to strains due to impulse with degraded modulus.

3. The variation of modulus degradation through the thickness is important for predicting failure.

4. The feasibility of AGT impulse simulation of response of 3DQP to hot spectra depends on the timing of thermal degradation of material modulus. Exact reproduction of initial thermal stress is not of significant importance.

## 7.0 UGT/AGT COMPARISONS

### 7.1 UGT/AGT Overlays of Measured Strain

Correlation coefficients were calculated comparing the measured strain records for four AGT flyer plate simulation experiments with the measured strains from UGT ring 381-1.

The AGT rings were the following:

7.1.4/4
7.1.4/6
7.1.4/15
7.1.4/16

The overplots of the experimental data from 7.1.4/4 and 7.1.4/6 with the data from ring 381-1 are presented in Reference 1. Such overplots for rings 7.1.4/15 and 7.1.4/16 are given here as Figures 41 and 42. Correlation coefficients for these comparisons are given in Table 8. It is observed from the quality of these correlations that the 180° strain experienced by UGT ring 381-1 was successfully simulated by each of the four AGT rings.

### 7.2 Modulus Degradation Study

Preliminary modulus degradation assessments based on resonant frequency measurements for the first extensional mode $f_o$ pre and posttest on rings 381-1, 7.1.4/4, 7.1.4/6, 7.1.4/15, and 7.1.4/16 are reported in Table 9.

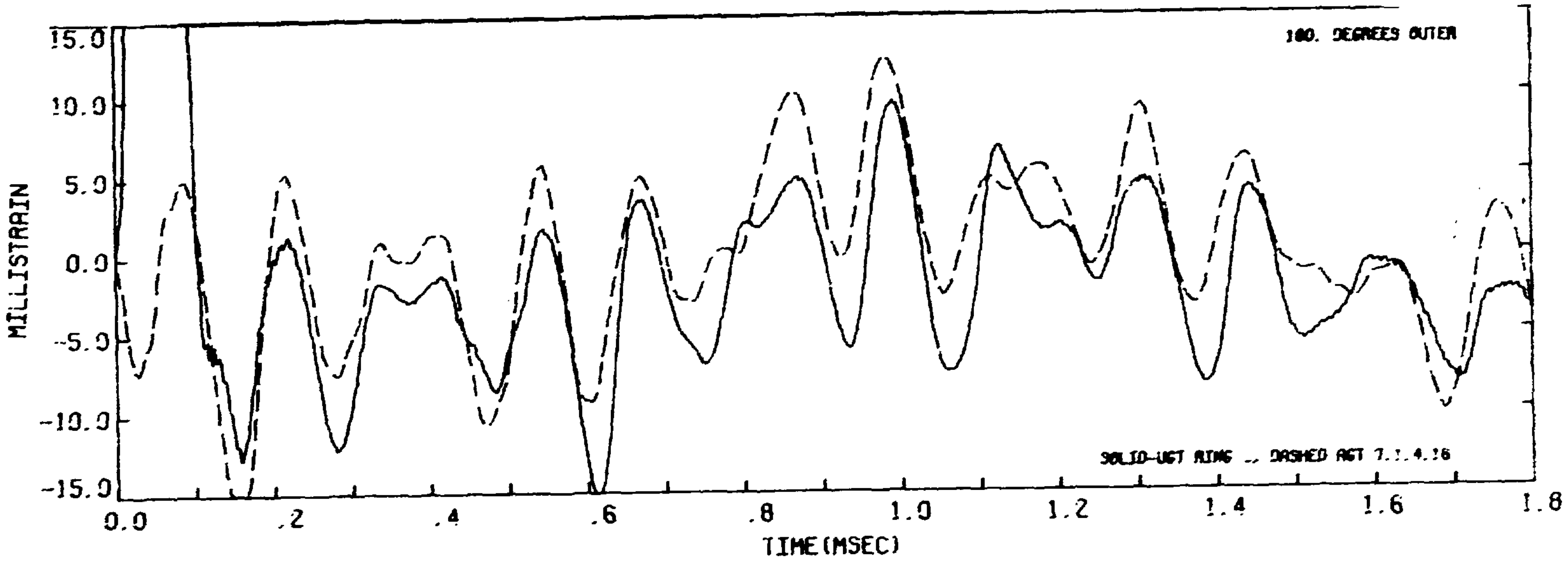

FIGURE 41

COMPARISON OF AGT AND UGT STRAINS.
RING 7.1.4/16 VERSUS M381-1

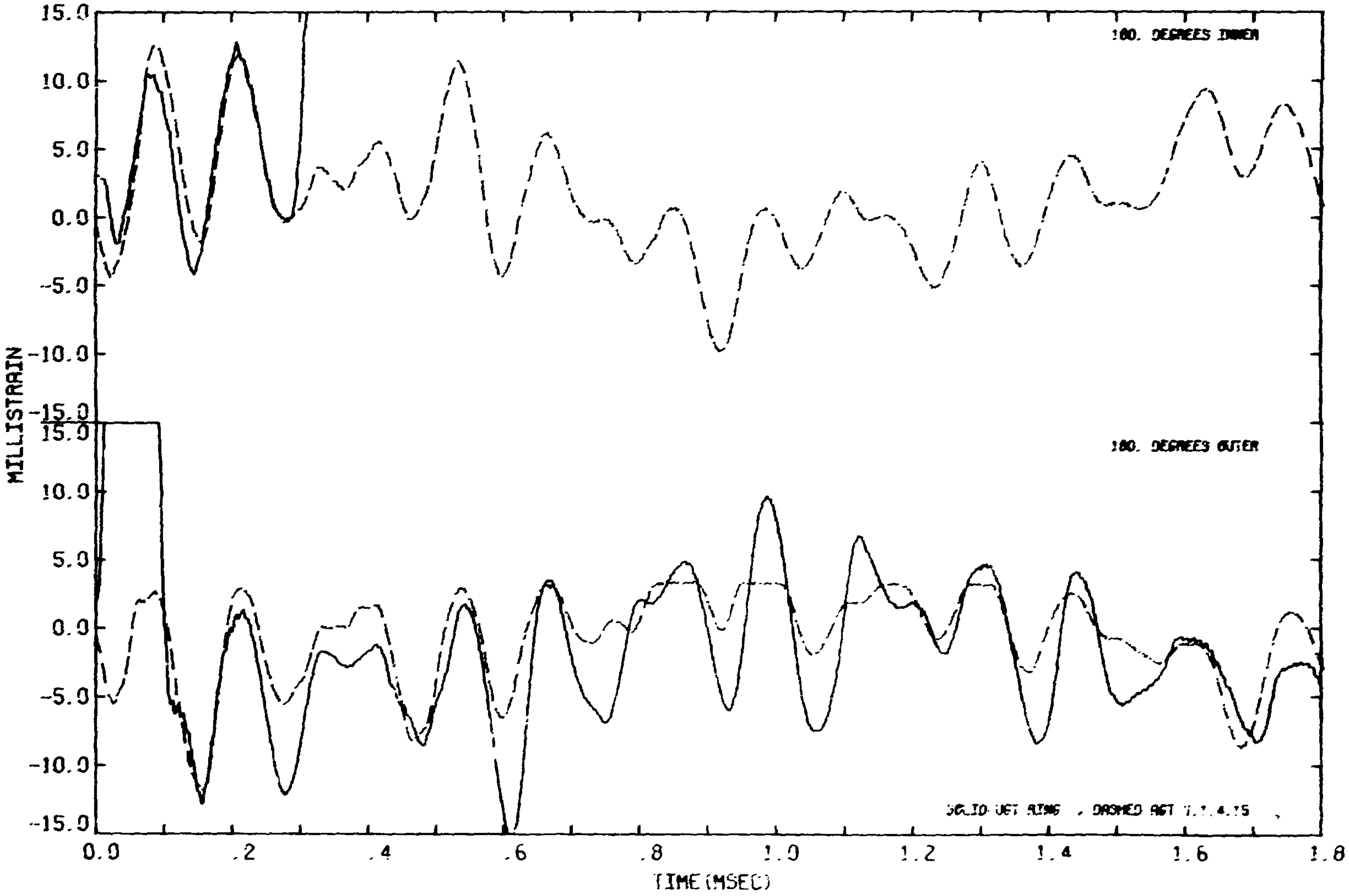

FIGURE 42.

COMPARISON OF AGT AND UGT STRAINS.
RING 7.1.4/15 VERSUS M381-1

In this table $E_o$ is the virgin modulus and $\Delta E/E_o$ is the fractional degradation of modulus at 0°. A cosine distribution of degradation between ±90° is assumed in this calculation.

These numbers allow a preliminary comparison of one type of degradation suffered by the four AGT rings compared to that experienced by ring 381-1. The indication is that, except for ring 7.1.4/4, the modulus degradation in the AGT rings closely matches that of UGT ring 381-1.

Table 8. UGT Measured Strain Versus AGT Measured Strain Correlation Coefficients

| RINGS | GAGE LOCATION | TIME INTERVAL (ms) | CORRELATION COEFFICIENT |
|---|---|---|---|
| 381-1 vs 7.1.4/4 | 180° Inner | 0.096 to 0.333 | 0.943 |
| | 180° Outer | 0.162 to 0.652 | 0.918 |
| | | 0.162 to 1.95 | 0.775 |
| 381-1 vs 7.1.4/6 | 180° Inner | 0.092 to 0.333 | 0.975 |
| | 180° Outer | 0.170 to 0.648 | 0.876 |
| | | 0.170 to 1.95 | 0.754 |
| 381-1 vs 7.1.4/15 | 180° Inner | 0.025 to 0.304 | 0.971 |
| | 180° Outer | 0.116 to 0.583 | 0.887 |
| | | 0.116 to 1.95 | 0.744 |
| 381-1 vs 7.1.4/16 | 180° Outer | 0.116 to 0.583 | 0.873 |
| | | 0.116 to 1.95 | 0.738 |

Table 9 Preliminary Modulus and Degradation Assessments

| RING | $f_o$(pretest) | $f_o$(posttest) | $E_o$ (GPa) | $\Delta E/E_o$ |
|---|---|---|---|---|
| 381-1 | Not Measured | 6649 | 26.6* | 0.28* |
| 7.1.4/4 | 6939 | 6506** | 26.1 | 0.38 |
| 7.1.4/6 | 6948 | 6629 | 26.2 | 0.28 |
| 7.1.4/15 | 6954 | 6631 | 26.3 | 0.29 |
| 7.1.4/16 | 6960 | 6610 | 26.2 | 0.31 |

*Based on correlation of six resonant frequencies

**Counted from 90° strain record.

# 8.0 RESONANT FREQUENCY STUDIES

## 8.1 Analytical Technique

The frequencies of the vibrational modes of a ring, that are active during impulsive response, can be measured one-by-one by structural resonance testing. Theoretical calculations of the resonant frequencies involve the mechanical properties of the material of the ring as well as the geometric configuration. Analytical correlation of the measured frequencies can be used to evaluate those properties which significantly influence the resonant frequencies.

For circular metal rings with constant properties, this calculation can be done satisfactorily with classical ring theory. The mechanical behavior of nonhomogeneous layered composites is determined by average properties and these average properties vary with fabrication technique. If the radius, thickness, and density distribution of a composite ring are known, it is found that the frequencies of membrane modes 0 and 1 are determined by circumferential modulus, but the flexural mode frequencies n = 2, 3 . . . involve both circumferential modulus and transverse shear modulus. Properties such as the radial and axial moduli, axial shear moduli, and Poisson's ratios have much smaller influences. Internal damping also is not expected to significantly influence resonance.

Calculation of resonant frequencies for composite rings, therefore, requires a theory which includes transverse shear flexibility. For symmetric rings the calculation can be

[redacted]

done using two-dimensional elasticity theory without ring theory constraints; but, if the ring is nonsymmetric for any reason, such as circumferential variations of thickness, moduli, or density, the two-dimensional theory must be treated numerically in two directions and, thus, becomes impractical. The frequency analysis of nonsymmetric composite rings, therefore, requires transverse shear theory dealt with numerically in the circumferential direction.

KSC's NFDR code (Natural Frequencies of Degraded Rings) was written to deal with this type of problem and has been used in the 3DQC Program to correlate resonant frequencies for material property assessment. The theory in this code assumes that the subject ring is thin and single-layered. The material properties used are average values for a given circumferential position. The code accepts arbitrarily specified continuous circumferential variations of circumferential modulus E, transverse shear modulus G, density, and thickness. In the frequency analysis of degraded rings in the 3DQC Program the following degradation functions have been employed:

$$E = E_o - \Delta E \cos \frac{\pi\theta}{120} \quad , \quad |\theta| \leq 60°$$

$$E = E_o \quad , \quad |\theta| > 60°$$

$$G = G_o - \Delta G \quad , \quad |\theta| \leq 45°$$

$$G = G_o \quad , \quad |\theta| > 60°$$

Linear Variation from

$G_o - \Delta G$ to $G_o$ , $45° < |\theta| \leq 60°$

$E_o$ and $G_o$ represent the virgin moduli and are assumed constant. $\Delta E$ and $\Delta G$ are the maximum values of degradation distributions which are assumed to be symmetric about the center of impulse. The symmetry assumption has been considered reasonable and is a requirement if a systematic relationship between degradation and impulse prevails.

In considering the concept of deriving property values and degradation parameters from analytical correlation of resonant frequencies, the question arises as to the sensitivity of the various frequency measurements to these properties and their variations. In order to discern one set of parametric values from another, the measured frequencies and their analytical correlation must have the required sensitivity to indicate which set of parametric values is the better choice. In order to address this question, two analytical sensitivity studies were done.

In the first study the subject specimen was assumed symmetric and undegraded. Frequencies for wave numbers 0 to 6 were computed for a range of values of $E_o$ and $G_o$. The parameters assumed in this study are the following:

| | |
|---|---|
| Radius | 9.10 cm |
| Thickness | 1.16 cm |
| Density | 1.67 g/cm$^3$ |
| $E_o$ | 19.1 to 33.2 GPa |
| $G_o$ | 1.68 to 2.52 GPa |
| $\Delta E$ | 0.0 |
| $\Delta G$ | 0.0 |

The results are given graphically in Figures 43 to 47.

The following conclusions can be drawn:

1. $f_o$ and $f_1$ are unaffected by $G_o$ but are very sensitive to the choice of $E_o$. $E_o$ should be derivable from an accurate pretest measurement of $f_o$ alone.
2. The sensitivity of $f_2$ to $G_o$ is inadequate
3. The sensitivity of $f_3$ to $f_6$ to $G_o$ is good.
4. The sensitivity of all the frequencies to $E_o$ is good.

In the second study the values $E_o$ and $G_o$ were held fixed and $\Delta E$ and $\Delta G$ were given a range of values. The parameters assumed in this analysis are typical of 3DQP and are listed as follows:

| | |
|---|---|
| $E_o$ | 26.6 GPa |
| $G_o$ | 2.39 GPa |
| Density | 1.67 g/cm$^3$ |
| Thickness | 1.15 cm |
| Radius | 9.10 cm |
| $\Delta E/E_o$ | 0.00 to 32.0% |
| $\Delta G/G_o$ | 0.00 to 32.0% |

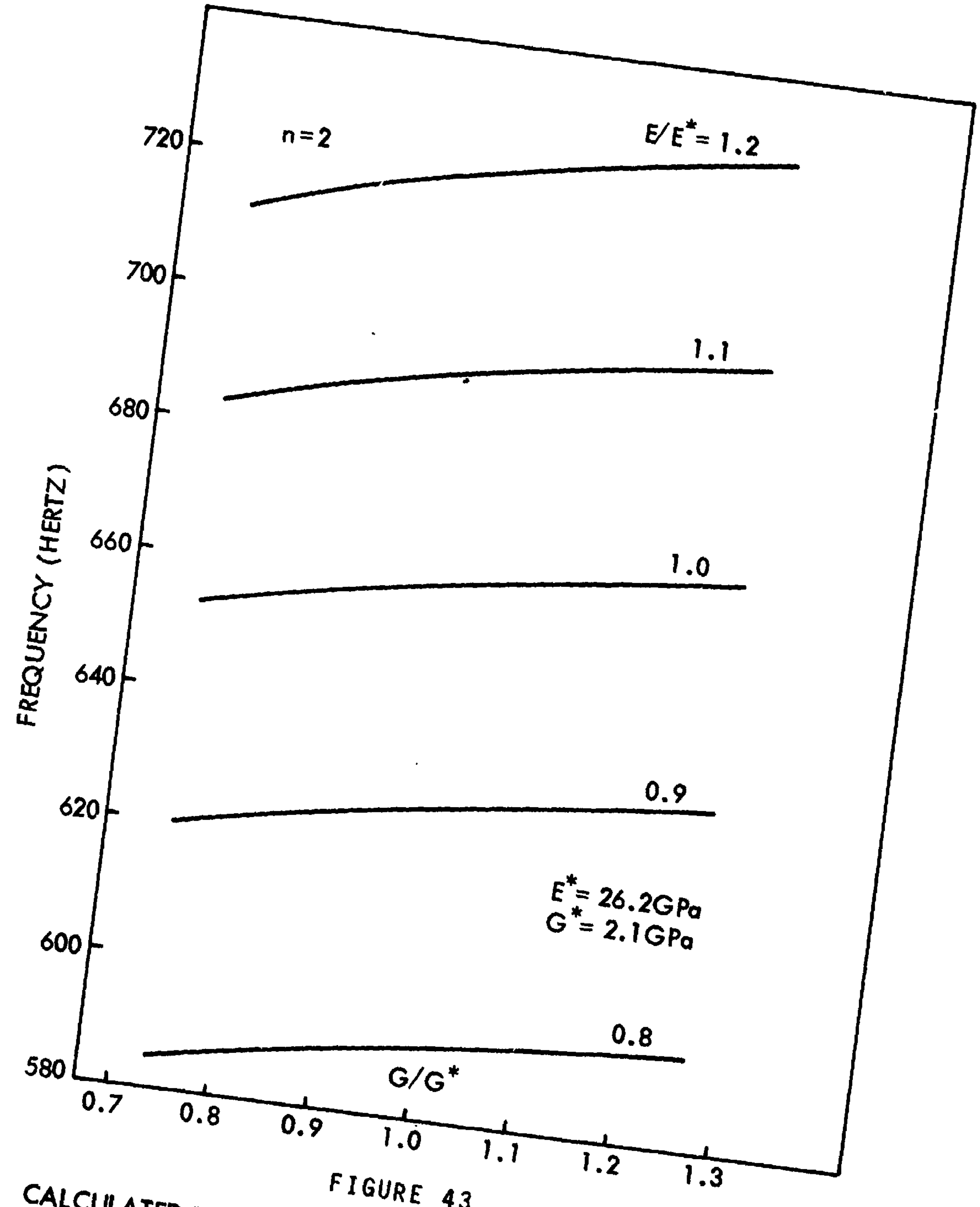

FIGURE 43

CALCULATED RESONANT FREQUENCY VERSUS SHEAR MODULUS.
NOMINAL 3DQP RING, RADIUS 9.1 CM, THICKNESS 1.16 CM

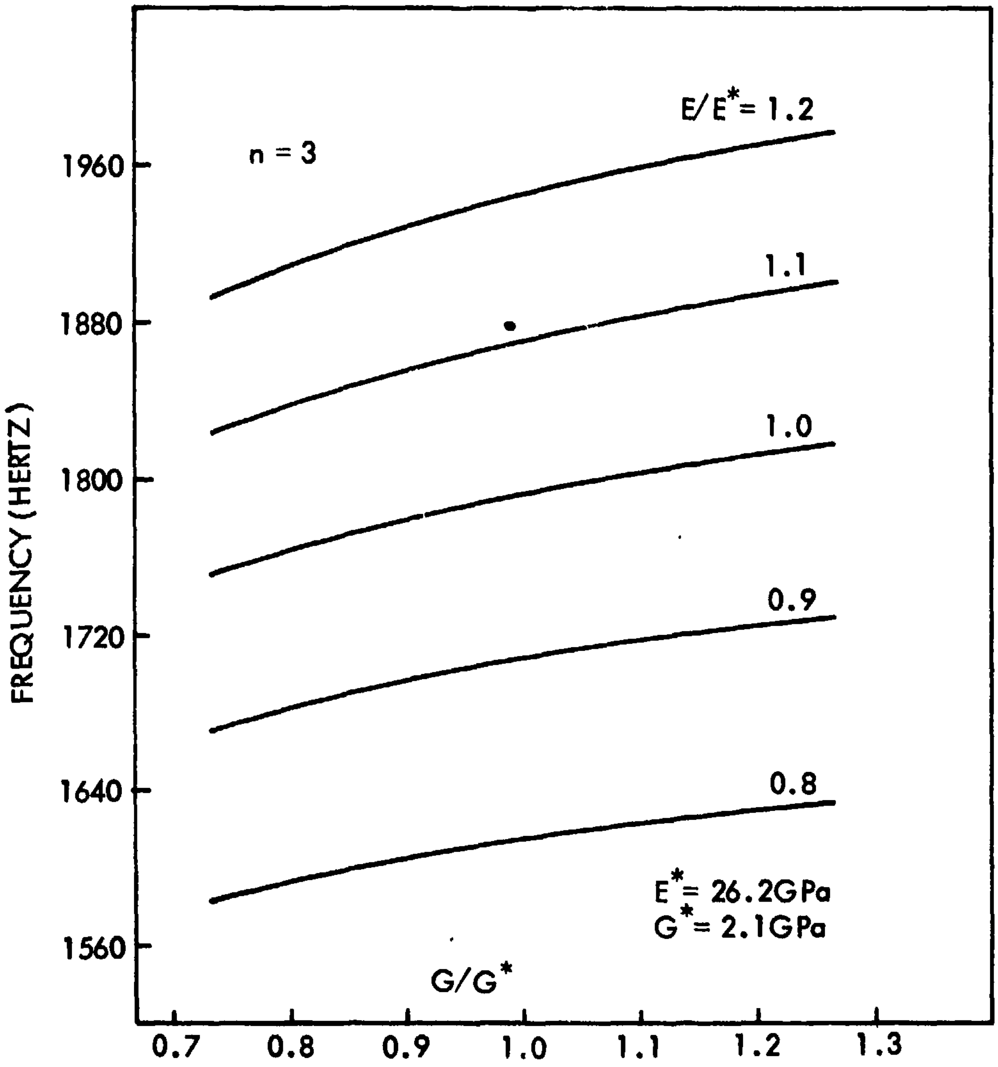

FIGURE 44

CALCULATED RESONANT FREQUENCY VERSUS SHEAR MODULUS. NOMINAL 3DQP RING, RADIUS 9.1 CM, THICKNESS 1.16 CM

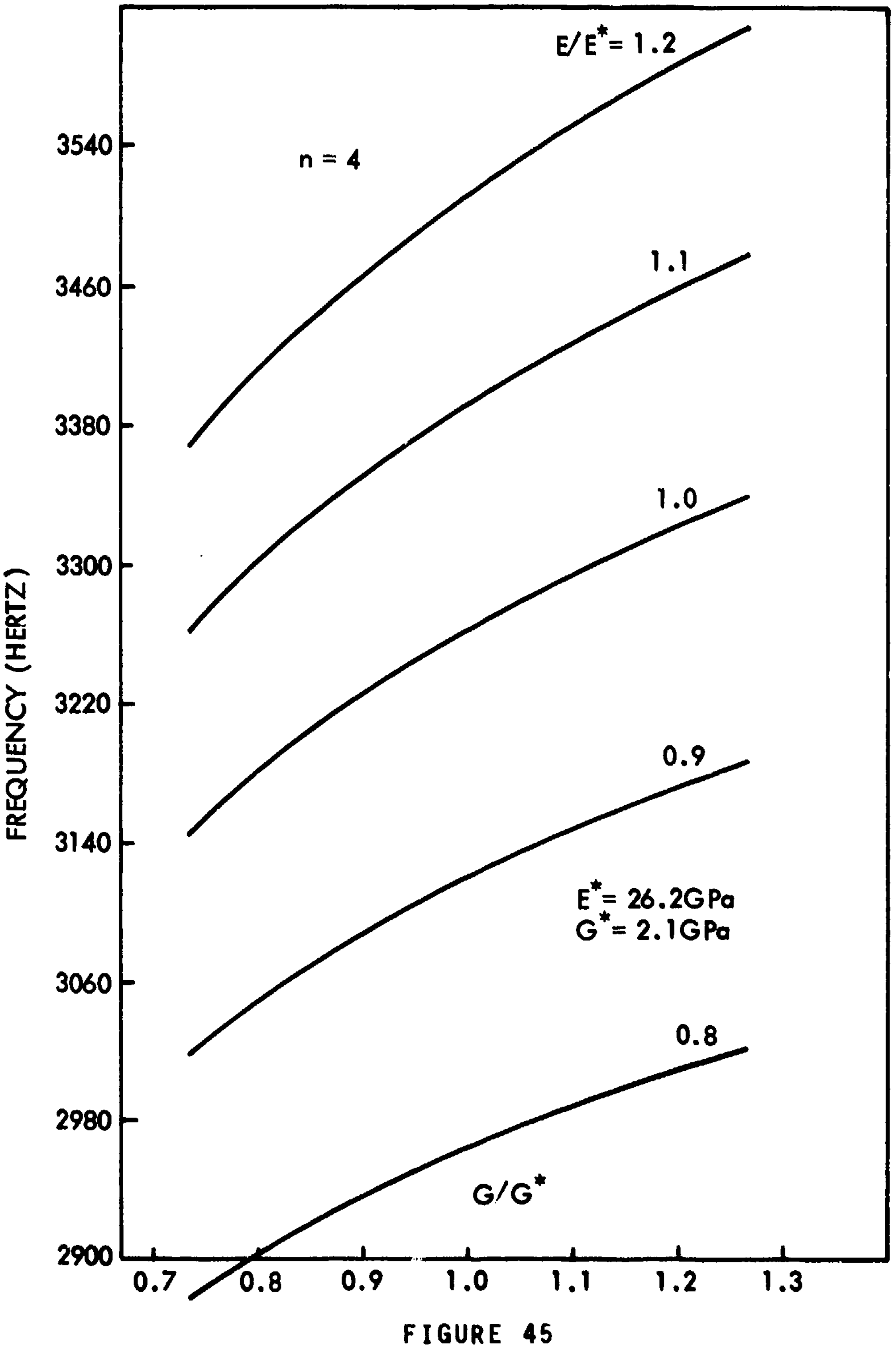

FIGURE 45

CALCULATED RESONANT FREQUENCY VERSUS SHEAR MODULUS. NOMINAL 3DQP RING, RADIUS 9.1 CM, THICKNESS 1.16 CM

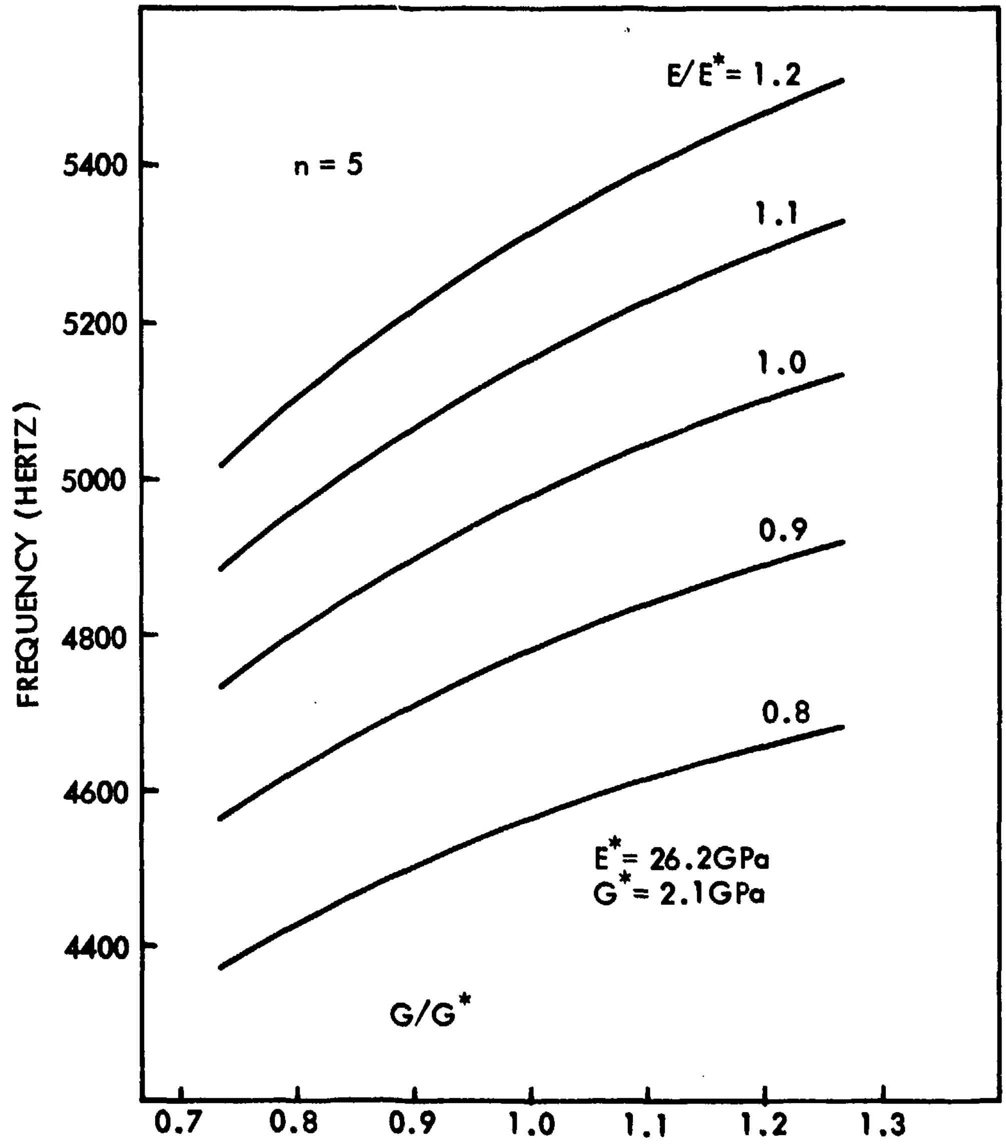

FIGURE 46

CALCULATED RESONANT FREQUENCY VERSUS SHEAR MODULUS.
NOMINAL 3DQP RING, RADIUS 9.1 CM, THICKNESS 1.16 CM

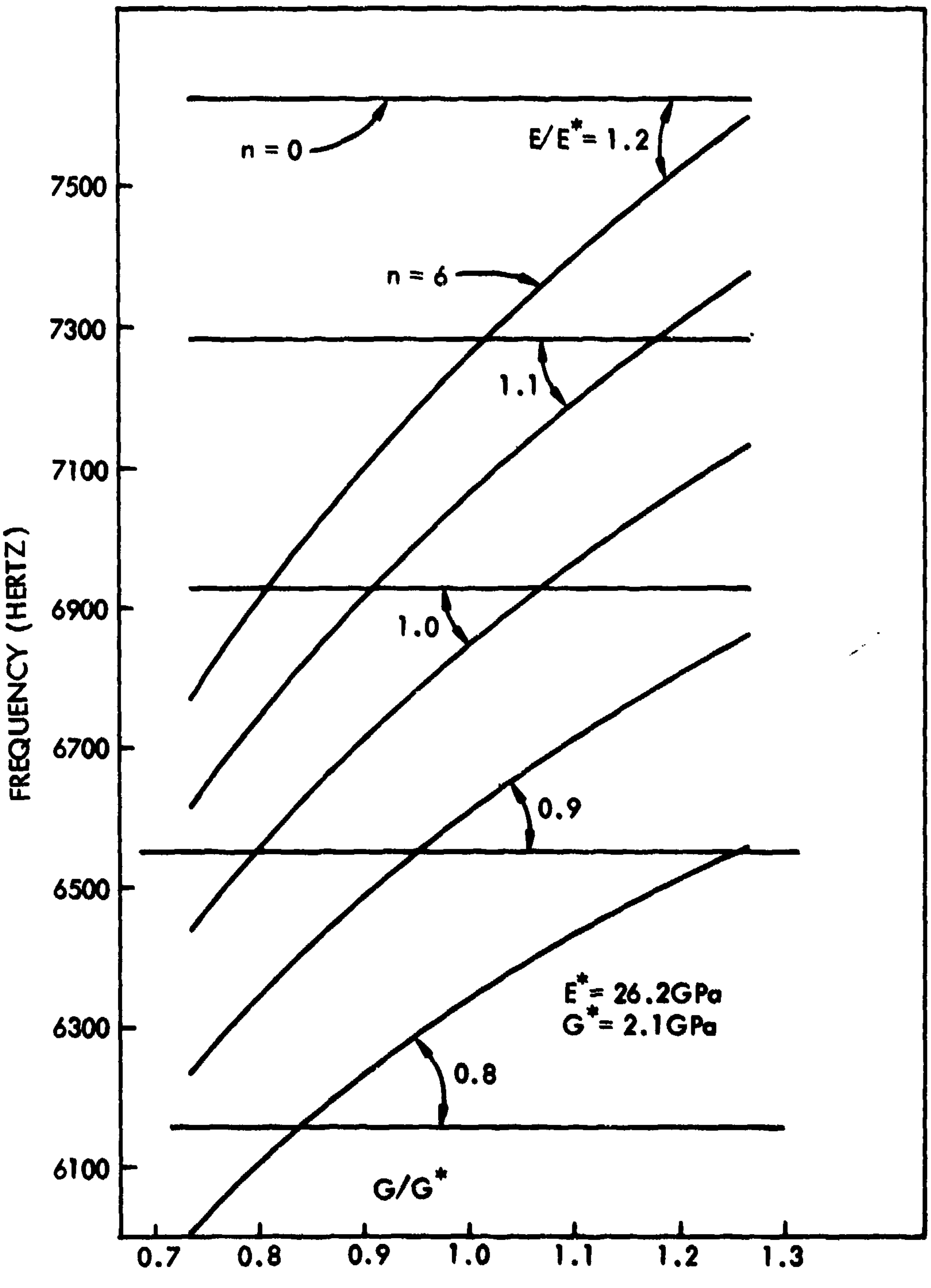

FIGURE 47

CALCULATED RESONANT FREQUENCY VERSUS SHEAR MODULUS. NOMINAL 3DQP RING, RADIUS 9.1 CM, THICKNESS 1.16 CM

The results of this study are given graphically in Figure 48 to 50.

The following conclusions are drawn:

1. $f_o$ is quite sensitive to $\Delta E$ but completely insensitive to $\Delta G$. $\Delta E$ should be derivable from an accurate posttest measurement of $f_o$ alone.

2. The sensitivity of $f_2$ and $f_3$ to $\Delta G$ is inadequate.

3. The sensitivity of $f_2$ to $\Delta E$ is not good.

4. The sensitivity of $f_3$ to $f_6$ to $\Delta E$ is good.

5. The sensitivity of $f_4$ to $f_6$ to $\Delta G$ is good.

From these studies taken together it is apparent that the $f_o$ measurement pre and posttest is very important. If these are not accurate, the task of calculating the properties is much more difficult, because it is necessary to rely on the simultaneous correlation of a set of frequencies. Pretest measurements are practically imperative in order to have a condition when $\Delta G$ and $\Delta E$ do not yet exist. $f_4$ and $f_5$ are important for calculating $\Delta G$, and $f_6$ is an important measurement, because, at least for the rings in this program, it is numerically close to $f_o$, and it is necessary to determine which is which, so that $f_6$ is not erroneously taken for $f_o$.

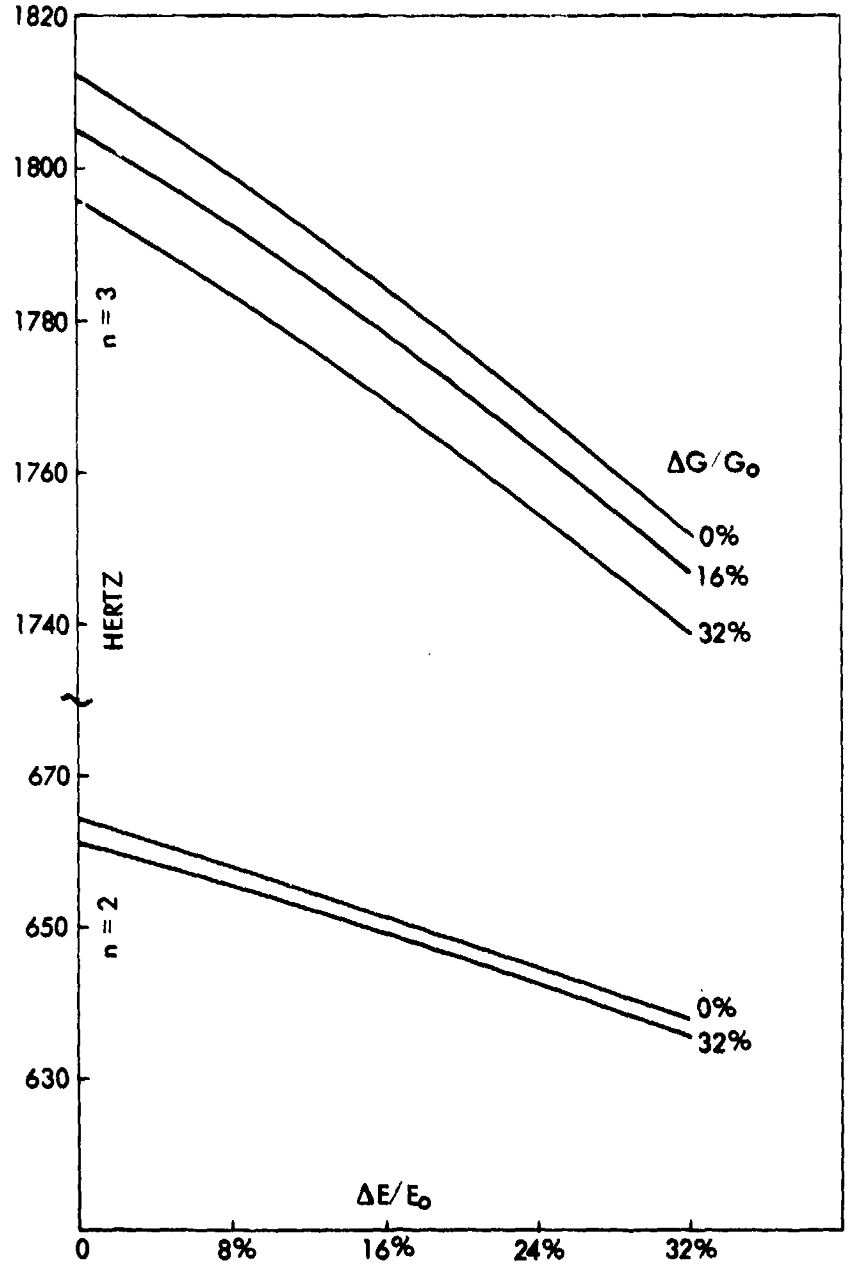

FIGURE 48

CALCULATED RESONANT FREQUENCY VERSUS MODULUS DEGRADATION. NOMINAL 3DQP RING, RADIUS 9.1 CM, THICKNESS 1.15 CM

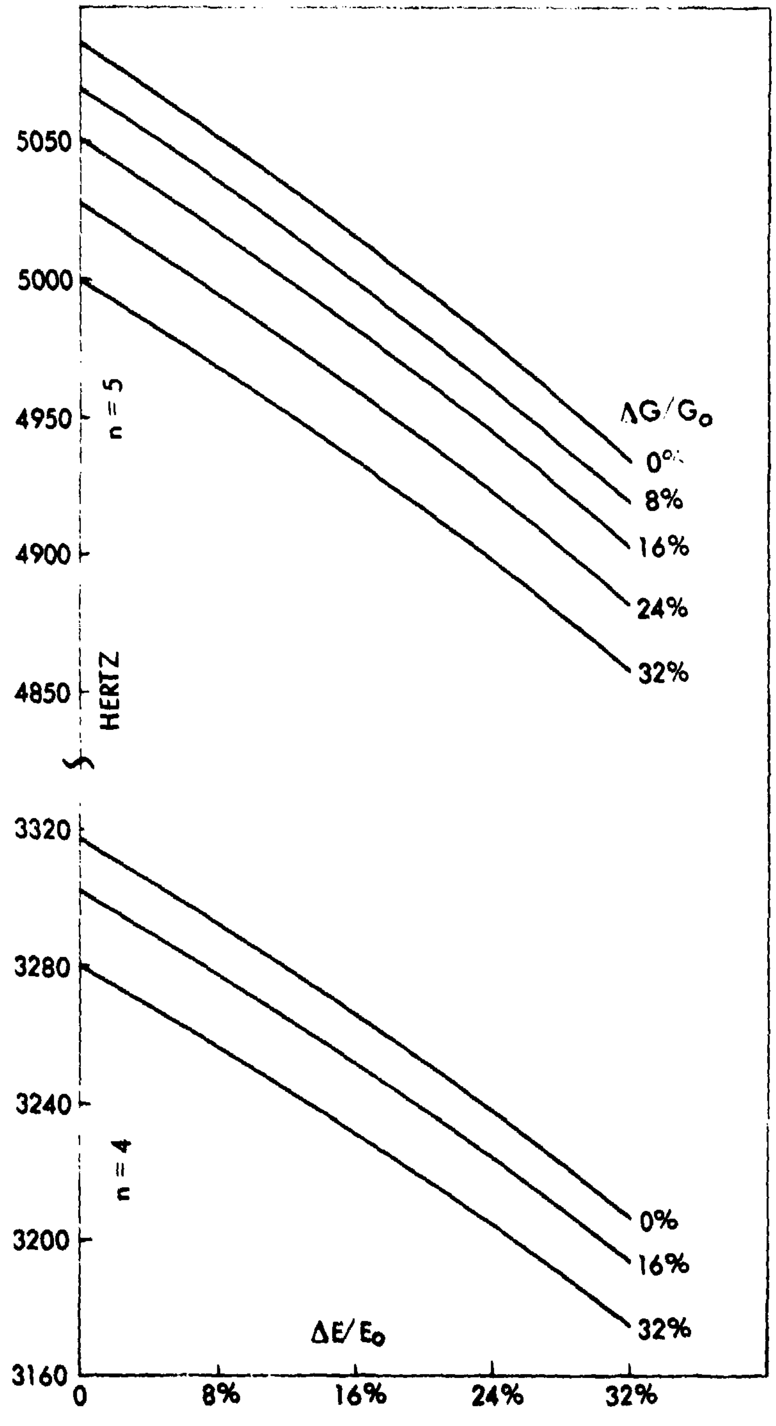

FIGURE 49

CALCULATED RESONANT FREQUENCY VERSUS MODULUS DEGRADATION. NOMINAL 3DQP RING, RADIUS 9.1 CM, THICKNESS 1.15 CM

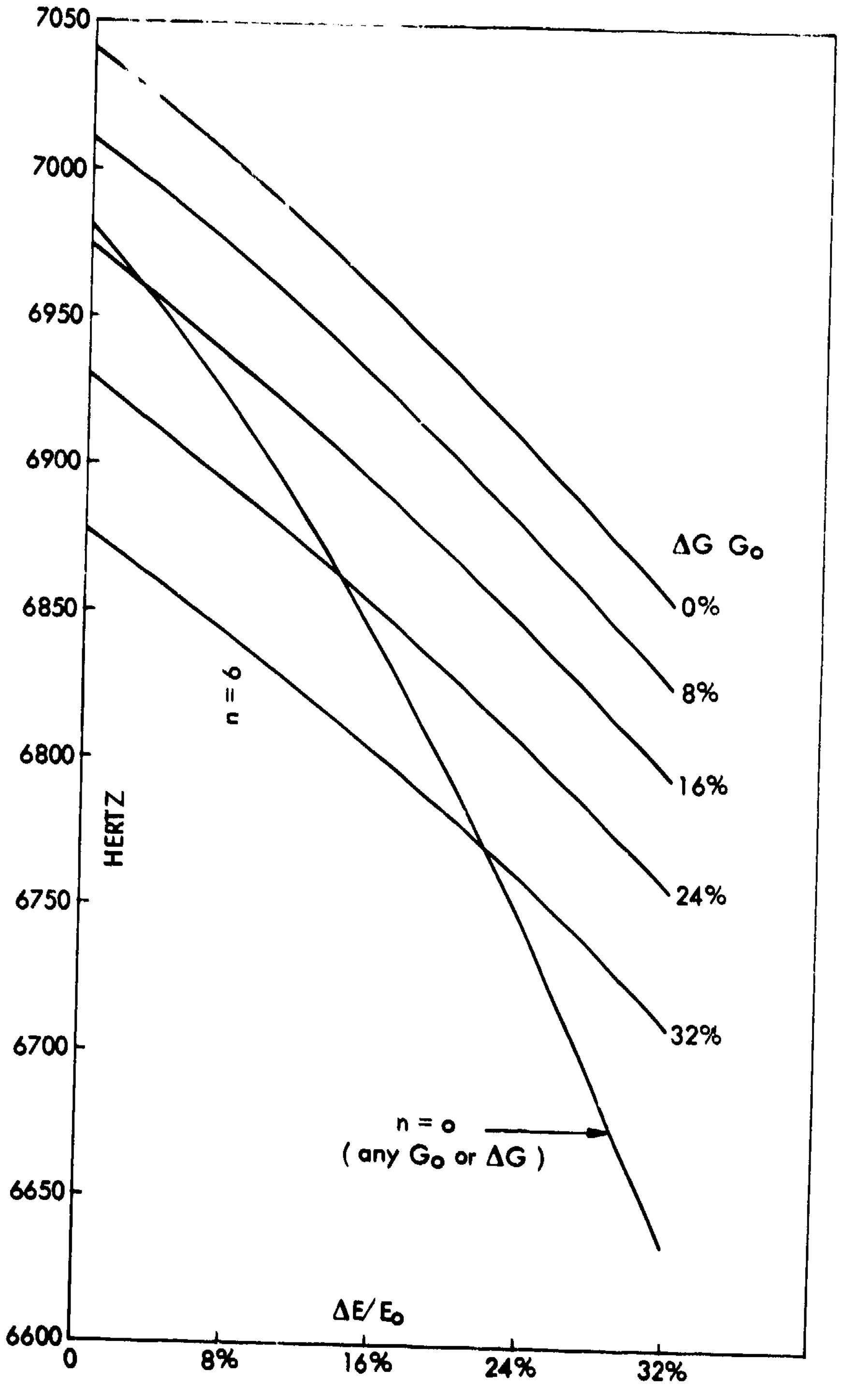

FIGURE 50

CALCULATED RESONANT FREQUENCY VERSUS MODULUS DEGRADATION. NOMINAL 3DQP RING, RADIUS 9.1 CM, THICKNESS 1.15 CM

## 8.2 Incremental Machining Experiment

### 8.2.1 Description of the Experiment

Five 3DQP rings were subjected to a progressive or incremental machining experiment. Those rings were the underground tested rings M381-1, M277-6, and M483-3 and flyer plate impacted rings 7.1.4/4 and 7.1.4/6. The experiment consists of subjecting the specimens to a sequence of cycles of resonant frequency measurement and incremental removal of material from the outer surface. In preparation for the experiment each UGT ring is ground clean of surface nonuniformities inside and outside and each AGT ring is similarly cleaned inside.

The purpose of the experiment was to obtain a quantitative description of the variation of the degradation of the influential material properties through the thickness caused by the impulse that these rings had experienced. The ultimate goal is to compare the through-the-thickness characteristics of degradation produced by UGT impulse with those produced by flyer plate simulation tests.

The resulting data consists of a set of resonant frequencies (usually n = 0, 2, 3, 4, 5, and 6) for each ring for several thicknesses in the sequence. For each thickness condition, for which resonant frequencies were measured, calculations are done to determine the sectional average values of the influential material properties that must characterize the ring in order that the measured frequencies can be correlated with theoretical results. For these calculations the NFDR code is used.

As has been described, the NFDR code accepts arbitrarily prescribed variations of the properties around the circumference. In this study the following degradation functions are postulated:

$E = E_o - \Delta E \cos \pi\theta/120, \qquad |\theta| \leq 60°$

$E = E_o, \qquad |\theta| > 60°$

$G = G_o - \Delta G, \qquad |\theta| \leq 45°$

$G = G_o, \qquad |\theta| > 60°$

$G =$ linear variation from $(G_o - \Delta G)$ to $G_o$, $45° < |\theta| < 60°$

Values of $E_o$, $G_o$, $\Delta E$, and $\Delta G$ are deduced for which the calculated frequencies correlate the measured frequencies.

Let the thicknesses in the sequence be denoted by $h_i$ and let the incremental thickness removed between two conditions to be denoted by $\Delta Z_i = h_i - h_{i+1}$. Also let the degradation magnitudes be denoted by $\Delta E_i$ and $\Delta G_i$ and the average circumferential and shear moduli, evaluated at 0°, be denoted by $\bar{E}_i$ and $\bar{G}_i$.

These are related by:

$$\bar{E}_i = E_o - \Delta E_i$$

and

$$\bar{G}_i = G_o - \Delta G_i.$$

If the average circumferential modulus has been obtained for each thickness in the sequence, we can then write the following equations:

$$h_1\bar{E}_1 = h_2\bar{E}_2 + E_1\Delta Z_1$$

$$h_2\bar{E}_2 = h_3\bar{E}_3 + E_2\Delta Z_2$$

$$h_3\bar{E}_3 = h_4\bar{E}_4 + E_3\Delta Z_3$$

$$\vdots$$

where $E_1$, $E_2$, $E_3$, . . . are the local values of circumferential modulus in the sequentially removed layers $\Delta Z_1$, $\Delta Z_2$, $\Delta Z_3$, . . ., respectively, which is exactly the desired information.

G cannot presently be similarly treated because of contradictions inherent in the shell theory treatment of transverse shear.

### 8.2.2 Preliminary Results

A summary of the ring configurations for which resonant frequencies have been measured is given in Table 10. Because of the present cumbersomeness of the analysis, the results reported at this time are incomplete and these will be rechecked when the automation of the analysis is completed. Partial results are available for rings M381-1 and 7.1.4/6. These results are given in Tables 11 and 12 and plots of circumferential modulus through the thickness are given in Figures 51 and 52.

Table 10 Incremental Machining Experiment
Resonant Frequency Test Configurations

| RING NO. | CONFIGURATION | 1 | 2 | 3 | 4 | 5 |
|---|---|---|---|---|---|---|
| M381-1 | Thickness (cm) | 1.153 | 1.039 | 0.699 | 0.254 | 0.203 |
| | O.D. (cm) | 19.36 | 19.14 | 18.46 | 17.57 | 17.47 |
| M277-6 | Thickness | 0.706 | 0.582 | 0.467 | 0.254 | 0.203 |
| | O.D. | 19.36 | 19.12 | 18.89 | 18.46 | 18.36 |
| M483-3 | Thickness | 0.986 | 0.864 | 0.699 | -- | -- |
| | O.D. | 19.12 | 18.88 | 18.55 | -- | -- |
| 7.1.4/4 | Thickness | 1.292 | 1.194 | 0.699 | 0.254 | 0.203 |
| | O.D. | 19.58 | 19.38 | 18.39 | 17.50 | 17.40 |
| 7.1.4/6 | Thickness | 1.189 | 1.080 | 0.699 | 0.254 | 0.203 |
| | O.D. | 19.58 | 19.36 | 18.60 | 17.71 | 17.61 |

Table 11 Incremental Machining Experiment
M381-1 Results

$E_o$ = 26.6 GPa

$G_o$ = 2.4 GPa

| Configuration | 1 | 2 | 3 |
|---|---|---|---|
| $\Delta E/E_o$ | 0.28 | 0.31 | 0.36 |
| $\Delta G/G_o$ | 0.28 | 0.31 | 0.37 |
| E Removed Material | | 26.6 GPa | 21.0 GPa |

## Table 12 Incremental Machining Experiment
## 7.1.4/6 Results

$E_o$ = 26.1 GPa

$G_o$ = 2.60 GPa

| Configuration | 1 | | 2 | | 3 |
|---|---|---|---|---|---|
| $\Delta E/E_o$ | 0.27 | | 0.27 | | 0.37 |
| $\Delta G/G_o$ | 0.26 | | 0.26 | | 0.37 |
| E Removed Material | | 21.9 GPa | | 23.2 GPa | |

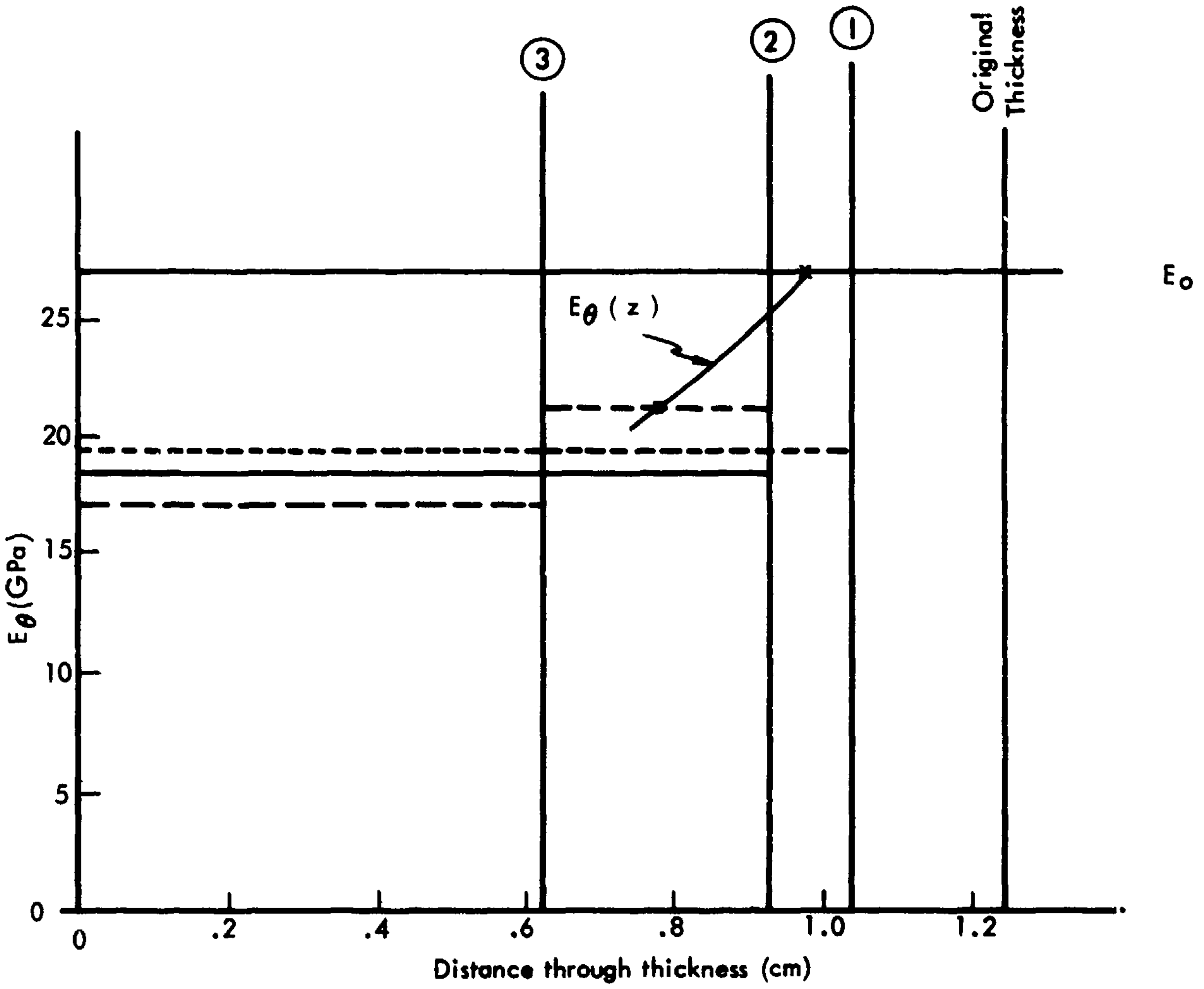

FIGURE 51

PROGRESSIVE MACHINING PRELIMINARY RESULT.
CIRCUMFERENTIAL MODULUS AT $\theta=0^\circ$
RING M-381-1

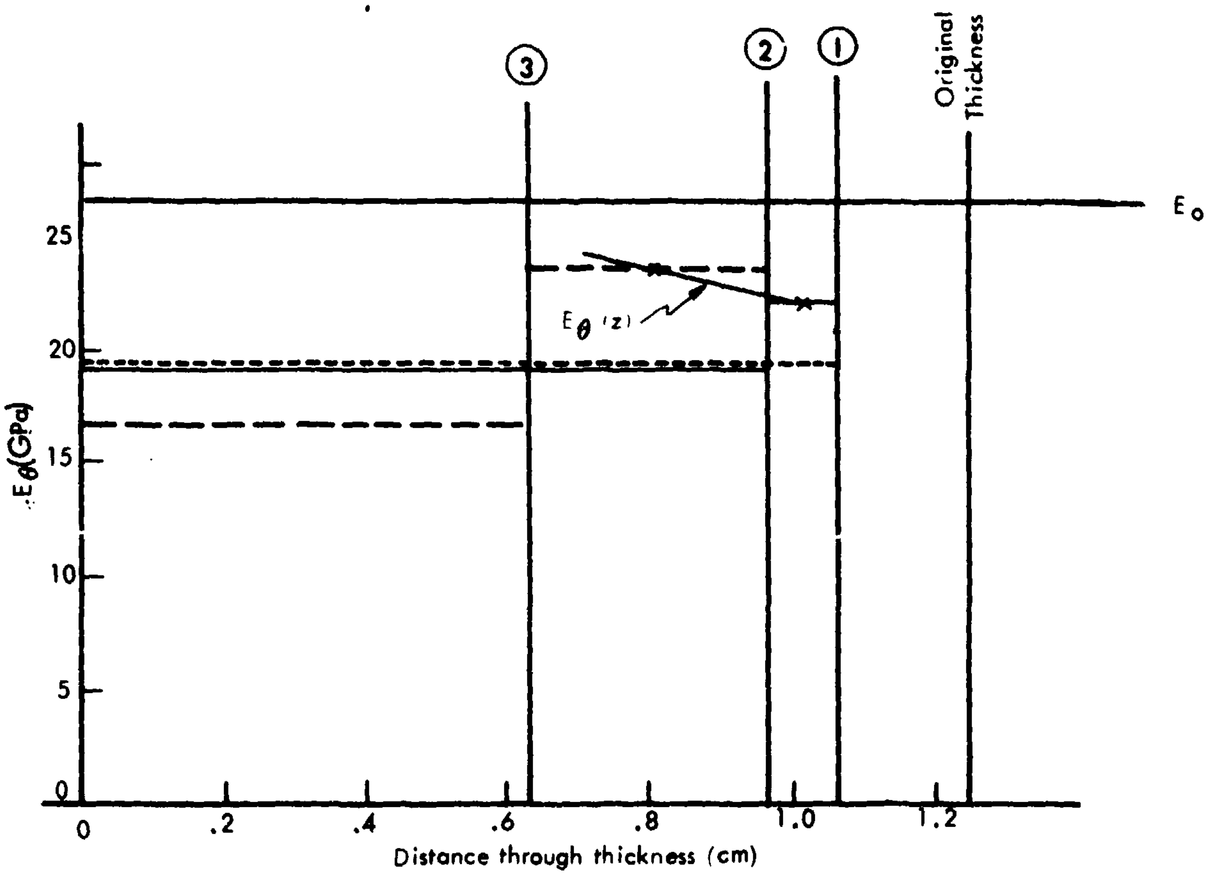

FIGURE 52

PROGRESSIVE MACHINING PRELIMINARY RESULT.
CIRCUMFERENTIAL MODULUS AT $\theta=0^\circ$
RING 7.1.4/6

## 9.0 CONCLUSIONS AND SUMMARY

A brief summary of the conclusions reached from this program are as follows:

- Arc samples from cylinder 7.1.3, 7.1.4, and 4.1.5 suffered the same failure mode at common load levels
- Front surface mylar did not affect damage mode
- Increasing prompt impulse while holding other loading parameters constant opened mid-plane damage on 7.1.3 materials
- Ring samples had 5 - 20 percent higher retained strength properties and slightly higher retained modulus than the arc samples
- Ring 7.1.4#15 duplicated several effects experienced by Ring Z, including degraded modulus, strain-time and rear surface damage. Mid-plane damage was not sufficiently connected across enough cell widths to be considered a duplication of Ring Z, however, such that damage mode was not perfectly simulated. This ring is similar to 7.1.4#6 in simulation of Ring Z effects
- Ring 7.1.4#16 was an acknowledged overtest conducted in an attempt to develop mid-plane delamination. A near mid-plane delamination

was achieved, while rear surface damage was exactly duplicated. Degraded modulus and strain-time indicated too high a load level

- KSC shock tube data matches trends shown by past experimenters, i.e., that the risetime of the rear surface particle velocity waveform can differentiate A and C process 3DQP. Absolute differences in risetime between the KSC and Aerospace Work were 1.0 μsec for C and 1.5 μsec for A process 3DQP

In summary the 3DQC program successfully demonstrated the ability to create a desired damage mode and level which simulated the UGT condition. Although the discrepancy between arc and ring specimens was not resolved within the scope of this program, the following parameters were duplicated to the errors shown:

| Parameter | Ring Z Result | AGT Result | % Difference |
|---|---|---|---|
| damage location | 25/30 plies | 26/38 plies | 20 |
| p-t peak | 7.3 kbar | 7.4 kbar | 2 |
| 180° $\epsilon$-t | (from 0.116 msec to 0.583 msec) | | 11 |
| dynamic modulus degradation | 28% | 29% | 3 |
| total impulse | 13.5 | 13.6 | 1 |

As described in Reference 1 and this report, this comprehensive test program was a major step in the development of magnetically driven flyer plate technology. New test techniques were devised, repeatibility was established and - perhaps most importantly - an analytical understanding of the combined x-ray response and flyer plate system performance was demonstrated. It is believed that these same techniques can be extended to other materials with equal success.

## REFERENCES

1. Doane, W. S., Meagher, T. F. V., Oscarson, J., and Webter, L. D. Magnetic Flyer Facility Correlation and UGT Simulation (U) DNA 4622-F, May 1978, (CFRD).

2. Pears, C., Fornaro, G., Outline For UK Data Exchange, a handout for the presentation made in the UK 27 November 1978. (U)

3. Shock Tube Report Rich

4. Webster, L. D., The Method of Finite Elements Applied To Unidirectional Fiber Reinforced Composites (U), A Kaman Nuclear Report, 23 Janauary 1967.

5. Hollister, H., McNeice, J., and Lew M. Husser Sword Series, Husky Ace Event, Project Officers Report (U), KSC Report K-74-478(R), POR-6803, December 1974 (SRD)

6. Gurtman, G. A., 3DQP AGT/UGT Correlation Study (U), DNA 4597F (CFRD)

## APPENDIX A

Eight shots were conducted in January, 1978, to investigate methods to either eliminate or minimize flyer plate edge curl at the 13,000 - 15,000 tap impulse levels attained during this program. Techniques used to achieve the goal must be consistent with test setup and operational procedures established for years at KSC.

Details of the edge curl study are shown in Figure A1. As mentioned in this figure, a streak camera was used to monitor the flyer plate impact conditions. Calipers were used to measure the pre and posttest widths to monitor the width destortion of the flyer plates due to edge curl melting. The parameter varied to minimize edge curl was the flyer plate to backstrap plate width ratio.

Six shots were conducted at 0.254 cm free run since it was believed that the longer free run represented a worst case. Operational free runs were 0.058 cm, only 20 - 25 percent of the worst case value. Data from five of these shots are presented in Figure A-2; a streak record was not obtained on one of the six shots.

The five shots achieved a flyer planarity of 250 - 500 ns. Taken as an absolute asimultaneity, this is a poor result at the high flyer velocities achieved. However, the asimultaneity was only at the very edge of the flyer, while the central portion of the flyer was extremely flat as shown in Figure A-2. The posttest flyer width change was only 3 - 5 percent, extremely good at 15,000 - 19,000 tap flyer plate levels achieved. Posttest inspection of the flyer revealed very little edge melt or flyer crumple; these observations of the posttest flyer condition are thought to be significant in view of the high impulse levels.

Two shots were conducted at operational free run distances, 0.058 cm rather than 0.254 cm as above. These tests were run to establish when the flyer crush and edge curl happened. In particular, the test was conducted to determine if the flyer changed ist width before or after impact at operational free run distances. Scribe lines were placed on the flyer, with several lines placed on each flyer edge. The flight of the flyer was viewed through a lucite witness plate with a streak camera. By this method a continuous record of the flyer width versus time was obtained until the lucite spalled. From these two shots it was determined that the flyer width change must occur after impact, which was 5 - 6 μsec after bank fire. The lucite witness plate broke up approximately 10 μsec after bank fire, with no significant width change having developed in the flyer.

A shot summary detailing these eight shots are presented in Table A-1.

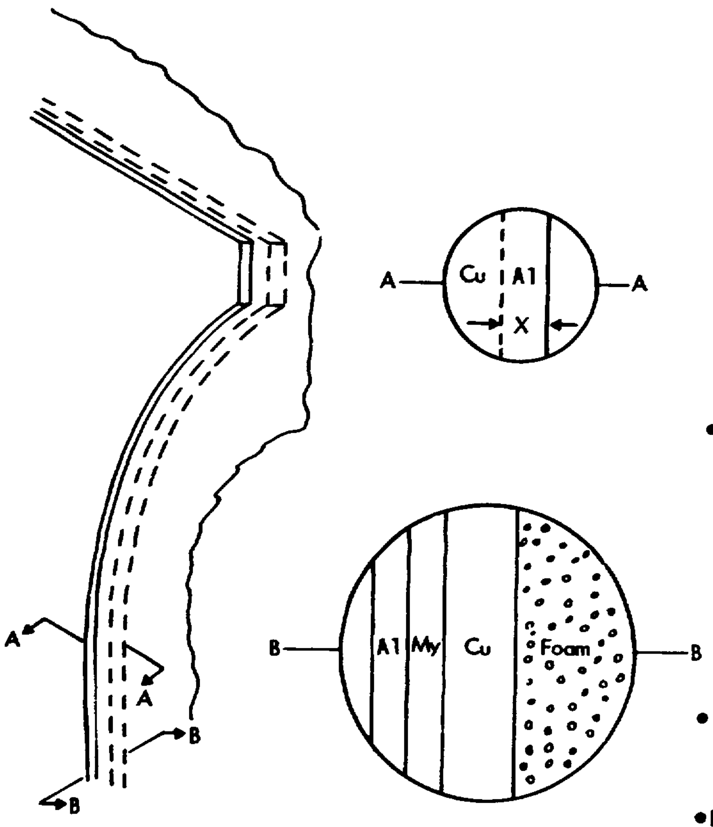

- **STUDY GOALS**
  - Eliminate/ Minimize Flyer Width Change Due To Edge Curl
  - Maintain Integrity Of Test Setup
    - Flat, Smooth Flyer
    - Uniform Flyer/ Target Spacing
- **APPROACH**
  - Flat Flyers -0.0635 cm Thick A1 Flyer
    -0.127 cm Thick Cu Backstrap
  - Vacuum Mandrel To Form Flyer
  - Foam Backstrap To Maintain Shape
- **VARIABLE**
  - Flyer Plate To Backstrap Width
- **DIAGNOSTIC**
  - Streak Camera
    Writing Rate : 10mm/ μsec
    Time Resolution : ~ 50 n sec
    Space Resolution : ~ 0.05 cm

FIGURE A-1
EDGE CURL STUDY FLYER GEOMETRY

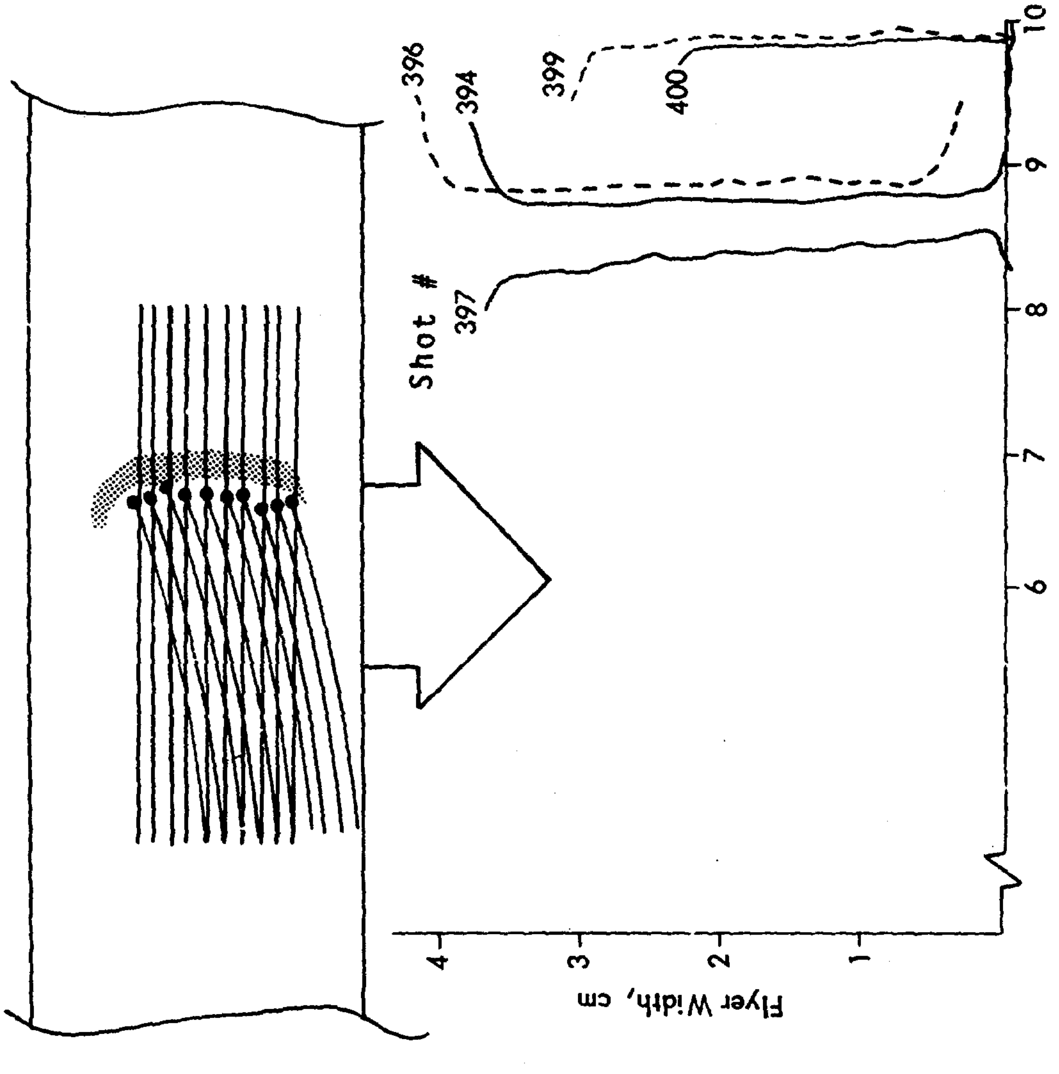

FIGURE A-2 FLYER PLANARITY DATA FROM THE EDGE CURL STUDY DATA OBTAINED BY STREAK CAMERA TECHNIQUES

# DISTRIBUTION LIST

## DEPARTMENT OF DEFENSE

Assistant to the Secretary of Defense
Atomic Energy
ATTN: Executive Assistant

Defense Advanced Rsch. Proj. Agency
ATTN: TIO

Defense Intelligence Agency
ATTN: DT-2

Defense Nuclear Agency
ATTN: SPSS
ATTN: SPAS
ATTN: SPTD
ATTN: STSP
4 cy ATTN: TITL

Defense Technical Information Center
2 cy ATTN: DD

Field Command
Defense Nuclear Agency
ATTN: FCTMD
ATTN: FCPR

Field Command
Defense Nuclear Agency
Livermore Division
ATTN: FCPRL

Joint Chiefs of Staff
ATTN: SAGA/SFD
ATTN: J-5 Force Planning & Program Div.
ATTN: SAGA/SSD
ATTN: J-5 Nuclear Division

Joint Strat. Tgt. Planning Staff
ATTN: JLTW-2
ATTN: JLA
ATTN: JPTM

Undersecretary of Defense for Rsch. & Engrg.
ATTN: Strategic & Space Systems (OS)

## DEPARTMENT OF THE ARMY

BMD Advanced Technology Center
Department of the Army
ATTN: ATC-T, M. Capps

BMD Program Office
Department of the Army
ATTN: Technology Division

BMD Systems Command
Department of the Army
ATTN: BMDSC-H, N. Hurst

Deputy Chief of Staff for Ops. & Plans
Department of the Army
ATTN: DAMO-NCZ

Deputy Chief of Staff for Rsch., Dev., & Acq.
Department of the Army
ATTN: DAMA-CSS-N

## DEPARTMENT OF THE ARMY (Continued)

Harry Diamond Laboratories
Department of the Army
ATTN: DELHD-N-RBC, D. Schallhorn
ATTN: DELHD-N-P
ATTN: DELHD-N-P, J. Gwaltney

U.S. Army Ballistic Research Labs
ATTN: DRDAR-BLE, J. Keefer
ATTN: DRDAR-BLV, W. Schuman, Jr.
ATTN: DRDAR-BLV

U.S. Army Material & Mechanics Rsch. Ctr.
ATTN: DRXMR-HH, J. Dignam

U.S. Army Materiel Dev. & Readiness Cmd.
ATTN: DRCDE-D, L. Flynn

U.S. Army Missile Command
ATTN: DRSMI-RKP, W. Thomas

U.S. Army Nuclear & Chemical Agency
ATTN: Library

U.S. Army Research Office
ATTN: Technical Library

## DEPARTMENT OF THE NAVY

Naval Research Laboratory
ATTN: Code 6770, G. Cooperstein
ATTN: Code 2627
ATTN: Code 7908, A. Williams

Naval Sea Systems Command
ATTN: SEA-0351
ATTN: SEA-0352, M. Kinna

Naval Surface Weapons Center
ATTN: Code K06, C. Lyons
ATTN: Code F31
ATTN: Code R15, J. Petes
ATTN: Code K06

Naval Weapons Evaluation Facility
ATTN: L. Oliver

Office of the Chief of Naval Operations
ATTN: OP 604C
ATTN: OP 604E14, R. Blaise
ATTN: OP 981

Strategic Systems Project Office
Department of the Navy
ATTN: NSP-272
ATTN: NSP-273

## DEPARTMENT OF THE AIR FORCE

Aeronautical Systems Division
Air Force Systems Command
ATTN: ASD/ENFTV

Air Force Rocket Propulsion Laboratory
ATTN: LKCP, G. Beale

This document is being sent to the below listed contractors for the use of the individuals listed. Recipient contractors are requested to validate individuals' clearances before forwarding document to same.

### DEPARTMENT OF THE AIR FORCE (Continued)

Air Force Materials Laboratory
ATTN: MBC, D. Schmidt
ATTN: MBE, G. Schmitt
ATTN: LLM, T. Nicholas

Air Force Systems Command
ATTN: SOSS
ATTN: XRTO

Air Force Weapons Laboratory
Air Force Systems Command
ATTN: SUL
ATTN: DYV
ATTN: DYT
ATTN: NT
ATTN DYS

Ballistic Missile Office
Air Force Systems Command
ATTN: MNNH
ATTN: MNNR

Deputy Chief of Staff
Research, Development, & Acq.
Department of the Air Froce
ATTN: AFRD
ATTN: AFRDQSM

Foreign Technology Division
Air Force Systems Command
ATTN: SDBG
ATTN: SDBS, J. Pumphrey
ATTN: TQTD

Headquarters Space Division
Air Force Systems Command
ATTN: DYS

Headquarters Space Division
Air Force Systems Command
ATTN: RSS
ATTN: RSMA
ATTN: RSSE

Strategic Air Command
Department of the Air Force
ATTN: XPFS
ATTN: DOXT
ATTN: XPQM
ATTN: XOBM

### DEPARTMENT OF ENERGY

Department of Energy
ATTN: Document Control for OMA/RD&T

### DEPARTMENT OF ENERGY CONTRACTORS

Lawrence Livermore Laboratory
ATTN: L-92, C. Taylor
ATTN: L-96, L. Woodruff
ATTN: L-125, J. Keller
ATTN: D. Hanner

### DEPARTMENT OF ENERGY CONTRACTORS (Continued)

Los Alamos Scientific Laboratory
ATTN: R. Skaggs
ATTN: J. McQueen/J. Taylor
ATTN: D. Shover
ATTN: R. Dingus

Sandia Laboratories
Livermore Laboratory
ATTN: H. Norris, Jr.
ATTN: T. Gold

Sandia Laboratories
ATTN: M. Cowan
ATTN: C. Broyles
ATTN: C. Mehl

### DEPARTMENT OF DEFENSE CONTRACTORS

Aerospace Corp.
ATTN: R. Crolius
ATTN: H. Blaes
ATTN: R. Strickler

AVCO Research & Systems Group
ATTN: P. Grady
ATTN: J. Stevens
ATTN: G. Weber
ATTN: J. Gilmore
ATTN: W. Broding
ATTN: Document Control

Battelle Memorial Institute
ATTN: M. Vanderlind

Boeing Co.
ATTN: B. Lempriere

California Research & Technology, Inc.
ATTN: K. Kreyenhagen

Effects Technology, Inc.
ATTN: R. Parrise/M. Rosen
ATTN: R. Wengler/R. Bick

Ford Aerospace & Communications Corp.
ATTN: P. Spangler

General Electric Co.
ATTN: P. Cline
ATTN: D. Edelman
ATTN:N N. Dispenzierre
ATTN: G. Harrison

General Electric Company—TEMPO
ATTN: DASIAC

General Research Corp.
ATTN: R. Rosenthal

Institute for Defense Analyses
ATTN: Classified Library
ATTN: J. Bengston

ION Physics Corp.
ATTN: R. Evans

This document is being sent to the below listed contractors for the use of the individuals listed. Recipient contractors are requested to validate individuals' clearances before forwarding document to same.

DEPARTMENT OF DEFENSE CONTRACTORS (Continued)

Kaman AviDyne
ATTN: R. Ruetenik

Kaman Sciences Corp.
ATTN: R. Sachs/R. O'Keefe
ATTN: T. Meagher
ATTN: F. Shelton

Lockheed Missiles & Space Co., Inc.
ATTN: F. Borgardt

Lockheed Missiles & Space Co., Inc.
ATTN: O. Burford
ATTN: R. Walls

Lockheed Missiles & Space Co., Inc.
ATTN: T. Fortune

Martin Marietta Corp.
ATTN: L. Kinnaird

McDonnell Douglas Corp.
ATTN: L. Cohen
ATTN: H. Berkowitz
ATTN: J. Peck
ATTN: E. Fitzgerald

Pacific-Sierra Research Corp.
ATTN: G. Lang

Physics International Co.
ATTN: J. Shea

Prototype Development Associates, Inc.
ATTN: N. Harington
ATTN: J. McDonald

R & D Associates
ATTN: P. Rausch
ATTN: C. MacDonald
ATTN: W. Graham, Jr.
ATTN: F. Field

DEPARTMENT OF DEFENSE CONTRACTORS (Continued)

Rand Corp.
ATTN: R. Rapp

Science Applications, Inc.
ATTN: W. Layson
ATTN: W. Seebaugh

Southern Research Institute
ATTN: C. Pears

SRI International
ATTN: H. Lindberg
ATTN: D. Curran
ATTN: G. Abrahamson

Systems, Science & Software, Inc.
ATTN: G. Gurtman
ATTN: T. McKinley
ATTN: R. Duff

Terra Tek, Inc.
ATTN: S. Green

TRW Defense & Space Sys. Group
ATTN: W. Wood
ATTN: L. Donahue
2 cy ATTN: P. Dai/D. Jortner

TRW Defense & Space Sys. Group
ATTN: W. Polich
ATTN: R. Mortensen
ATTN: V. Blankenship
ATTN: J. Farrell

Science Applications, Inc.
ATTN: W. Yengst

**Defense Special Weapons Agency**
6801 Telegraph Road
Alexandria, Virginia 22310-3398

TRC

13 April 1998

MEMORANDUM TO DEFENSE TECHNICAL INFORMATION CENTER
ATTN: OCQ/MR BILL BUSH

The following reports have been reviewed by the Defense Special Weapons Agency Security Office:

321
~~DNA-4622F, AD-C015969, DTL-78,1304~~ Completed
DNA-5056F, AD-C021924, ✓DTL-80,0808
DNA-5826F, AD-C040572, ✓DTL-87,0355 C FRD
DNA-5826F-SUP, AD-C041417, ✓DTL-871167 CFRD

The Security Office has **declassified** all of the listed reports. Further, distribution statement **"A"** applies to all of the reports.

Ardith Jarrett
ARDITH JARRETT
Chief, Technical Resource Center

Completed
15 May 2000
B.W.